

MSc Thesis on

**VEGETATION OPTICAL DEPTH:  
ITS POTENTIAL AS AN AGRICULTURAL DROUGHT INDICATOR**

A case study on pepper fields in Indonesia



Anna Luisa Hemshorn de Sánchez  
TU Delft & VanderSat



VanderSat

Master of Science  
**Civil Engineering**  
**Water Management**

Supervisors

Prof. Dr. ir. Susan Steele-Dunne  
Dr. Richard de Jeu  
Dr. ir. Edo Abraham  
Dr. Philip Vardon



# ABSTRACT

Droughts are a serious threat to the planet. Especially in agriculture, the consequences are devastating leading to reduced yields or crop failure with further implications for economics, politics and society. Being able to monitor and predict agricultural droughts is an important step to reduce agricultural vulnerability and secure livelihoods. However, few drought indicators measure the actual crop response towards the hydrological conditions. Remote sensing bears great potential for this challenge due to its worldwide continuous coverage and relatively low costs. Vegetation Optical Depth (VOD), a remote sensing method, is a measure of above-ground vegetation water content based on passive microwaves, which are not affected by atmospheric distortion. The present research aims at analysing the potential of VOD as an agricultural drought indicator. A case study on pepper fields in Indonesia was conducted using daily VOD data between 2012 and 2018 at a downscaled spatial resolution of 100 x 100 m. Correlations between VOD anomalies and anomalies of other meteorological drought indicators were calculated. VOD was found to be correlated with the Standardized Precipitation Evaporation Index (SPEI) by 0.47, with the El Niño Southern Oscillation (ENSO) by -0.46 and with the Indian Ocean Dipole (IOD) by -0.46. These correlations indicate that other factors influence the VOD, which should be considered as an independent dataset. This study provides evidence that VOD is capable of capturing agricultural droughts. A cross-comparison was conducted with the Normalized Difference Vegetation Index (NDVI), which is often compared to VOD as an alternative measure. Results in the investigated area suggest that, although VOD has a lower spatial resolution, it performs better than NDVI. Finally, a roadmap was proposed towards developing a drought indicator based on the VOD anomalies. This roadmap aims at modelling future VOD based on the relation between SPEI and VOD by using the added value of VOD that this study reveals. This study is especially relevant for other tropical areas with a high cloud density.

# TABLE OF CONTENTS

1	Introduction.....	1
2	Theoretical background.....	4
2.1	Definition of droughts.....	4
2.2	Commonly used drought indices.....	5
2.2.1	Meteorological drought indices.....	5
2.2.2	Hydrological drought indices.....	7
2.2.3	Soil moisture indices.....	7
2.2.4	Combined drought index.....	9
2.2.5	Vegetation indicators.....	9
2.3	Vegetation Optical Depth (VOD).....	11
2.3.1	History.....	11
2.3.2	Derivation.....	11
2.3.3	Bands, resolution and downscaling.....	16
2.3.4	Differences between VOD and NDVI.....	18
3	Indonesia: a case study.....	19
3.1	General Information.....	19
3.1.1	Climate.....	19
3.1.2	Economy.....	23
3.2	Field visit in the pepper fields.....	24
3.2.1	Plant and field shape.....	26
3.2.2	Life cycle.....	28
3.2.3	Irrigation and droughts.....	32
4	Methodology.....	34
4.1	Study area.....	34
4.2	Datasets.....	35
4.2.1	Vegetation Optical Depth.....	35
4.2.2	Normalized Difference Vegetation Index (NDVI).....	36
4.2.3	Multivariate ENSO Index (MEI).....	36
4.2.4	Dipole Mode Index (DMI).....	36
4.2.5	Standardized Precipitation Evaporation Index (SPEI).....	36
4.2.6	Hansen deforestation maps.....	37
4.2.7	Yield data.....	37
4.3	Spatial patterns in VOD.....	37
4.3.1	Comparison of VOD and NDVI to general land use patterns.....	37
4.3.2	Derivation of spatial characteristics of VOD of pepper fields.....	37
4.3.3	Identification of spatio-temporal characteristics of large-scale VOD.....	37
4.4	Temporal patterns in VOD.....	38
4.4.1	Calculation of VOD anomalies.....	38
4.4.2	De-trending of VOD anomalies.....	38
4.4.3	Derivation of temporal characteristics of VOD of pepper fields.....	38
4.4.4	Comparison of VOD to other drought indicators.....	39
4.4.5	Comparison of NDVI to other drought indicators.....	40
4.4.6	Comparison of yields to VOD.....	40
5	Results & Discussion.....	41
5.1	Spatial patterns.....	41

5.1.1	VOD and NDVI.....	41
5.1.2	Derivation of spatial characteristics of VOD of pepper fields .....	42
5.1.3	Spatial changes in large-scale VOD over time.....	45
5.2	Temporal patterns.....	46
5.2.1	Effect of applying a moving average or temporal aggregation.....	46
5.2.2	VOD trends .....	47
5.2.3	Derivation of temporal characteristics of VOD of pepper fields.....	47
5.2.4	VOD, NDVI and other drought indicators.....	51
5.2.5	Yields and VOD.....	60
5.3	Guideline to convert VOD to a drought index .....	60
6	Conclusions & Recommendations .....	62
6.1	Conclusions.....	62
6.2	Recommendations .....	63
7	Bibliography.....	64
8	Appendix .....	69
8.1	Details for the analysed fields.....	69
8.2	Additional spatial analysis of <i>LSquare04</i> .....	70
8.3	Pepper field versus large-scale surrounding .....	71
8.3.1	Anomaly time series.....	71
8.3.2	Scatter plots .....	72
8.4	Correlations between different drought indices .....	74
8.4.1	ENSO .....	74
8.4.2	IOD.....	78
8.4.3	SPEI.....	82

# LIST OF FIGURES

Figure 1: Frequencies, wavelength and spectra (Imgur Stack Exchange, no date).....	9
Figure 2: Relationship between Brightness temperature and emissivity for low frequencies.....	12
Figure 3: Rough surface emissivity and resulting reflectivity.....	13
Figure 4: Brightness temperature according to (Mo et al., 1982) including vegetation effects (image: de Jeu, 2003).....	14
Figure 5: Physical soil and canopy temperature according to (Parinussa et al., 2016).....	14
Figure 6: Schematization of simultaneous VOD and soil moisture retrieval (LPRM).....	15
Figure 7: Relation between VOD and MPDI (de Jeu, 2003).....	16
Figure 8: Intensity and Gauss distribution (VanderSat, 2016).....	17
Figure 9: Ellipses (VanderSat, 2016).....	17
Figure 10: Map of Indonesia with islands (capital letters) and provinces (lower case letters) of interest.....	19
Figure 11: Mean precipitation and temperature in Indonesia (The World Bank Group, 2018).....	20
Figure 12: Composite maps of meteorological drought (SPI3) in September–October–November during warm ENSO years ((a) all, (b) weak, (c) moderate, and (d) strong El Niño years) (Setiawan et al., 2017).....	21
Figure 13: Palm oil plantation.....	24
Figure 14: Rubber plantation.....	24
Figure 15: Tin mine in Bangka.....	25
Figure 16: Cornfield in Lampung.....	25
Figure 17: Pepper and some other land uses from a Google Earth image.....	26
Figure 18: Pepper plants growing on sticks in North Bangka.....	26
Figure 19: Pepper plants growing on sticks in central Bangka.....	27
Figure 20: Industrial pepper field of 36 ha in Bangka.....	27
Figure 21: Pepper plants on living trees on Lampung with large canopy (left) and with small canopy (right).....	27
Figure 22: Seedlings in polybags.....	28
Figure 23: Segment structure of the pepper plant.....	29
Figure 24: Recently planted pepper plant.....	29
Figure 25: Irregular ripening process within the same plant.....	30
Figure 26: Soaking of pepper in open surface water bodies to become white pepper.....	30
Figure 27: Black and white pepper.....	31
Figure 28: Pepper plant with yellow disease.....	31
Figure 29: Pepper plant with root rot disease.....	32
Figure 30: Irrigation dredge.....	32
Figure 31: Study areas on Bangka.....	34
Figure 32: Study areas on Lampung.....	35
Figure 33: Google Earth image of <i>BSquare02</i> (left) and <i>LSquare07</i> (right).....	41
Figure 34: Mean NDVI (top), mean NDVI with VOD contours (middle) and mean VOD (bottom) of 2016 of <i>BSquare02</i> ... 43	43
Figure 35: Mean NDVI (top), mean NDVI with VOD contours (middle) and mean VOD (bottom) of 2016 of <i>LSquare07</i> ... 44	44
Figure 36: 4-monthly VOD anomaly before, during and after the drought in <i>BSquare02</i> (left) and <i>LSquare07</i> (right).....	45
Figure 37: VOD (X-Band) time series of <i>BPepperField06</i> – raw data, moving average and climatology.....	46
Figure 38: VOD anomalies of fields and squares in <i>BSquare02</i> , <i>BSquare04</i> , <i>LSquare03</i> and <i>LSquare07</i> .....	48
Figure 39: VOD time series of selected fields in the entire period (left) and a selected period during the offset (right)....	49
Figure 40: Spatial VOD images before or after and during offset of selected fields.....	50
Figure 41: Field-specific Pearson and Spearman correlations of VOD and other drought indicators.....	53
Figure 42: VOD, NDVI and MEI anomalies for selected Pepper Fields in Bangka (top) and Lampung (bottom).....	55
Figure 43: VOD, NDVI and IOD anomalies for selected Pepper Fields in Bangka (top) and Lampung (bottom).....	57
Figure 44: VOD, NDVI and SPEI anomalies for selected Pepper Fields in Bangka (top) and Lampung (bottom).....	59
Figure 45: Yearly pepper yield from 2012 to 2017 of Indonesia (Directorate General of Estate Crops et al., 2016).....	60
Figure 46: Road map to convert VOD into an agricultural drought predictor.....	61

# LIST OF TABLES

Table 1: Other meteorological drought indices.....	7
Table 2: Hydrological drought indices .....	7
Table 3: Soil moisture indices.....	8
Table 4: Combined drought index .....	9
Table 5: Other vegetation indices.....	10
Table 6: Bands, frequencies and foot print sizes (VanderSat B.V., 2016).....	16
Table 7: Intensity of El Niño years from 1980-2018 (Australian Government - Bureau of Meteorology, no date) .....	21
Table 8: Timeframe for the 4-month VOD mean in the drought and the non-drought year .....	38
Table 9: Mean, min and max anomaly before, during and after the drought in 2015 with reference to the normal year 2016.....	45
Table 10: Increasing or decreasing trends of the VOD anomaly time series per pepper field .....	47
Table 11: Summary of correlations between VOD anomalies and other drought indices .....	52
Table 12: Summary of correlations between NDVI and other drought indices.....	52



# 1 INTRODUCTION

Droughts represent a severe threat to humans and ecosystems. Compared to other atmospheric hazards, droughts are often characterized by a larger spatial coverage and a longer duration (Ding *et al.*, 2013). Even though they are among the most slowly developing extreme meteorological phenomena, they are still the least predictable (Mishra *et al.*, 2010). Although droughts are often related to arid climates, almost all regions including wet and humid climates are susceptible to them (Dai, 2011; Carrão *et al.*, 2016). In particular, populated and agriculturally extensively exploited areas are characterized by a high drought risk (Carrão *et al.*, 2016). From an economic point of view, annual yield variations, crop failure and pasture losses represent the main direct impacts of this natural hazard within the agricultural sector (Boyer, 1982; Ding *et al.*, 2013). This may even have a catalytic effect on social and political conflicts (Kelley *et al.*, 2015). Due to this complexity of the impacts on the environment, the economy and the society, the consequences of droughts are difficult to quantify (Wilhite, 2000).

At a global scale, recent drying has been influenced on the one hand by natural climatic variations in atmospheric circulation patterns such as El Niño Southern Oscillation (ENSO) and Asian monsoons (Dai, 2011). On the other hand, anthropogenic activities caused an increase in greenhouse gas emissions leading to higher atmospheric moisture demand, thus, altering the atmospheric circulation patterns (Dai, 2011). Additionally, population growth and the associated increased water demand as well as other anthropogenic triggers such as excessive irrigation, over-farming and deforestation will aggravate the impacts of droughts (Mishra *et al.*, 2010). The central role of humans in this complex issue also includes the opportunity to reduce future damage if more knowledge were available on sustainable limits of agriculture and water use. Instead of managing droughts after they occurred, as currently common practice (Hayer *et al.*, 2004, Svoboda *et al.*, 2015; Wilhite *et al.*, 2007, 2014 cited in Carrão *et al.*, 2016), drought monitoring and prediction could help to reduce the agricultural vulnerability in order to secure livelihoods.

A range of drought indices was developed in this context. Most of these are based on indirect measures such as precipitation or temperature (Torres *et al.*, 2013). However, the site-specific soil and vegetation properties, e.g. soil water content, play a significant role in the manifestation of droughts (Martínez-Fernández *et al.*, 2016). The indirect indices became the common practice because of the deficient availability of the required ground data (Van Lanen *et al.*, 2013).

Through its continuous and worldwide coverage, remote sensing offers cost-efficient opportunities to meet this challenge, especially at continental to global scales or in locations where in-situ measurements are difficult to obtain. Due to its simplicity and efficiency, the Normalized Difference Vegetation Index (NDVI) has become the most used indicator of vegetation productivity on global scale studies (Andela *et al.*, 2013; Sruthi *et al.*, 2015). This index operates in the optical spectrum and measures the chlorophyll abundance at the planet's surface (Myneni *et al.*, 1995). Therefore, it can be used as a pre-drought indicator value to study vegetation cover changes as well as trends in the occurrence of agricultural droughts (Van Dijk *et al.*, 2013; Sruthi *et al.*, 2015). Despite the various advantages of NDVI and similar remote sensing based vegetation indices, they also have downsides, as for instance, lacking data in case of cloud cover or a high concentration of aerosols (Morton *et al.*, 2014, Saleska *et al.*, 2016, Samanta *et al.*, 2010 cited in Liu *et al.*, 2018). Furthermore, in the densely vegetated tropical areas, NDVI saturates, impeding proper analysis. One approach to face this challenge is to complement NDVI with the highly negatively correlated Land Surface Temperature (LST) data (Sruthi *et al.*, 2015).

The microwave spectrum bears promising potential. Temperature, soil moisture as well as the shielding effect of water in the above-ground vegetation biomass define the intensity at which the Earth naturally emits passive microwaves (Jackson *et al.*, 1991; Kerr *et al.*, 1990; Guglielmetti *et al.*, 2007 cited in Liu *et al.*, 2015). For this reason, soil moisture and vegetation water content can be measured with passive microwaves.

Vegetation Optical Depth (VOD) is a dimensionless parameter (Andela *et al.*, 2013) that describes the transparency of vegetation in the microwave domain (retrieved through remote sensing) (Kirdiashev *et al.*, 1979 cited in Andela *et al.*, 2013). It is highly correlated with the total vegetation water content in the biomass above the ground (Jackson *et al.*, 1991; Jackson *et al.*, 1982, 1990; Owe *et al.*, 2001; Wigneron *et al.*, 1993). In contrast to NDVI, this method includes the biomass of woody as well as of leafy components (Yi Liu *et al.*, 2012). The large advantage of VOD over NDVI is that it can penetrate through clouds and aerosols. Furthermore, the longer wavelengths of VOD achieve a deeper penetration into the canopy leading to a saturation at a higher vegetation density than NDVI (Yi Liu *et al.*, 2012).

The application of VOD has been studied in different directions. Nevertheless, it is a field that has not been studied extensively yet and its full potential is still to be explored. Liu *et al.* (2013) applied this method to prove that nearly all steppe grasslands in Mongolia experienced a significant reduction in biomass at a rapid rate that corresponds to variations in rainfall, crop production, livestock, deforestation and fires. Similarly, Liu *et al.* (2015) used VOD to estimate the global Aboveground Biomass Carbon (ABC) during the past two decades looking at both forest and non-forest biomes. Results showed that the strong response of water-limited environments to precipitation variability heavily influences inter-annual ABC patterns. Liu *et al.* (2012) applied a recently developed long-term VOD record (1988-2008) to analyse the response of vegetation water content in various land-cover types to anthropogenic and environmental influences. This record allowed identifying different trends and causes per land-cover type. Andela *et al.* (2013) employed VOD as well as NDVI to study the long-term vegetation changes in drylands around the world. By analysing co-trends between both methods and considering the sensitivity of NDVI towards leafy components, a trend towards woody vegetation encroachment replacing the herbaceous vegetation components could be identified. Moreover, Liu *et al.* (2007) used satellite-derived soil moisture content and VOD to demonstrate that registered drought conditions in Eastern Australia can be identified with this method and that they could be explained to a large extent by the El Niño Southern Oscillation Index (SOI) and to a lesser extent by the Indian Ocean Dipole (IOD) index. Similarly, Van Dijk *et al.* (2013) compared VOD, NDVI as well as a model-based crop water use as crop growth indicators to estimate the impact of droughts on yields in Australia and to compare it with actual yield data. Results showed that each of the test variables could explain 66% - 68% of the recorded crop-yield variations. Furthermore, this study underlines that only rainfall-based indicators are insufficient to characterize droughts. More recently, Liu *et al.* (2018) found that VOD is able to capture droughts in the Amazon rainforest. The study highlights that during the onset of droughts, when rainfall is below and radiation above average, large-scale positive anomalies in VOD were observed. This is most likely caused by enhanced canopy growth. When rainfall deficit is persisting resulting in water and heat stress that exceeds a certain threshold, widespread negative VOD anomalies are observed.

South Asia is one of the most drought-vulnerable regions worldwide, which is also related to the insufficient socio-economic capacity to manage its effects (Carrão *et al.*, 2016). In particular, in Indonesia drought-related expansions of peat fires release sequestered carbon impacting on other areas of the world (Field *et al.*, 2009). The resulting high concentration of aerosols in combination with the high cloud and vegetation density in this region challenges optical data retrieval (e.g. NDVI). VOD could represent a cost-efficient alternative to monitor droughts, facilitate pre-managing measures in this region and reduce the impact.

Based on this background, the aim of this study is to assess the potential of VOD as an agricultural drought indicator for pepper fields in Indonesia. This research will in particular address the following questions:

- How does the VOD of pepper fields compare to large-scale VOD?
- How does the VOD compare with other drought indicators? Does it have an added value over NDVI?
- How does the VOD capture agricultural drought events?
- How can the VOD be transformed to an agricultural drought indicator?

The pepper fields are compared to their surroundings by looking into spatial images and also into temporal anomalies. For the temporal analysis, anomalies of the fields are compared to the anomalies of their

surroundings. The analysis corresponding to the second research question is also split into a spatial and a temporal part. Spatially, VOD and NDVI are compared to a Google satellite image to assess their general performance and also to understand the behaviour in the subsequent temporal analysis. Temporally, correlations between VOD anomalies and the anomalies of El Niño Southern Oscillation (ENSO), the Indian Ocean Dipole (IOD) and the Standardized Precipitation Evaporation Index (SPEI) are calculated. As a cross-comparison, correlations between NDVI and the other indicators are calculated. The third question on the performance on VOD of capturing agricultural drought events is answered qualitatively by combining the information obtained in the field visit, with literature and yearly pepper yields of Indonesia. Finally, a guideline is proposed to convert VOD into an agricultural drought indicator or even predictor, based on the limitations discovered in this study and existing work on drought indices.

In the next chapter, the required theoretical background for this thesis is given. First, the different definitions of droughts are presented to understand the differences between various existing drought indicators, which are presented subsequently. The description of the indicators with their benefits and shortcomings forms the base for the selection of indicators to be compared to VOD within this research. Furthermore, this chapter describes the theory behind the retrieval of VOD, which is important to understand the results. In chapter 3, the case study of pepper fields in Indonesia is introduced. First, some general information on the climate and economy is given. This includes a literature research on droughts occurred in the past years in Indonesia that is relevant to discuss the results. Second, the information on agricultural practices obtained on the fieldwork is presented. In chapter 4, the methodology is explained. First, the study area and the datasets are introduced and then the different analysis procedures, that are required to answer the research questions, are explained. Subsequently, the results are described and discussed in chapter 5. Finally, in chapter 6, the conclusions of this research are summarized by answering the four research questions. Furthermore, recommendations for future research are given.

## 2 THEORETICAL BACKGROUND

This chapter provides relevant theory for this study. First, the multiple definitions of droughts are explained, which is necessary to understand the differences between drought indicators. Secondly, commonly used drought indicators are presented, from which four are chosen to be compared to VOD in this study. Third, the theory behind the Vegetation Optical Depth retrieval is explained, which helps to understand the results.

### 2.1 Definition of droughts

To analyse droughts, it is important to be aware that there is not a common agreement on the definition of droughts. Depending on the perspective out of which a drought is analysed, its definition and so its indicator varies across the literature. This obstructs the comparability among different studies. In particular, when assessing the impacts, it is important to be aware of the varying underlying concepts of drought indicators to prevent false conclusions (Van Lanen *et al.*, 2013). The common denominator of these diverse definitions is that droughts originate from a deviation from normal conditions (Wanders *et al.*, 2010). Mishra *et al.* (2010) analysed different drought definitions and found that these mainly differ from the variable used to describe the drought and, therefore, classified into the following four categories.

- **Meteorological drought:** refers to a period of time with below-normal precipitation over a region. This is either identified as a deficit compared to average values or through a comparison of the drought duration and intensity with the cumulative precipitation shortages. (Mishra *et al.*, 2010; Dai, 2011)
- **Hydrological drought:** is defined as a period of time with below long-term mean levels in surface and subsurface waters resources (Mishra *et al.*, 2010; Dai, 2011).
- **Agricultural drought:** describes a period of time where soil moisture decline affects crop yield, crop growth and agricultural production. This decline in soil moisture can be caused by a below-average reduction in precipitation, intense but less frequent rainfall events, changes in temperature or above-normal evaporation. The plant water demand does not only vary with weather conditions but also with the biological features and the growth stage of the plant (Mishra *et al.*, 2010). Although soil moisture is the key variable to analyse agricultural droughts, it is not considered by most drought indices. (Dai, 2011; Sruthi *et al.*, 2015; Martínez-Fernández *et al.*, 2016)
- **Socio-economic drought:** refers to the failure of water resource systems in meeting the water demand, requiring water as an economic good (AMS, 2004 cited in Mishra & Singh, 2010).

Hydrological droughts, as well as agricultural droughts, are often triggered by a lack of precipitation (Dai, 2011). Nevertheless, other elements such as more intense but less frequent precipitation, erosion and poor water management can not only intensify but also cause these type of droughts (Dai, 2011).

Some studies also classify into meteorological, hydrological and soil moisture (Hisdal *et al.*, 2001 cited in Wanders *et al.*, 2010). The focus on the present research is on agricultural droughts.

Droughts are mainly described in terms of various statistics that summarize the duration, the intensity and the spatial extent of the event (Wilhite, 2000). The diversity of droughts concerning these three aspects complicate the inter-comparison of droughts even more (Wanders *et al.*, 2010). Furthermore, it is important to differentiate correctly between hazard, exposure, vulnerability and risk. Hazard describes the probability that an event of a certain severity occurs. The number of elements (population, assets, services, etc.) that can be affected by an event is defined as the exposure. The susceptibility of elements to suffer the negative impacts of droughts is described as the vulnerability. The product of these three (with normalized statistics: 0 (min) - 1 (max)) is the likelihood of drought impact defined as drought risk. (Carrão *et al.*, 2016)

## 2.2 Commonly used drought indices

Several drought indices have been developed to define drought parameters (intensity, duration, spatial extent), detecting droughts and assessing the effect of drought (Mishra *et al.*, 2010). Each drought index has its benefits and restrictions, which also depend on the region where it is used. So far, research has shown that it is difficult to apply a single indicator at a global scale (Fleig *et al.*, 2006; Sheffield *et al.*, 2009; Van Lanen *et al.*, 2007 cited in Wanders *et al.*, 2010). In the following, the commonly used drought indices are presented with their corresponding benefits and shortcomings. The indices are ordered according to the variable they use (as by (Wanders *et al.*, 2010)).

### 2.2.1 Meteorological drought indices

These indices are based on observed precipitation. They are independent of physical properties on-site. However, they suffer from a high variety in temporal and spatial distribution of precipitation. The use of monthly values or moving averages can diminish this problem (Wanders *et al.*, 2010).

#### 2.2.1.1 Standardized Precipitation Index (SPI)

The Standardized Precipitation Index (SPI) has been recognized as the standard and best suitable indicator to report meteorological droughts, in particular, assessing drought intensity (Wanders *et al.*, 2010; Keyantash *et al.*, 2018). It is based on long-term precipitation records for a specific area and time period. This precipitation data can be retrieved either from ground stations or from satellites. The time series are fitted to a probability distribution and then transformed to a normal distribution in order to be able to apply the same SPI scale across areas and periods with different rainfall amounts. By doing so, the mean SPI is always zero and the SPI represents the number of standard deviations from the long-term mean (SADC Regional Remote Sensing Unit, 2000; Mishra *et al.*, 2010). It can be applied to a variety of time scales and therefore gives information about different parts of the hydrological system. On short timescales, it monitors water storage, which respond quickly to precipitation anomalies, such as soil moisture. On longer timescales, the SPI is rather related to water resources, which reflect long-term precipitation anomalies, such as groundwater, stream flow and reservoir storage. (Mishra *et al.*, 2010; Keyantash *et al.*, 2018)

The benefits and shortcomings of the SPI are listed below.

Benefits	Shortcomings
<ul style="list-style-type: none"> <li>▪ Applicable for different time scales, corresponding to different water resources</li> <li>▪ Applicable for dry and wet periods</li> <li>▪ Easier computation and better comparison across regions with different climates compared to PDSI (see 2.2.2)</li> <li>▪ Applicable to calculate current precipitation deficit but also the current percentage of the average precipitation of a certain time period</li> </ul>	<ul style="list-style-type: none"> <li>▪ Evaporation not considered → limited estimation of soil moisture and demand</li> <li>▪ Sensitive to reliability and quantity of data used to fit the distribution (30-50 years of data record recommended)</li> <li>▪ Sensitive to the probability distribution used (gamma, Pearson Type III, extreme value, exponential, etc.)</li> <li>▪ Potentially biased fitting distribution, if SPI is calculated for long time scales (&gt;24 months) due to data length limitations</li> <li>▪ The potential impacts of precipitation intensity on runoff, stream flow, and water availability are not considered</li> </ul>

Source: (Tsakiris *et al.*, 2007; Mishra *et al.*, 2010; Keyantash *et al.*, 2018)

#### 2.2.1.2 Standardized Precipitation Evaporation Index (SPEI)

Due to the limitation of the SPI being unable to consider change in evaporation the Standardized Precipitation Evaporation Index (SPEI) was developed. This index works like the SPI but considers evaporation, which is one of the major drawbacks of the SPI. The calculation of the evaporation depends on the dataset that is used. Although this index identifies meteorological droughts, important stakeholders, such as the insurance company SWISSRE use this index in the agricultural context. Thus, it is relevant to this case.

### 2.2.1.3 Multivariate ENSO Index (MEI)

There are phenomena that influence the global weather patterns. The El Niño Southern Oscillation (ENSO) is one of these phenomena. It describes the shift of the winds and ocean currents at the western coast of South America that occurs every two to seven years. Normally, the water in the West Pacific is warm and pushed by trade winds to the west whereas the water in the east is cold due to a shallow thermocline caused by the cold tongue of water at the sea surface. During el Niño years, the trade winds weaken and warmer water moves eastward. Over the Central Pacific air rises weakening the trade winds over the West Pacific. During La Niña years, the trade winds strengthen and more upwelling occurs in the Pacific Ocean. The atmospheric circulation strengthens the trade winds (Pietrzak *et al.*, 2017). While the return period is predictable varying from two to seven years, the intensity is difficult to predict as it varies strongly. The duration is 14 to 22 months. El Niño often starts in the beginning of the year and maximises between November and January.

The Southern Oscillation, which describes the variations in atmospheric pressure between the eastern equatorial Pacific and Indo-Australian areas, is closely related to El Niño. This phenomenon has been converted to indices like the air-pressure-based Southern Oscillation Index (SOI), the sea-surface-temperature-based Oceanic Niño Index (ONI) or the Multivariate ENSO Index (MEI) to quantify this phenomenon. The MEI is based on the six main observed variables over the Tropical Pacific: sea surface temperature, surface air temperature, sea-level pressure, zonal and meridional components of the surface wind and total cloudiness fraction of the sky (NOAA, 2018). These indices are not considered as drought indices. However, several studies have shown a relation between the ENSO and drought occurrence, especially in Indonesia, Australia, India, the Philippines, Brazil and East and South Africa as well as Central America and the US (Ropelewski *et al.*, 1987; University Corporation for Atmospheric Research pursuant to NOAA, 1994; Chiew *et al.*, 1998; Hendon, 2003; Schoennagel *et al.*, 2005; National Drought Mitigation Centre - University of Nebraska, 2018). See below for a list of benefits and limitations of this index.

#### Benefits

- Strong link between droughts and the ENSO in certain regions
- Predictive value concerning timing

#### Shortcomings

- Not a drought indicator as such
- Different indicators for the ENSO itself
- Only applicable to regions affected by the ENSO
- Droughts cannot be entirely explained by the ENSO

Source: (Chiew *et al.*, 1998)

### 2.2.1.4 Dipole Mode Index (DMI)

The Indian Ocean Dipole (IOD) is a coupled ocean-atmosphere phenomenon that influences the climate variability in the tropical Indian Ocean and the surrounding countries like Indonesia (Saji *et al.*, 1999; Webster *et al.*, 1997-98 cited in Lestari *et al.*, 2018). When the IOD is positive, low SST anomalies occur in the west of Sumatra and high SST anomalies occur in the western and central tropical Indian Ocean. This leads to south-easterly wind anomalies along the coast of Sumatra and Java resulting in a deficit precipitation over Indonesia and Australia and an excess precipitation in East Africa, India and Southeast Asia (Lestari *et al.*, 2018). This phenomenon is often quantified with the Dipole Mode Index (DMI), which is a measure of the anomalous SST gradient between the western (50E-70E and 10S-10N) and the south-eastern equatorial Indian Ocean (90E-110E and 10S-0N). (NOAA, 2017)

#### Benefits

- Strong link between droughts and the IOD in certain regions
- Predictive value concerning timing

#### Shortcomings

- Not a drought indicator as such
- Different indicators for the IOD itself
- Only applicable to regions affected by the IOD
- Droughts cannot be entirely explained by the IOD

Source: (Lestari *et al.*, 2018)

### 2.2.1.5 Other meteorological indices

Below other meteorological drought indices are listed. However, these are not used for further analysis.

Table 1: Other meteorological drought indices

Meteorological Indicator	Description	Benefits	Shortcomings
Rainfall Deciles	<ul style="list-style-type: none"> <li>Compares monthly accumulates to long-term mean</li> <li>Observed data is ranked and classified with deciles</li> </ul>	<ul style="list-style-type: none"> <li>Easy to calculate</li> <li>Less data required compared to other indices</li> </ul>	<ul style="list-style-type: none"> <li>Long-term records required</li> <li>Less suited for dry climates or climates with a strong seasonality</li> </ul>
Effective Drought Index (EDI)	<ul style="list-style-type: none"> <li>Calculates water accumulation with a weighting function of time passage on a daily time-scale</li> </ul>	<ul style="list-style-type: none"> <li>Standardised index → comparable across different climatic regions</li> </ul>	<ul style="list-style-type: none"> <li>Data series of &gt;30 years required to transform the EDI values into a reliable normal distribution</li> </ul>
Number of consecutive dry days	<ul style="list-style-type: none"> <li>Gives the number of maximum consecutive dry days per year</li> <li>Indicates relative dryness of a certain year by changes in <math>P</math></li> </ul>	<ul style="list-style-type: none"> <li>Easy to calculate</li> </ul>	<ul style="list-style-type: none"> <li>Long-term records required</li> </ul>
Rainfall Anomaly Index (RAI)	<ul style="list-style-type: none"> <li>Uses average <math>P</math> of a week/month/year to calculate relative drought</li> </ul>	<ul style="list-style-type: none"> <li>Different time scales</li> <li>Similar to PDSI results (see 2.2.2)</li> </ul>	<ul style="list-style-type: none"> <li>Choice of time scale based on <math>P</math> distribution</li> </ul>

$P$  = Precipitation; Source: (Hayes *et al.*, 1999; Mekis *et al.*, 2004; Kim *et al.*, 2009; Wanders *et al.*, 2010; Mishra *et al.*, 2011)

### 2.2.2 Hydrological drought indices

Hydrological drought indicators use observed or simulated stream flow, groundwater storage or ground water levels to characterize droughts. Some of the existing hydrological drought indices are listed below.

Table 2: Hydrological drought indices

Hydrological Index	Description	Benefits	Shortcomings
Surface Water Supply Index (SWSI)	<ul style="list-style-type: none"> <li>Calculates probability of exceedance based on historical data (<math>Q</math>, reservoir storage, snowpack and <math>P</math>)</li> <li>Same index value as the PDSI</li> <li>Monthly time-scale</li> </ul>	<ul style="list-style-type: none"> <li>Unique for every catchment</li> <li>Able to cope with snow and resulting delayed runoff and large topographic variations</li> </ul>	<ul style="list-style-type: none"> <li>Unique for every catchment → difficult inter-basin/global comparison</li> </ul>
Groundwater resource Index (GRI)	<ul style="list-style-type: none"> <li>Uses <math>P</math>, air temperature and air pressure data to simulate groundwater storage</li> </ul>	<ul style="list-style-type: none"> <li>Appears to be a better indicator than the SPI in the Mediterranean area</li> </ul>	<ul style="list-style-type: none"> <li>Only tested on a single study (Mendicino <i>et al.</i>, 2008)</li> </ul>
Total Storage Deficit Index (TSDI)	<ul style="list-style-type: none"> <li>Uses <math>P</math>, <math>E</math> and <math>Q</math> from the basin outlet</li> <li>Combines the PDSI and water storage anomalies from Gravity Recover And Climate Experiment satellite observations</li> </ul>	<ul style="list-style-type: none"> <li>Capable of representing long-term dryness and wetness</li> </ul>	<ul style="list-style-type: none"> <li>Only two case studies so far (Yirdaw <i>et al.</i>, 2008; Agboma <i>et al.</i>, 2009)</li> <li>Not applied yet to a global scale</li> </ul>

$P$  = Precipitation;  $E$  = Evaporation;  $Q$  = Stream flow

Source: (Wanders *et al.*, 2010)

### 2.2.3 Soil moisture indices

Soil moisture drought indices indicate drought situations based on observed or simulated soil moisture, meaning the amount of water stored in the unsaturated zone. Especially for describing agricultural droughts, the soil moisture can be a better description of the dryness, considering that precipitation changes can be

different from the soil moisture changes (Dai, 2011). Therefore, these indicators are often used to describe agricultural droughts. When only using soil moisture for the drought analysis, the prediction becomes problematic in arid regions (Sheffield *et al.*, 2009). Some of the soil moisture drought indicators also use meteorological data such as precipitation. (Wanders *et al.*, 2010)

Table 3: Soil moisture indices

Soil Moisture Index	Description	Benefits	Shortcomings
Palmer Drought Severity Index (PDSI)	<ul style="list-style-type: none"> <li>Estimates soil moisture supply and demand with a two-layer soil model (fed with <math>P</math> and <math>T</math> data)</li> <li>One of the most prominent drought indices in the USA</li> </ul>	<ul style="list-style-type: none"> <li>Accounts for <math>E</math></li> <li>Long existing index → well tested and verified</li> <li>Accounts for <math>T</math> and soil characteristics</li> <li>Standardised → comparable across climatic regions and time scales</li> </ul>	<ul style="list-style-type: none"> <li>Drought start and end not clearly defined → slow response to developing/diminishing droughts</li> <li>Simplified two-layer model</li> <li>Assumes runoff occurrence during saturation of both layers only → runoff underestimation</li> <li>Assumes uniform land use and soil properties across regions</li> <li>Snow and hail are seen as rain</li> </ul>
Palmer Z-Index	<ul style="list-style-type: none"> <li>Derived from PDSI calculation</li> <li>Describes <math>SM</math> anomaly of the current month</li> </ul>	<ul style="list-style-type: none"> <li>Same as of the PDSI</li> <li>Time-independent → faster response to changes in <math>SM</math></li> </ul>	<ul style="list-style-type: none"> <li>Same as of the PDSI</li> </ul>
African Flood and Drought Monitor (of Princeton University)	<ul style="list-style-type: none"> <li>Drought index based on low <math>SM</math> percentiles</li> <li>Historic and real-time data modeled with the Variable Infiltration Capacity land surface hydrological model with observations and modeled/remotely sensed meteorology</li> </ul>	<ul style="list-style-type: none"> <li>Near-real-time</li> <li>0.25° and daily resolution</li> <li>At basin or continental scale</li> <li>Stable and robust system providing continuous data</li> <li>Open source</li> </ul>	<ul style="list-style-type: none"> <li>More comprehensive evaluations are needed on the drought products utility of the system</li> <li>Focused on Africa only</li> </ul>
Soil Moisture Deficit Index (SMDI)	<ul style="list-style-type: none"> <li>Based on <math>SM</math> and <math>E</math> values simulated in a SWAT model</li> <li>Used for agricultural droughts</li> <li>Weekly time-scale</li> </ul>	<ul style="list-style-type: none"> <li>Detects short-term dry conditions</li> <li>Independent of season and climate</li> <li>Highly correlated with SPI and PDSI</li> </ul>	<ul style="list-style-type: none"> <li>Has neither been tested in other study areas than the US nor at global scale</li> <li>Based on estimated values from hydrological models/climatic variables → large uncertainty</li> </ul>
Crop Moisture Index (CMI)	<ul style="list-style-type: none"> <li>Evaluates short-term variations in <math>SM</math></li> <li>Calculates excess <math>P</math> (based on long-term mean) and <math>SM</math> infiltration based on excess <math>P</math> and observed <math>T</math></li> <li>Used for agricultural droughts</li> <li>Weekly time-scale</li> </ul>	<ul style="list-style-type: none"> <li>Suitable for predicting short-term droughts</li> <li>Suitable during warm seasons (growing season)</li> </ul>	<ul style="list-style-type: none"> <li>Increases with potential <math>E</math> → with higher potential <math>E</math> the <math>SM</math> increases which does not occur in nature</li> <li>CMI responds quickly to short-term conditions → misleading information about long-term conditions</li> <li>Not suitable for winter droughts</li> </ul>
Soil Moisture content	<ul style="list-style-type: none"> <li>Detects a drought when <math>SM</math> content is below a certain threshold</li> </ul>	<ul style="list-style-type: none"> <li>Has been used on a global scale</li> </ul>	<ul style="list-style-type: none"> <li>Varying indicator performance per catchment → difficult comparison</li> </ul>

$P$  = Precipitation;  $T$  = Temperature;  $SM$  = Soil Moisture;  $E$  = Evaporation;

Source: (Palmer, 1965; Mishra *et al.*, 2010; Wanders *et al.*, 2010; Princeton University, 2013; Carrão *et al.*, 2015)

### 2.2.4 Combined drought index

This category refers to an indicator that uses precipitation, soil moisture as well as storage or discharge data. Thus, it is potentially capable of describing the drought throughout the entire hydrological cycle.

Table 4: Combined drought index

Combined Index	Description	Benefits	Shortcomings
Aggregate Drought Index (ADI)	<ul style="list-style-type: none"> <li>Uses <math>P</math>, <math>E</math>, <math>Q</math>, reservoir storage, soil moisture content and snow water content</li> <li>Monthly time-scale</li> </ul>	<ul style="list-style-type: none"> <li>Assesses various drought types</li> <li>Direct mathematical formulation → easy to apply to new observational data</li> </ul>	<ul style="list-style-type: none"> <li>Requires observations of at least five variables</li> <li>Only tested in three Climates in California (Keyantash et al., 2004)</li> </ul>

$P$  = Precipitation;  $E$  = Evaporation;  $Q$  = Stream flow;

Source: (Keyantash et al., 2004; Wanders et al., 2010)

### 2.2.5 Vegetation indicators

In order to monitor agricultural droughts, the actual response of vegetation to hydrological circumstances is relevant. Low precipitation anomalies and even low soil moisture anomalies do not directly mean that yields are reduced. Additionally, the hydrological simulations with current models used in several of the previously mentioned indicators imply large uncertainties (Dai, 2011). Therefore, vegetation indices can monitor agricultural droughts although they are not defined as drought indices as such. They aim at measuring the condition of the vegetation. Hence, many studies have found the vegetation index to be one of the important parameters to map drought conditions and crop yield amongst others (Tucker et al. (1982); Justice et al. (1985); Hielkema et al. (1986); Kogan (1987a, b), (1995); Dabrowska-Zielinska et al. (2002), Narasimhan et al. (2005), Chakraborty et al. (2010) cited in Sruthi et al., 2015). Moreover, vegetation indices are always based on remote sensing data. It is a cost-efficient and valuable source of spatially and timely continuous data about the earth’s surface that allows monitoring vegetation dynamics over large areas (Mishra et al., 2010; Xue et al., 2017). Important to understand in this context is that these indices are based on different parts of the spectrum. Figure 1 gives an overview of the different frequencies and spectra.

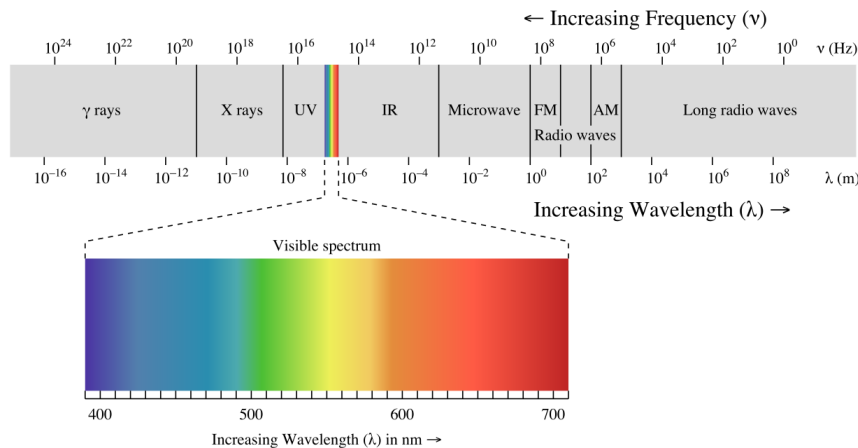


Figure 1: Frequencies, wavelength and spectra (Imgur Stack Exchange, no date)

Nevertheless, existing vegetation indices also suffer from shortcomings. The revisit time of the satellites, which is 16 days on average provides a relatively coarse temporal resolution for agricultural applications such as water management (Xue et al., 2017). Remote sensing data that is based on optical data is limited by atmospheric influences as for instance clouds (Xue et al., 2017). To overcome this obstacle, Sruthi et al. (2015) conducted a study to analyse water stress in Southern India by combining the Normalized Difference Vegetation Index (NDVI) with the highly negatively correlated Land Surface Temperature (LST). The authors found that with the combination of the two datasets agricultural drought could be identified and this method can serve to monitor agricultural droughts in order to develop an early warning system for farmers.

### 2.2.5.1 Normalized Difference Vegetation Index (NDVI)

Due to its simplicity and efficiency, the Normalized Difference Vegetation Index (NDVI) is currently the most commonly used vegetation index (Sruthi et al., 2015). It monitors vegetation cover changes through the following ratio of red ( $\lambda_{RED}$ ) and near-infrared reflectance ( $\lambda_{NIR}$ ) (Andela et al., 2013).

$$NDVI = \frac{\lambda_{NIR} - \lambda_{RED}}{\lambda_{NIR} + \lambda_{RED}}$$

The values range between 0 and 1 (Xue et al., 2017), indicating the amount of photosynthetically active vegetation and, therefore, the chlorophyll in the canopy, as leaves absorb red and reflect near-infrared radiation (Andela et al., 2013). Furthermore, it is correlated to the leaf area index (LAI) and the fraction of absorbed photosynthetically active radiation (PAR) (Andela et al., 2013). These parameters allow analysing trends in the occurrence of agricultural droughts (Sruthi et al., 2015). Due to the disadvantages of the NDVI (listed below) it is recommended to combine the NDVI with Land Surface Temperature (LST), which can deliver significant data about the climate and the physical properties of the surface (Sruthi et al., 2015). NDVI is often compared to Vegetation Optical Depth (VOD), which is the tested method in the present study.

Benefits	Shortcomings
<ul style="list-style-type: none"> <li>Open source data</li> <li>Simple</li> <li>High spatial resolution</li> </ul>	<ul style="list-style-type: none"> <li>Limited by atmospheric effects (clouds, cloud shadow, aerosols)</li> <li>Saturation on dense vegetation</li> <li>Only senses the top layer of the canopy</li> <li>Sensitive to effects of soil brightness and colour</li> </ul>

Source: (Yi Liu et al., 2012; Sruthi et al., 2015; Xue et al., 2017)

### 2.2.5.2 Other vegetation indices

Table 5: Other vegetation indices

Vegetation Index	Description	Benefits	Shortcomings
Difference Vegetation Index (DVI)	<ul style="list-style-type: none"> <li>DVI = NIR – Red</li> </ul>	<ul style="list-style-type: none"> <li>Senses vegetation amount</li> <li>Simple</li> </ul>	<ul style="list-style-type: none"> <li>Does not compensate atmospheric errors</li> </ul>
Ratio Vegetation Index (RVI) (Or Simple Ratio (SR))	<ul style="list-style-type: none"> <li>RVI = NIR/Red</li> <li>Widely used for green biomass monitoring</li> </ul>	<ul style="list-style-type: none"> <li>High correlation with LAI, Leaf Dry Biomass Matter and chlorophyll content</li> <li>Less affected by atmos. and topography than DVI</li> <li>Simple</li> </ul>	<ul style="list-style-type: none"> <li>At sparse vegetation cover (&lt;50%) atmospheric effects dominate causing errors</li> </ul>
Vegetation Condition Index (VCI)	<ul style="list-style-type: none"> <li>Compares current NDVI to previous years</li> <li>VCI of month i</li> </ul> $VCI_i = \frac{NDVI_i - NDVI_{min}}{NDVI_{max} - NDVI_{min}} * 100$	<ul style="list-style-type: none"> <li>More suitable for long-term drought monitoring</li> </ul>	<ul style="list-style-type: none"> <li>Depends on NDVI quality</li> <li>In regions without seasonality values are unpredictable and sharply fluctuating</li> </ul>
Vegetation Health Index (VHI)	<ul style="list-style-type: none"> <li>Considers VCI and thermal condition of vegetation</li> </ul>	<ul style="list-style-type: none"> <li>Evaluates thermal stress on vegetation</li> </ul>	<ul style="list-style-type: none"> <li>Lower drought accuracy than PDSI</li> </ul>
Normalized Difference Water Index (NDWI)	<ul style="list-style-type: none"> <li>NDWI = <math>\frac{\rho(0.86\mu m) - \rho(1.24\mu m)}{\rho(0.86\mu m) + \rho(1.24\mu m)}</math> where <math>\rho(\lambda)</math> is the reflectance at wavelength <math>\lambda</math> (different <math>\lambda</math> than in NDVI)</li> <li>Complements NDVI</li> </ul>	<ul style="list-style-type: none"> <li>Less sensitive to atmos. scattering than NDVI</li> <li>These two wavelengths penetrate equally deep</li> <li>Sense the liquid water content in the vegetation</li> </ul>	<ul style="list-style-type: none"> <li>Equivalent water thickness is not detectable over partly vegetated areas as soil background reflectance cannot be removed</li> </ul>

Source: (Kogan, 1990; Bannari et al., 1995; Gao, 1996; Liu et al., 2012; Choi et al., 2013; Jiao et al., 2016; Xue et al., 2017)

## 2.3 Vegetation Optical Depth (VOD)

The main focus of this study is on Vegetation Optical Depth (VOD). This section describes the theory behind the retrieval model applied in this research. VOD (denoted  $\tau$ ) is a measure of the opacity of a medium (canopy) to radiation passing through it and is closely related to the aboveground biomass water content (de Jeu *et al.*, 2004). This includes the water present in the leafy but also in the woody components of the vegetation (Shi *et al.*, 2008). VOD is derived from Passive Microwave Remote Sensing (PMRS) (Yi Liu *et al.*, 2012). So far, microwave technology is the only remote sensing technique that measures a direct response to the absolute water quantity in the surface soil and the above ground vegetation. Radiometers on board of satellites measure the brightness temperature, which depends on several factors such as the surface temperature of the soil and vegetation, the soil-moisture-dependant dielectric constant of the soil, the VOD-dependant transmissivity of the vegetation and the vegetation-induced scattering of the albedo. A method presented by (Owe *et al.*, 2001) allows solving the soil moisture and Vegetation Optical Depth simultaneously. This method is known as the Land Parameter Retrieval Model (LPRM) and is further explained in 2.3.2. (de Jeu, 2003)

### 2.3.1 History

Satellite remote sensing is already being applied for water-related purposes for several decades. The first studies focused on the visible and infrared spectrum, which, for example, revealed valuable information on for example, land use or surface temperature. However, this radiometry is constrained by clouds and aerosols. In contrast, the microwave radiometry is not affected by these atmospheric contaminants. For this reason, the first microwave satellites (EMSR and SMMR) were launched in the 1970s. In order to better understand the physics of microwave radiation in the soil, Wilheit (1975) developed one of the first radiative transfers models. This and further radiative transfer models served to develop soil moisture models, such as the one of Njoku *et al.* (1977), which considers rapidly changing moisture profiles and non-uniform temperature profiles. Choudhury *et al.* (1979) presented a soil moisture model, which also took the effect of surface roughness on brightness temperature into consideration. Moreover, Wang *et al.* (1980) developed a model that improves the description of the dielectric behaviour of different soil-water mixtures. (de Jeu, 2003)

In 2001, Owe *et al.* (2001) presented the Land Parameter Retrieval Model (LPRM), that serves to retrieve VOD and soil moisture simultaneously from low-frequency passive microwave observations (<20 GHz) (Yi Liu *et al.*, 2012; Andela *et al.*, 2013). In 2005, the LPRM was further improved in efficiency by Meesters *et al.* (2005) and tested with different passive microwave sensors (Owe *et al.*, 2008; Andela *et al.*, 2013). Six years later, Liu *et al.* (2011) produced the first long-term (1987-2008) passive microwave satellite-based vegetation product by merging the data of three satellite-based passive microwave instruments and using the LPRM algorithm. Specifically, the SSM/I (Special Sensor Microwave Imager, 1988-2007), TMI (on board of the Tropical Rainfall Measuring Mission satellite, 1998-2008) and AMSR-E (Advanced Microwave Scanning Radiometer – Earth Observing System, 2002-2008) were applied to produce this long-term record. Although the accuracy of VOD retrievals from AMSR-E was expected to have a better accuracy than the other two due to its longer wavelength, Yi Liu *et al.* (2012) showed that the errors related to sensor changes in this harmonized product are small (Andela *et al.*, 2013).

### 2.3.2 Derivation

PMRS consists in the measurement of the thermal radiation emitted naturally by the earth's surface in the centimetre wave band ( $\lambda = 0.1$  to 100 cm). The physical temperature and the emissivity of the radiating body are the main variables influencing this radiation. Compared to the longwave infrared region ( $\lambda = 1$  to 100  $\mu\text{m}$ ), the emitted radiation is extremely low (~a factor 1000 lower). Radiometers are able to measure the intensity of the earth's surface thermal emission (microwave brightness temperature  $T_b$ ) up to the thermal sampling

depth, which is thought to be several tenths of the wavelength deep (Schmugge, 1983; de Jeu *et al.*, 2004). This is approximately 0 to 5 cm at L-band frequency ( $\lambda = 21$  cm), depending on the moisture content.

### 2.3.2.1 The dielectric constant

The dielectric constant is a key element in PMRS. This electric property of matter is a measure of the polarity of a medium. It is dependent on temperature, pressure and frequency (Owen *et al.*, 1961). Additionally, this constant is a dimensionless number that consists of a real and a complex component as shown below.

$$\epsilon = \epsilon' + \epsilon''i$$

The first term ( $\epsilon'$ ) determines the propagation characteristics of the energy as it moves upward through the soil and the latter ( $\epsilon''i$ ) term the energy losses. In the following, the dielectric constant is simplified using only the real component. (de Jeu, 2003)

$$k = |\epsilon|$$

Dry soil has a dielectric constant of  $k \approx 4$ , whereas water has a dielectric constant of  $k \approx 80$  for low frequencies (<10 GHz). The development of the dipole structure of water molecules in response to an applied electric magnetic field explains the larger value of water (Schmugge, 1983). This results in values ranging from 4 to 44 for soil-water mixtures. The exact values of these non-homogeneous mediums are mainly dependant on the moisture content, temperature, salinity textural composition and frequency. Soil moisture and dielectric constant of the soil are almost linearly related, except for low moisture conditions. When a small amount of water is present in the soil, the bonds between the soil particle surfaces become much stronger. The described relationship between the dielectric constant and the soil moisture also varies per soil type: smaller particles such as clays or fine sands have a higher surface area-to-volume ratio and are, thus, able to hold more water molecules at higher potentials. Furthermore, the dielectric constant, is directly related to the surface emissivity (see Figure 2) (de Jeu *et al.*, 2004). The large contrast resulting from the presence of different amounts of water influence the emissivity of the soil and makes it possible to quantify soil moisture at the surface. The following schematization describes the relation between the brightness temperature measured by radiometers on board of satellites and the dielectric constant, which is dependent on the water content (see Figure 2). (de Jeu, 2003)

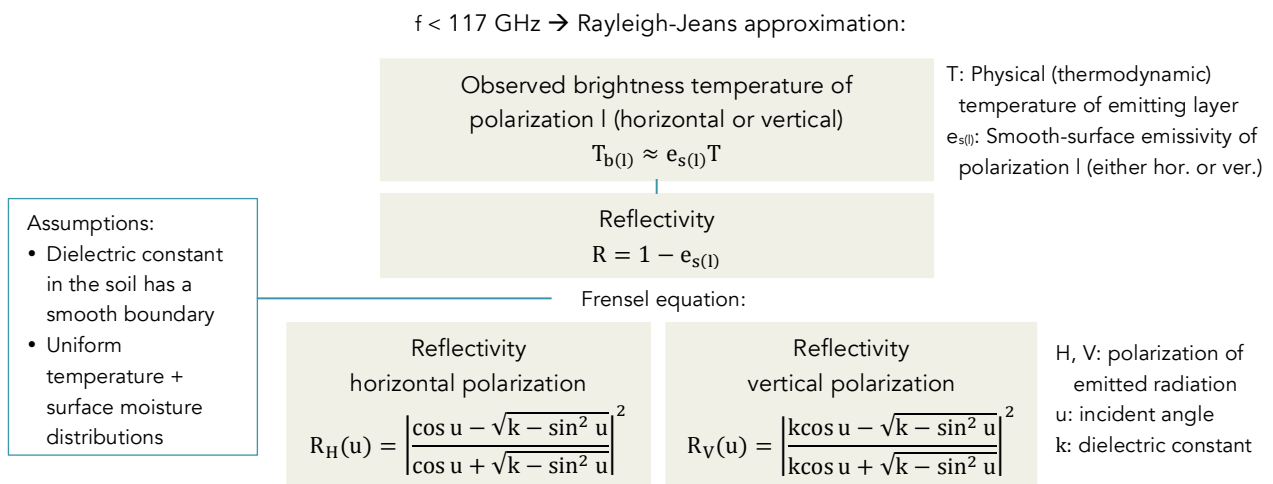


Figure 2: Relationship between Brightness temperature and emissivity for low frequencies

The absolute soil emissivity is higher at vertical polarization but the sensitivity to changes in surface moisture is significantly lower compared to the horizontal polarization (de Jeu, 2003).

### 2.3.2.2 Surface roughness

Surface roughness influences the emission in several ways. With a higher surface roughness, the surface area increases leading to scattering. This results in an increase of the apparent emissivity. Furthermore, the sensitivity to soil moisture changes and, therefore, the measurable emissivity from dry to wet conditions are reduced. For frequencies larger than 10 GHz, which are usually affected by atmospheric attenuation, the elevation and the slope of the surface resulting from surface roughness influence the path between the soil surface and the sensor. Different roughness models were developed to approach the impact of surface roughness on the emissivity. For the presented approach, the model of Wang *et al.* (1981) is used to describe the dimensionless rough surface emissivity calculated as a function of soil moisture, soil texture and indirectly of the effective temperature as well as corrected for soil roughness and polarization mixing influences. (de Jeu, 2003)

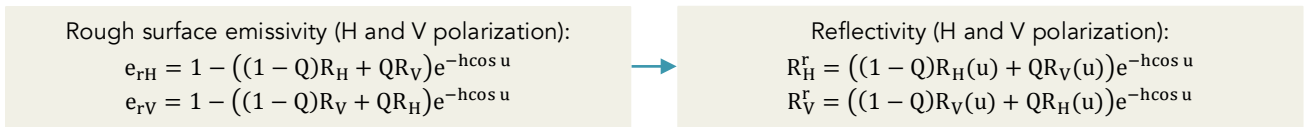


Figure 3: Rough surface emissivity and resulting reflectivity

Where  $H$  and  $V$  are the two polarizations,  $Q$  the polarization mixing factor,  $R_H$  and  $R_V$  the Fresnel reflectivities and  $h$  a dimensionless roughness characterizing height. (Schalie *et al.*, 2015).

### 2.3.2.3 Atmosphere

Atmospheric gases, such as, oxygen, water vapour, etc., can absorb the radiation emitted by the earth's surface and reduce the amount that arrives at the sensor. Nevertheless, the impact for frequencies lower than 15 GHz is relatively small and negligible for frequencies lower than 10 GHz. More significant are the effects of water droplets present in the atmosphere. The impact varies with the phase state of the water and the particle size relative to the wavelength. Furthermore, sky background radiation reflecting towards the sensor as well as a direct radiation from the atmosphere, both attenuated by the atmospheric transmissivity, should be taken into consideration. (de Jeu, 2003)

### 2.3.2.4 Vegetation

It is important to mention that the measured brightness temperature is not only composed by the emission of the bare soil, but also by the emissivity of the vegetation itself as well as the one reflecting from the vegetation to the soil and consequently to the atmosphere. In areas with a highly dense canopy, the soil radiation will be replaced by canopy radiation. Furthermore, the wavelength and the vegetation water content define the magnitude of the absorption by the canopy. In soil moisture sensing, the most commonly used wavelengths are in the L-band ( $\lambda \approx 21$  cm) and the C-band ( $\lambda \approx 5$  cm), where the former can penetrate deeper into vegetation of any significant density. Also for the influence of the vegetation on the brightness temperature, different models were developed.

For this research, the model of (Mo *et al.*, 1982) is used as it is considered to be simple but physically based and capable of estimating the soil's radiation effectively even under vegetation. This model describes the upwelling radiation from land surface (brightness temperature) with the following simple radiative transfer equation (see Figure 4). The first term describes the radiation emitted by the soil and attenuated by the surrounding vegetation. The second term defines the upward radiation emitted directly by the vegetation. The last term accounts for downward radiation emitted by the vegetation that is reflected upward by the soil and attenuated by the surrounding vegetation. The attenuation through vegetation is described by the dimensionless transmissivity  $T_{(l)}$  of the vegetation, which is a function of the Vegetation Optical Depth  $\tau_{(l)}$  including a correction for the observation angle  $u$  as shown below. (de Jeu, 2003)

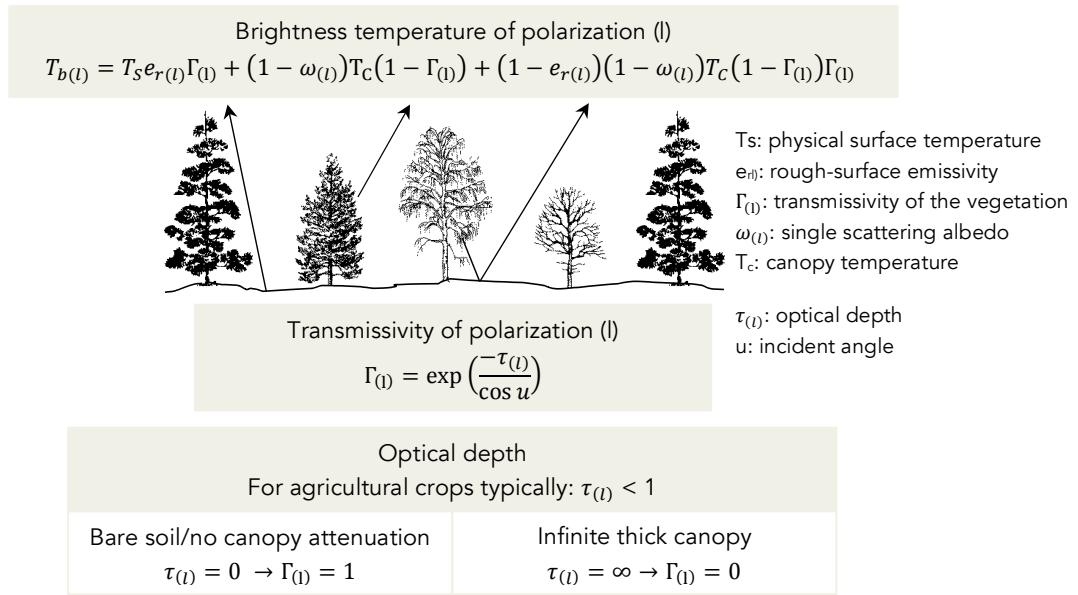


Figure 4: Brightness temperature according to (Mo et al., 1982) including vegetation effects (image: de Jeu, 2003)

The optical depth increases with higher vegetation densities and higher frequencies. For frequencies below 10 GHz,  $\tau_{(I)}$  a linear relation to vegetation water content was found. At higher frequencies, the relationship is still to a large degree unknown. With increasing VOD, soil emissions are attenuated more by the canopy and the signal is saturated by the emission from the vegetation. As a result, the sensor sensitivity to soil moisture variations decreases with increasing canopy thickness or VOD (Ulaby et al., 1986 cited de Jeu, 2003). At C-band, the horizontal signal saturates significantly at an optical depth of 0.75 achieving a total saturation at  $\tau_{(I)}=1.5$ . This can occur at even lower VOD values under dry conditions. (de Jeu, 2003)

The dimensionless single scattering albedo  $\omega_{(I)}$  expresses the scattering of the emitted microwaves through vegetation. As it theoretically depends on the plant geometry, it varies per plant species. However, in reality, it is often considered to be stable over time (van der Schalie et al., 2017). According to de Jeu (2003), a limited amount of experimental studies have determined values varying between 0.04 to 0.12 for selected crops and around 0.05 for natural vegetation. Although the influence of polarization on  $\tau_{(I)}$  and  $\omega_{(I)}$  is still to be studied in further detail, it seems that for random canopies the optical depth is independent of polarization and that for vegetation with some systematic orientation such as vertical stalks differences can be observed between  $\tau_H$  and  $\tau_V$ , that increase with the incident angle. (de Jeu, 2003)

### 2.3.2.5 Temperature retrieval

$T_s$  and  $T_c$  are the thermodynamic temperatures of the soil and the canopy. In analogy to de Jeu (2003), for the present method, the surface temperature  $T_s$  is assumed to be equal to the temperature at a depth of 28% of the wavelength. Previous studies have shown that, at a frequency of 37 GHz, the brightness temperature is mainly dependant on soil surface temperature (Holmes et al., 2009). For this reason, the equation is solved in that frequency to obtain the soil temperature resulting in the following equation by Parinussa et al. (2016). However, other sources for this temperature could also be used.

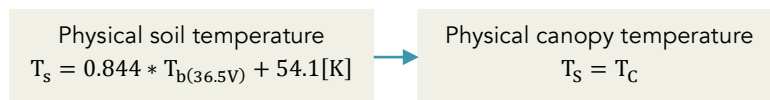


Figure 5: Physical soil and canopy temperature according to (Parinussa et al., 2016)

### 2.3.2.6 Land Parameter Retrieval Model (LPRM)

The previously explained theory comes together in the Land Parameter Retrieval Model (LPRM) (de Jeu, 2003; Owe et al., 2001, 2008). This model uses dual-polarized low frequency passive microwave observations

to retrieve VOD and the soil dielectric constant simultaneously based on the function for the Brightness temperature in vertical and horizontal polarization by (Mo et al., 1982), shown in Figure 4. It is applicable in wide range of low microwave frequencies like L-Band, C-Band, X-Band and Ku-Band (Parinussa et al., 2016). Figure 6 gives a schematic overview of this method, which is based on the previously explained formulas. The inputs to the model are the polarized brightness temperatures and the incident angle measured by the radiometers. The Polarization Mixing Factor  $Q$  is a constant value and  $\omega_H$  is a global value that was optimised by Van der Schalie (2017). The only remaining unknown is the dielectric constant that represents the soil moisture and the roughness parameter  $h$ , which is directly linked to the soil moisture and varies depending on the soil moisture that is used. The model is solved analytically with the dimensionless Microwave Polarization Difference Index (MPDI) by Meesters et al. (2005). Additionally, the model is run in an iterative manner with a wide range of scenarios for the dielectric constant of the soil (or soil moisture). The scenario resulting in the smallest absolute difference between the observed and calculated brightness temperature is taken as the "true" values. This index does not require any information on vegetation and can therefore be used as an independent vegetation index.

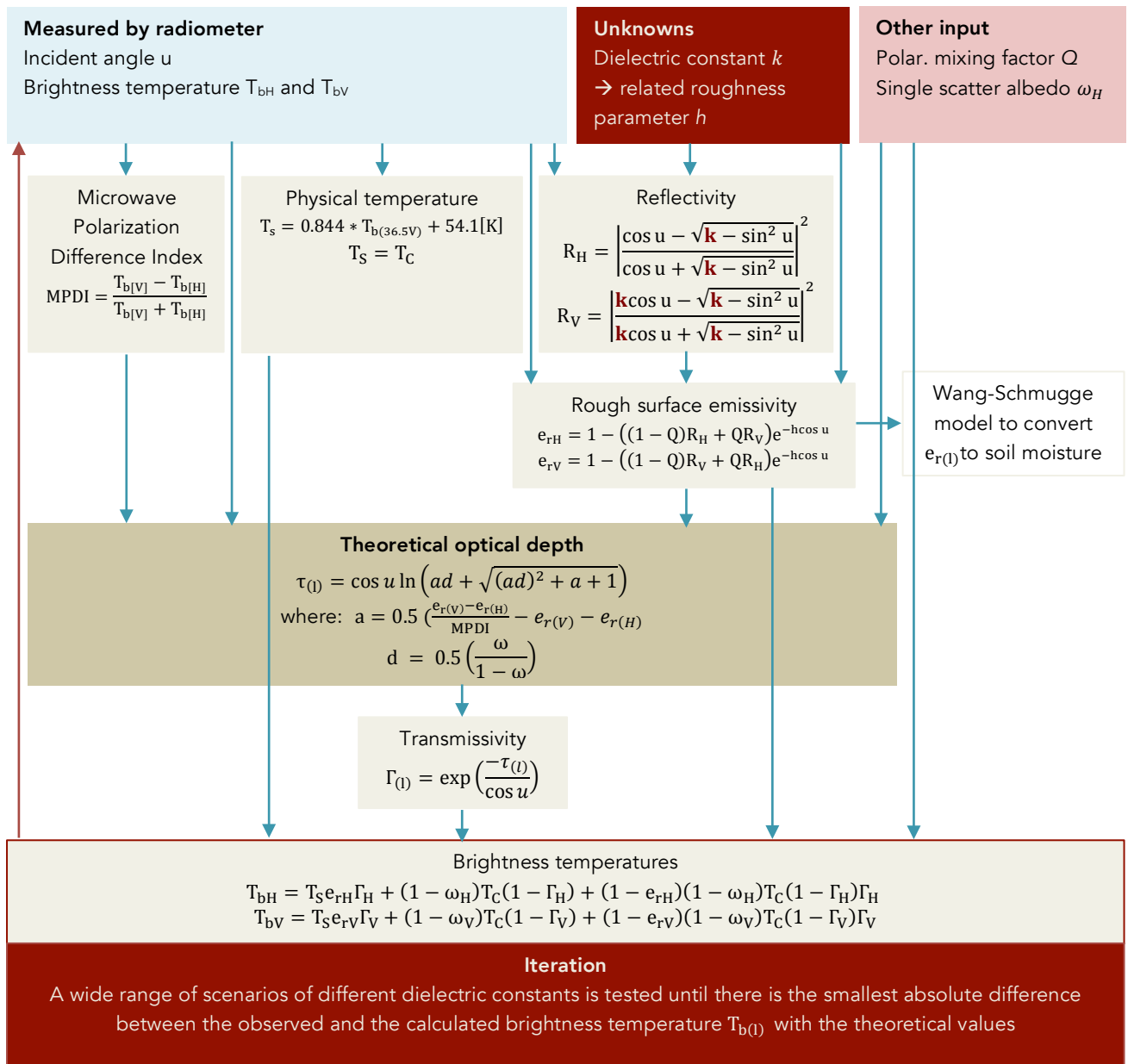


Figure 6: Schematization of simultaneous VOD and soil moisture retrieval (LPRM)

The MPDI describes a ratio function between the measured horizontal and vertical polarized brightness temperature (de Jeu *et al.*, 2004). When vegetation density and therefore VOD, is low the difference between the wet and the dry curve is large. This can be seen in the graph shown below (see Figure 7). In contrast, if a lot of vegetation is present, the difference between the wet and the dry curve becomes smaller. This means that the VOD saturates at some point. Nevertheless, it saturates at a higher biomass level than the NDVI, because it penetrates deeper into the canopy due to the longer microwave lengths (Liu, 2013). It also becomes visible that the relationship between the optical depth and the MPDI is strongly dependant on surface moisture (see dielectric constant  $k$ ).

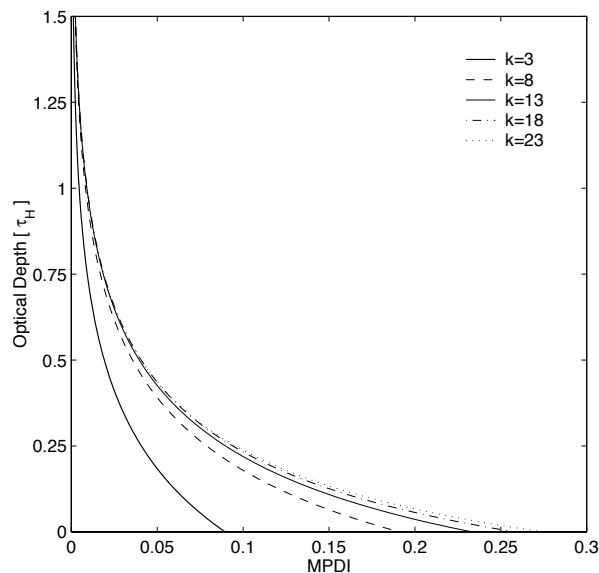


Figure 7: Relation between VOD and MPDI (de Jeu, 2003)

The MPDI is used to eliminate the dependency of the temperature. As the influence of vegetation and soil temperature on the MPDI is negligible, the changes in the index can be attributed to variations either in soil moisture conditions or in vegetation (de Jeu *et al.*, 2004).

From the rough surface emissivity, the soil moisture can be calculated with the Wang-Schmugge Model (Wang *et al.*, 1980). However, this is not discussed further in detail here.

The relation between the optical depth and the water content can be described as follows:

$$\tau = \tau_o + \tau_u = c_\tau (\Theta_o m_o + \Theta_u m_u)$$

where the subscripts  $o$  and  $u$  stand for overstory and understory,  $\theta$  is vegetation water content,  $m$  the aboveground biomass, and  $c_\tau$  the constant of proportionality. (Andela *et al.*, 2013)

### 2.3.3 Bands, resolution and downscaling

The VOD and other products at VanderSat are available at four different frequencies. Each frequency has a different foot print size as shown in Table 6.

Table 6: Bands, frequencies and foot print sizes (VanderSat B.V., 2016)

Name	Band [GHz]	Polarization	Spatial Resolution (3-dB footprint size) [km x km]
C-Band	6.93	V, H	62 x 35
X-Band	10.8	V, H	42 x 24
Ku-Band	18.7	V, H	22 x 14
Ka-Band	36.5	V, H	12 x 7

Additionally, VOD is currently available at a daily step. With the proprietary downscaling method of VanderSat, the VOD can be obtained at a resolution of 100 x 100 m (VanderSat B.V., 2016). This method is briefly described here.

The satellite measures the brightness temperature per footprint. The footprint has an oval shape in which the highest signal density is in the centre of this footprint decreasing towards the edges. The distribution of the contribution of the signal is assumed to be a Gaussian distribution. Figure 8 illustrates the relation between the Gaussian distribution, the signal intensity and the curve width. For example, when the intensity is at half of the maximum, the curve width is  $2.355\sigma$  and the values above the -3dB limit contribute approximately with 75% to the brightness temperature value of the total footprint. At an intensity reduction of -30dB, approximately 100% of the contribution is reached. Table 6 contains the height and the length of the ellipse of this 75% limit. With this concept, the footprint can be divided into several ellipses with the same centre contributing with different percentages to the footprint brightness temperature, as shown in Figure 9.

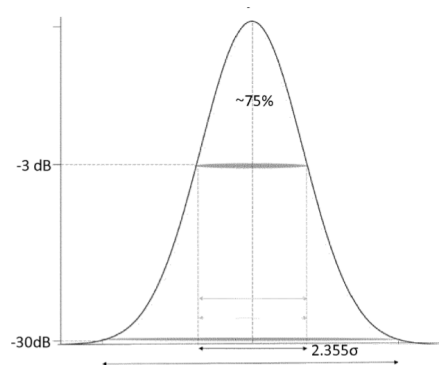


Figure 8: Intensity and Gauss distribution (VanderSat, 2016)

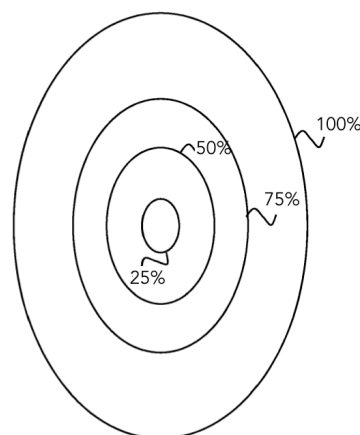


Figure 9: Ellipses (VanderSat, 2016)

Next, a high-resolution land water map is built by using ESA Sentinel satellite images and static land cover maps to mask out water surfaces. These maps are updated frequently. Then, the brightness temperature is corrected for the percentage of water pixels with an assumed brightness temperature of only water surface such that a *land brightness temperature* is obtained. In the final step, the brightness temperature of every 100 x 100 m pixel is calculated as a weighted sum of all overlaying ellipses of different footprints. The weight depends on the percentage associated with the ellipse. In the tropics, there are approximately 4 to 6 footprints contributing to a single value.

The downscaling in tropical areas suffers from two main drawbacks: the limited variety in brightness temperatures and the dynamics of open water bodies. Open water bodies are not well mapped, they change in shapes and the temperature of their surface is not well known and, therefore, has to be estimated. Apart from the mentioned issues, it is a reliable method except at the 37GHz frequency, where footprints do not fully overlap, which leads to blocky structures in the imagery.

#### **2.3.4 Differences between VOD and NDVI**

Being a remote sensing based technology without any required ground data, VOD offers the opportunity to obtain global data dating back to 1978. VOD is often compared to the NDVI as both use the presence and state of vegetation to monitor droughts (e.g. (Liu et al., 2012)). Due to its chlorophyll sensitivity, NDVI rather senses the greenness of vegetation, whereas VOD is sensitive to biomass water content and, therefore, to photosynthetic but also non-photosynthetic (leafy and woody) components of the vegetation (Liu, 2013). This is an important advantage of VOD because canopy greenness and vegetation water content do not necessarily change simultaneously and with the same trend (Ceccato et al., 2002). The sensitivity of VOD to changes in the woody components is larger than the one to leafy components (Liu, 2011).

Furthermore, VOD is based on longer wavelengths (microwaves) than NDVI (infrared). As a result, the penetration through the canopy is deeper and, consequently, VOD saturates at a higher biomass level. NDVI only senses the top of the vegetation canopy and saturates at relatively low vegetation (Yi Liu et al., 2012). Consequently, the spatial correlation between VOD and NDVI is more reliable in crop- and grasslands than in high vegetation density areas where NDVI saturates (Liu, 2011). Additionally, the longer wavelength also reduces the sensitivity to the atmosphere and weather conditions. (Andela, 2013; Liu, 2013)

On the other side, VOD also features some downsides. The presence of open water bodies can affect the emissivity and thus lead to an underestimation of the optical depth and an overestimation of retrieved soil moisture (Liu, 2013; Ye et al., 2015). To overcome this problematic, the water bodies are masked out as explained in 2.3.3. However, especially in the tropics, not all water bodies might be masked out properly. For this reason, areas with extensive lakes, reservoirs, rivers and flooded vegetation have to be interpreted with caution (Liu, 2013). According to (Andela et al., 2013), previous studies (de Jeu, 2003; Jones et al., 2011) showed that, also over sandy deserts and under frost conditions the conclusions, on the interpretation of the VOD signal should be drawn carefully. As microwaves are emitted at a lower energy level, a larger footprint (diameter of several kilometres) is required. This results in coarser resolutions than thermal and optical techniques (Liu, 2013). Even with the downscaling method, the resolution of 100 x 100 m is still lower compared to optical data. Due to the downscaling method, the radius of influence is larger than the resolution.

## 3 INDONESIA: A CASE STUDY

The presented research on VOD is conducted on the case study Indonesia. This archipelago is the fourth largest country on Earth and has 252 million inhabitants (The Worldbank, 2018). Its economy heavily relies on agricultural yields, representing 14% in 2016 (The Worldbank, 2017). Most of the agriculture is rain-fed, which leads to a strong dependence on the climate (Devendra, 2016). In combination with the exposure of the agriculture to the variable climate, this dependency raises concerns about the economic impact of droughts (Carrão *et al.*, 2016).

This study is embedded in the *SpiceUp* project, which is a G4AW<sup>1</sup> project aiming at optimizing the efficiency of pepper farms in Indonesia. For this reason, the focus of the present study is on pepper fields. The two main provinces of the project are Bangka-Belitung (in specific: Bangka island [2.2885° S, 106.0640° E]) and Lampung on Sumatra island [4.5586° S, 105.4068° E]. The areas of interest are shown in Figure 10. These two regions are well known for the production of white (Bangka) and black (Lampung) pepper, which was historically brought from India and has been cultivated for 2000 years (Tremblay, 2018). Pepper fields are challenging to analyse with satellites, since they are relatively small (often around 1 ha) and they grow along supporting sticks or trees, which have their own biomass.

First, this chapter provides general information on the region relevant for this case study (see 3.1). Furthermore, within this research, a field visit was conducted to obtain actual insight to the on-site conditions and select relevant areas. Finally, the outcomes of this field visit are described in 3.2.



Figure 10: Map of Indonesia with islands (capital letters) and provinces (lower case letters) of interest

### 3.1 General Information

#### 3.1.1 Climate

Overall, Indonesia is characterised by a hot and humid tropical rainforest climate (Af in the Köppen–Geiger climate classification system) (Köppen *et al.*, 1936; Peel *et al.*, 2007; Climate-Data.org, 2012). It is located around the equator in a low-pressure zone, where prevailing winds are calm. Due to its equatorial location, it barely experiences any changes in daylight hours throughout the year and has a relatively constant average

<sup>1</sup> Geodata for Agriculture and Water is a programme of the Dutch Ministry of Foreign affairs, executed by the Netherlands Space Office (Affairs, 2018)

temperature of 26.2°C (The World Bank Group, 2016). However, due to the monsoons, the annual precipitation of 2800 mm is spread heterogeneously over the year creating two main seasons.

Generally, the wet season concentrates on the period between December and March, when winds blow from the northwest bringing Pacific Ocean air masses. The peak of the wet season is in January. The dry season takes place between June and September peaking in August, when winds blow from southeast bringing Australian continental air masses. Figure 11 shows the mean precipitation and temperature of the entire country. However, these seasons shift depending on the exact location, also within the same province. (Hendon, 2003; The World Bank Group, 2016)

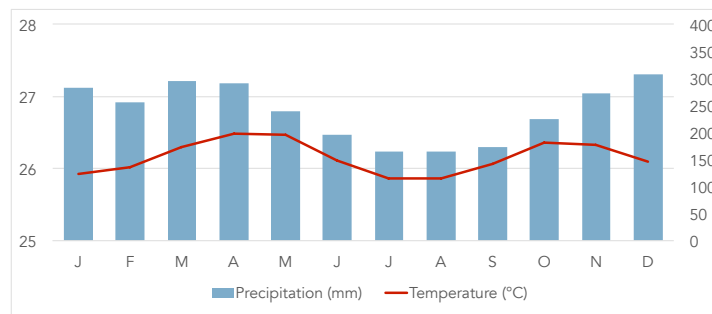


Figure 11: Mean precipitation and temperature in Indonesia (The World Bank Group, 2018)

In Lampung, the dry season lasts from June to October. During this period the rainfall is still around 140 mm per month but the rainfalls are much less heavy compared to the wet season (Fanin *et al.*, 2017).

In Bangka, the dry season lasts from March to October. However, more recently rains have lasted until April or later. In December, heavy storms with strong winds occur. Muntok (in the north of Bangka) is an exception in terms of climate as it has a tropical monsoon climate (Am in the Köppen–Geiger climate classification system), which means that the dry season is much shorter with its peak in August (Climate-Data.org, 2012).

Climate change has a significant impact on the probability of drought occurrence in this area. Recent warming of the tropical ocean has led to a weaker Walker circulation and, therewith, a decrease in precipitation. Despite the increasing tropical mean precipitation, a 25% increase in severe droughts from 1951-2000 to 2001-2050 is expected. (Lestari *et al.*, 2014)

### 3.1.1.1 Droughts and El Niño

Indonesia has experienced several droughts including very severe droughts in the last decades. Many studies aim at finding correlations with other phenomena such as Sea Surface Temperature (SST) or the Indian Ocean Dipole to explain these droughts. Multiple studies confirmed that the occurrence of droughts is strongly linked with El Niño Southern Oscillation (ENSO) (Hackert *et al.*, 1986; Hendon, 2003; Chang *et al.*, 2004; D'Arrigo *et al.*, 2006, 2008; Hamada *et al.*, 2012; Aulia *et al.*, 2016; Setiawan *et al.*, 2016, 2017). In these studies, either the closely related SST or indices as the SOI or ONI are used to represent the ENSO.

In Indonesia, during the rainy season and the first transitional season, from December to May, there is a low probability to be affected by El Niño, whereas in July to October, the risk is very high over several regions including Sumatra (Supari *et al.*, 2016). In most cases, the impacts of El Niño start in June with a drier climate (Supari *et al.*, 2016). This contributes to droughts and through the dry season, prolonged by El Niño, to crop failure in many agricultural areas (Aulia *et al.*, 2016). The opposite occurs during La Niña, meaning a wetter and prolonged wet season (Aulia *et al.*, 2016).

Table 7 shows the intensity of El Niño years measured with the SOI and with the SST. Although the timing of droughts is more or less foreseeable with the ENSO, the spatial distribution and intensity depends on the season and the intensity of the El Niño event, but also on local factors (Setiawan *et al.*, 2017). During el Niño years, the late onset of the Maritime Continent monsoon can also contribute to low precipitation anomalies leading to a non-linear relationship of the severity of a drought to the intensity of El Niño (Hamada *et al.*, 2002; Moron *et al.*, 2009; Lee and McBride, 2016 cited in Setiawan, 2017).



Further back in history, the droughts of 1982/83 and 1997/98 have been historic drought events (Van Nieuwstadt *et al.*, 2005). In the studied period of the present work (2012-2018), the only Indonesian drought described in the literature is the one of 2015/2016. The El Niño event of 2015/16 has been ranked in the same intensity due to the extreme SST anomalies. However, fires did occur at a less exceptional scale suggesting that the relationship between climate, land change and fire occurrence as well as the relationship between rainfall and El Niño might have changed over the years (Sloan *et al.*, 2017).

Lestari *et al.* (2018) analysed the dynamical development of the severe drought of 2015/2016 in Indonesia by comparing (TRMM) precipitation data to El Niño and Indian Dipole events. The authors used the monthly value of the Niño3.4 index (retrieved from SST anomalies in the equatorial Pacific Ocean) and the Dipole Mode Index (DMI) (retrieved from differences in SST anomalies between the western and eastern tropical Indian Ocean region) to represent the evolution of the two types of climate mode in this region. Over southern Sumatra, the low precipitation anomaly persisted from July 2015 to January 2016 and lead to a meteorological drought peak between September and October of 2015 with an anomaly of -450mm/month. El Niño started in April 2015, peaked in January 2016 and ended in April 2016, whereas the DMI revealed that the Indian Dipole event started in August 2015, peaked in September 2015 and ended in November 2015. These two peaks coincide with the low precipitation anomaly. The authors conclude that the severe drought of 2015/2016 is caused by the simultaneous occurrence of El Niño and the positive IOD event.

Sholihah *et al.* (2016) used the Vegetation Health Index (VHI) to identify the spatiotemporal extent of agricultural droughts over West Java and to classify the drought severity between the years 2000 and 2015. For this purpose, the authors used Landsat NDVI and Land surface temperature (LST) data to calculate the moisture vegetation/vegetation condition (VCI)<sup>2</sup> and the temperature condition (TCI)<sup>3</sup>. Based on the VCI and the TCI the Vegetation Health Index (VHI)<sup>4</sup> was calculated. This describes overall vegetation health and can indicate the severity of agricultural drought extent. The authors classified the conditions in 2015 as a “severe drought”, which is the second extreme class before “extreme drought”.

Also, other phenomena as the Indian Ocean Dipole (IOD) have shown to be related to droughts in Indonesia. Field *et al.* (2009) found the IOD to be an independent contributor to droughts in Indonesia. Additionally, Hamada (2012) observed that droughts in West Java, which is very close to Lampung and Bangka, occur with a positive El Niño but also a positive IOD. Similarly, Ashok *et al.* (2003) related the IOD to the low SST anomalies between Sumatra and Java contributing to droughts on the surrounding land.

### 3.1.1.2 Droughts and fires

Indonesia is characterised by the highest density of fire emissions in the world with most fires being generated in Sumatra and Kalimantan (Fanin *et al.*, 2017). The fires in Indonesia are mainly lit to clear vegetation waste, especially resulting from agricultural expansion and deforestation, maintaining or securing land tenure and regrowth (Field, 2009; Herawati *et al.*, 2011; Medrilzam *et al.*, 2014). They are often set on degraded and drained peatlands that are not capable of holding water anymore (Gaveau *et al.*, 2014). Peat is a layer of up to 20 m thickness, consisting of partially decomposed plant material and is thus characterized by a high proportion of organic matter (Fanin *et al.*, 2017). The fires are mainly set during the dry season (July to mid-November) leading to a much higher risk of forest and peat fires (Fernandes *et al.*, 2017). During abnormally dry El Niño years, the peat reaches such dry conditions that it can burn and release a high amount of sequestered carbon (Page *et al.*, 2002; Medrilzam *et al.*, 2014). The long duration of these fires is caused by the fact that the fires expand underground, where they have a large source of fuel and are only stopped by the return of the monsoon rains (Field *et al.*, 2008). This causes a strongly non-linear relationship between droughts in Indonesia and fires (Field *et al.*, 2016).

<sup>2</sup> VCI of month *i*:  $VCI_i = \frac{NDVI_i - NDVI_{min}}{NDVI_{max} - NDVI_{min}} * 100$

<sup>3</sup> TCI of month *i*:  $TCI_i = \frac{LST_{max} - LST_i}{LST_{max} + LST_{min}} * 100$

<sup>4</sup> VHI of month *i*:  $VHI_i = \alpha VCI_i + (1 - \alpha) TCI_i$  where the correlation factor of VCI and TCI:  $\alpha = 0.5$

Land use change is a strong contributor to this problematic. In the last decades a continuous peatland deforestation and conversion into managed land cover types, in particular, palm oil and pulp wood plantations, has taken place in Sumatra and other parts of Indonesia (Miettinen *et al.*, 2016). This increases the risk of expanding fires. Similarly, perturbed forests that have already been burned partly are more prone to fire occurrences (Sloan *et al.*, 2017).

These resulting gas and aerosol emissions affect not only the climate but also the air quality (Langmann *et al.*, 2009). Especially during El Niño years, the contribution of fires in Southeast Asia to fine particular matter and ozone is very high (Marlier *et al.*, 2013). This has serious health consequences for the population. For example, the emissions of these fires contribute to around 2% of the annual increase in adult cardiovascular mortality in this region (Marlier *et al.*, 2013).

The magnitude of the Indonesian fire events in 2015 contributes to the drought evidence described in 3.1.1.1. Around 2.6 million hectares were affected (Tacconi, 2016). Field *et al.* (2016) detected the fire season of 2015 and the resulting smoke pollution in Indonesia as the most severe since 2000 when NASA observations started. Also, longer-term records of airport visibility in Sumatra showed that 2015 was the worst case after 1997. In 2015 the fire season in Sumatra began in July. From September to October, large parts of the region were blanketed in thick smoke. This led to a 2-month hazardous exposure of millions of people to poor air quality. The MODIS fire detection confirmed the dense occurrence of active fires. Most of these were in peatland areas.

The greenhouse gases (GHG) emitted during this fires season were the second highest of the past two decades. During September and October 2015, the daily GHG emission was approximately 11 times higher than during normal years. As a consequence, over half a million people in the country suffered noticeable health effects. Furthermore, the fire and haze had a roughly estimated economic cost of US\$ 16.124 billion (1.8% of Indonesia's GDP in 2014). However, the total cost is likely to be much higher including the impact on other countries for example. Amongst others, the economic impact consisted of a reduced oil production due to ill workers, thousands of cancelled flights, further impacting on tourism and business and lost timber due to burned forests and plantations. Additionally, the reduced solar irradiance through the haze might have impacted agricultural crops (Tacconi, 2016)

### 3.1.2 Economy

In the last years, the gross domestic product share of agriculture in Indonesia has been around 14% (TheGlobalEconomy.com, 2016). Farming occupies a third of the labour force and is the main source of income for more than half of the economically poor households (Owen, 2015). To assure stable productions in the agriculture it is crucial to manage climatic variability, especially droughts. (Aulia *et al.*, 2016)

In 2015, the World Bank estimated that the drought of 2015 would reduce the rice production by 2.9% (2.1 million tonnes) and increase the rice prices by 10.2%. This mostly affects poorer households that spend a larger proportion of their income on food. (Owen, 2015)

Similarly, the World Food Programme conducted a survey in December 2015 in eastern Indonesia to assess the impacts of the drought. They survey revealed that 40% of the farmers relying primarily on their rice production lost more than half of their crop. Two thirds of the farmers stated that in the past three months their crop plantation was either delayed or not possible at all. Furthermore, 60% of the agricultural households reported to have lost income due to the drought and 10% had to reduce their money they were spending on food due to these conditions. (World Food Programme, 2016)

The pepper production in Indonesia relies heavily on the climate. During the drought of 1995, for example, Indonesian pepper production reduced by two-thirds within one year (Weiss, 2002). These strong fluctuations in production put the global supply under pressure and lead to highly volatile pepper prices, which are not only depending on global and domestic production but also on the international prices, especially of Vietnam (Yogesh *et al.*, 2013; Krishnakumar, 2016). In turn, the production in Vietnam, which is the largest producer and exporter of pepper, is also affected by droughts (International Pepper Community, no date)

### 3.2 Field visit in the pepper fields

The aim of the field visit was to obtain a general understanding of the cultivation of pepper. This included information on cropping cycles, irrigation practices, yields and droughts but also on adjacent land use and historical land use changes.

Both Bangka and Lampung, are mainly covered by natural forests and agricultural fields. However, the distribution of crops grown in both places is different. Bangka, which is a flatter region, with the exception of some hills in North Bangka, mainly contains natural forests, palm oil, rubber, tin mines, urban areas and pepper. Lampung, is much hillier and has more natural forest. The main crops grown in Lampung are cassava, corn and rice. Some of these land uses are shown in Figure 13, Figure 14, Figure 15 and Figure 16.



Figure 13: Palm oil plantation



Figure 14: Rubber plantation

The focus of this study is on pepper fields. Therefore, during the field visit mainly pepper fields were visited with the help of PT CAN, an organization within the *SpiceUp* project, which collects the pepper from the farmers and has a registration of all farmers involved. Pepper cultivation is considered to be a very risky business requiring skills, hard work and also luck (Wadley et al., 2005). Before the recent climate change, it used to generate yearly income, and is therefore a long-term investment in comparison to other crops such as palm oil (Personal communication, 2018).



Figure 15: Tin mine in Bangka



Figure 16: Cornfield in Lampung

### 3.2.1 Plant and field shape

Seen from space pepper plantations have a peculiar shape (see Figure 17). As they are climbing vines, they require supporting trees or poles to grow upwards resulting in a quadratic net of high vegetation column next to bare soil or very light vegetation. Additionally, they have shallow roots under the ground and usually hold a few major lateral roots that are able to penetrate soil depths of around 2 m. The trees should be planted with a 3-m distance between each other to avoid the expansion of diseases. However, most of the visited fields had distances of 1.5 to 2.5 m. For the same reason, the first 0.3 m from the soil upwards should be cleared from vegetation. Moreover, pepper plants should be exposed to the sunlight to avoid yield reduction. (Personal communication, 2018)

On Bangka, mainly sticks support the pepper plants (see Figure 18 and Figure 19). However, some plants also grow on living trees with controlled branches and leaves growth. Most fields visited in Bangka cover an area of 1-2 ha. There is one very large industrial pepper field of 36 ha (see Figure 20). Many of the visited fields suffer from the *Yellow Disease* and *Rot Root Cancer* (see 3.2.2). These kinds of diseases can easily spread, since the trees are often planted too close to each other and vegetation grows between them. (Personal communication, 2018)



Figure 17: Pepper and some other land uses from a Google Earth image



Figure 18: Pepper plants growing on sticks in North Bangka



Figure 19: Pepper plants growing on sticks in central Bangka



Figure 20: Industrial pepper field of 36 ha in Bangka



Figure 21: Pepper plants on living trees on Lampung with large canopy (left) and with small canopy (right)

In Lampung, the pepper is mainly supported by living trees (see Figure 21). The canopy of these trees varies significantly from field to field. One of the main reasons for using living trees here is that many of the forests are protected and can thus not be cleared. Therefore, the pepper has to be grown around the trees that are forbidden to be cut off. Furthermore, the fields on Lampung are very different from one another. In some fields, the canopies are dense leading to remarkably less dense pepper plants. Additionally, due to the lower amount of light in fields with large canopy trees on Lampung, the pepper plants are less dense. Other fields had small canopies and dense pepper plants.

### 3.2.2 Life cycle

In most of the cases, pepper fields are created in areas of previously natural forest. After clearing the forest, the ground is supplied with fertilizers for three months. The pepper seedling is prepared by taking one segment of a branch of a grown-up tree and by planting it into a polybag with some soil (see Figure 22). Figure 23 shows the segment structure of the pepper plant. The seedling preparation is mainly not done by farmers but by people engaged in the seedling business. These people buy a pepper segment and a polybag for 1000 Indonesian Rupiah (~0.06 €) each, water it for three months and sell it for 10 000 Indonesian Rupiah (~0.57 €). (Personal communication, 2018)



Figure 22: Seedlings in polybags



Figure 23: Segment structure of the pepper plant



Figure 24: Recently planted pepper plant

Then, the seedling is planted in the nutrient rich field and covered by palm tree leaves to provide the young plant with shade. In this period, the pepper is watered regularly. Once the pepper seedling is planted, it takes between one and two years before the first harvest can take place. (Personal communication, 2018)

In the beginning, the plant should be cut regularly, keeping it small in order to increase the strength of the root and stem. After flowering, it takes approximately nine months before the ripe berries can be harvested. Usually, all pepper berries ripen at the same time of the year around July or August. However, since the climate is changing, the pepper often matures heterogeneously from plant to plant but also within the same plant (see Figure 25). For this reason, most of the visited farmers harvest over the whole year. During the field visit, pepper farmers reported that the wet and dry seasons have recently changed and became unpredictable impacting their yields. (Personal communication, 2018)



Figure 25: Irregular ripening process within the same plant

In Lampung, black pepper is produced and in Bangka white pepper. These two differ only in the processing after harvesting the berries. The berries that are processed to be white pepper are gathered in large bags and left in water bodies for several weeks until the shell dissolves and the inner white core remains (see Figure 26 and Figure 27). The black pepper is made from the entire berry including the outer shell. White pepper can be sold on average for 60 000 Indonesian Rupiah/kg (3.44 €/kg) and black pepper for 30-40 000 Indonesian Rupiah /kg (~2.00 €/kg). (Personal communication, 2018)



Figure 26: Soaking of pepper in open surface water bodies to become white pepper



Figure 27: Black and white pepper

A pepper plant produces pepper for approximately 15 years. The most common disease of these plants is the *Yellow Disease*. It originates when the root is not strong enough to absorb nutrition on the ground and results in fewer and smaller leaves (see Figure 28). This leads to a slow decline of the entire plant until it dies. This process continues despite sufficient soil moisture availability. Once a pepper plant is ill, most farmers remove the plant, as it cannot recover to carry fruits again. Another common disease is the *Root Rot Disease* (see Figure 29). It is transmitted through water and is therefore most common during periods of heavy rain. It can also appear when young plants are watered too intensively. Measures to reduce the transmission risk of diseases are a good drainage to avoid stagnant water and the removal of the canopy of the living tree to reduce the moisture built up. Furthermore, a sufficient distance between the individual plants of 3 m should be kept and the soil between the trees should be cleared from vegetation. (Personal communication, 2018)



Figure 28: Pepper plant with yellow disease



Figure 29: Pepper plant with root rot disease

### 3.2.3 Irrigation and droughts

Pepper plants require around 2000 mm rain per year. If it does not rain enough, irrigation is needed to ensure constant yields. In the visited areas, none of the pepper fields is irrigated although yields were reported to be lower in drier years like in the year 2015. Especially in Lampung, several farmers reported to have experienced droughts in the past and were interested in irrigation advice (for which infrastructure would be needed). The only water used for the cultivation is during the first phase of the pepper life cycle to grow the seedling to a plant being able to attach to a support such as a stick or a tree. Some farmers dig round ditches around the individual plants to maintain the water for a longer period. Others, especially in the north of Bangka, where rain has recently increased throughout the dry season, farmers must deal with excess water and have developed draining techniques. Figure 30 shows a draining technique, in which the soil, where the pepper is planted, is slightly elevated in comparison to the surrounding. (Personal communication, 2018)



Figure 30: Irrigation dredge

Due to the inexistent irrigation, the water consumption related to the pepper production is very low. However, other crops, such as rice, maize and coconuts, are extensively irrigated. The water used in Lampung is to 98 % internal use, meaning that no external water needs to be imported. By exporting these crops to other islands, Lampung becomes one of the highest virtual water exporters of Indonesia. Moreover, Bangka is almost not exporting virtual water. (Bulsink *et al.*, 2010)

## 4 METHODOLOGY

In this chapter, the exact study area is shown, the different datasets are described, and the methods used to address the research objectives are explained. For the analysis ten of the visited pepper fields in Bangka and seven of the visited pepper fields in Lampung are selected. The locations are depicted in Figure 31 and Figure 32 and the details about the individual fields are given in Appendix 8.1

### 4.1 Study area

During the field visit mainly pepper fields were visited with the help of PT CAN, an organization within the *SpiceUp* project, which collects the pepper from registered farmers. The exact locations are depicted in Figure 31 and Figure 32.

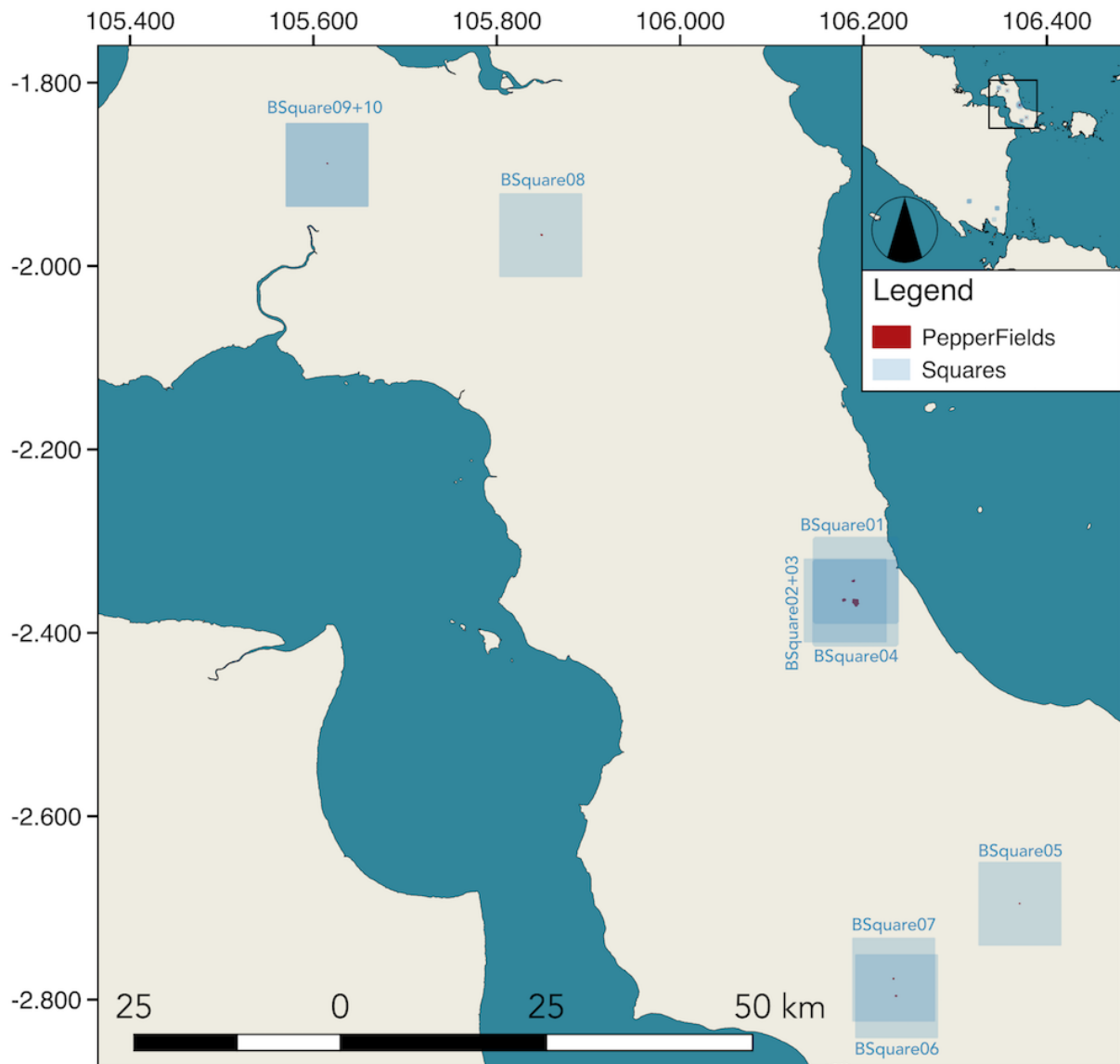


Figure 31: Study areas on Bangka

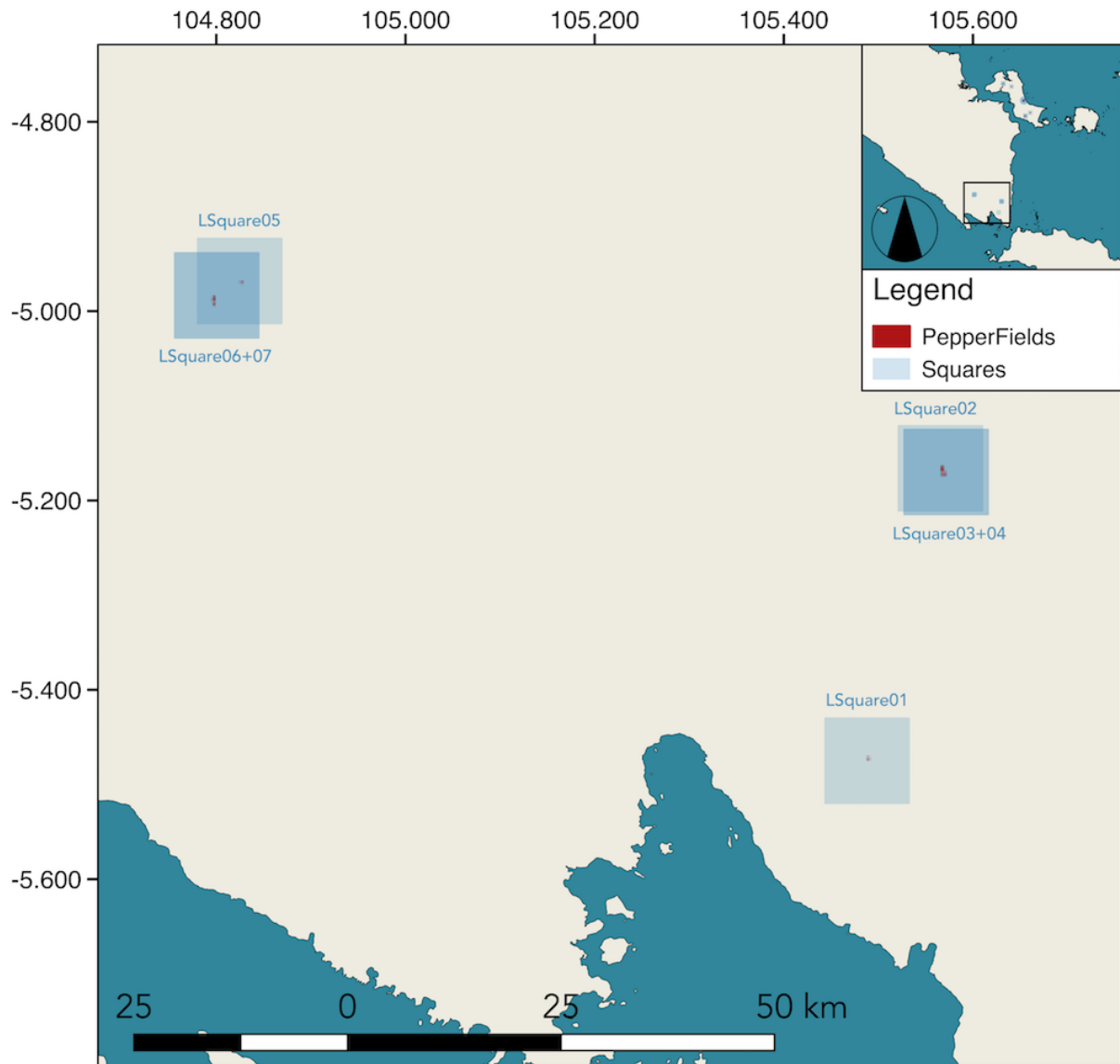


Figure 32: Study areas on Lampung

## 4.2 Datasets

### 4.2.1 Vegetation Optical Depth

The Vegetation Optical Depth data is provided by VanderSat at X-Band. The data is given in daily time steps. However, certain days lack of data values (on average 40% of missing data within the AMSR-2 VOD dataset). These gaps are most probably due to the revisit time, which becomes longer at the equator. For this reason, VanderSat also provides a 20-day moving average. By doing so, the VOD curve is smoothed and the gaps of missing data are filled.

From May 2002 until October 2011 the VOD was retrieved from the AMSR-E on NASA's EOS Aqua spacecraft. Since May 2012 it is retrieved from the AMSR-2 on JAXA's GCOM-W1 spacecraft (Kachi *et al.*, 2014). The VOD product of VanderSat suffers from a miscalibration between the two missions leading to a shift between the two time series for some regions of the world. Due to the large gap and the offset between the two missions, only the second, more recent mission of AMSR-2 is used. In the first weeks of the AMSR-2 missions, all the parameters on board of the mission were still being calibrated. Therefore, the data is only being used from the 15.08.12 when the values reached the average values of the time series. The end of the time series is set to the 01.05.2018, when the field visit took place.

#### 4.2.2 Normalized Difference Vegetation Index (NDVI)

In this study, two different NDVI data sets are used. For the spatial analysis, the Near-Infrared and the Red band from the Sentinel-2 MultiSpectral Instrument (Level-1C) are retrieved via the Google Earth Engine (see 4.3). These two bands have a spatial resolution of 10 m. This dataset does not correct for clouds but includes a cloud mask band with a resolution of 60 m and the image property *CLOUDY\_PIXEL\_PERCENTAGE*, which gives a granule-specific cloudy pixel percentage taken from the original metadata.

The Normalized Difference Vegetation Index data for time series analysis is retrieved as *MOD13A1: MODIS/Terra Vegetation Indices 16-day L3 Global 500 m SIN Grid V006* from the online Application for Extracting and Exploring Analysis Ready Samples (AppEEARS), courtesy of the NASA EOSDIS Land Processes Distributed Active Archive Center (LP DAAC), USGS/Earth Resources Observation and Science (EROS) Center, Sioux Falls, South Dakota (NASA EOSDIS LP DAAC, 2015). This dataset has an integrated cloud correction. As the name already suggests, it has a spatial resolution of 500 m. The timescale is given at an approximate 16-day interval. However, this interval is sometimes a day shorter or longer. The 16-day composite is generated using the two 8-day composite surface reflectance granules (MxD09A1) in the 16-day period.

#### 4.2.3 Multivariate ENSO Index (MEI)

In order to test the correlation between the VOD time series and the ENSO Index, the Multivariate ENSO Index (MEI) dataset from the NOAA website is used (NOAA, 2018). This dataset consists of bimonthly MEI values, which are given in 1/1000 of standard deviations. The dataset covers the time from December 1949 to May 2018. Missing values are left blank. However, there are no missing values in the timeframe that is used for this analysis. The values are normalized for each bimonthly time step. This means that the 44 values between 1950 and 1993 have a standard deviation of one and an average of zero.

#### 4.2.4 Dipole Mode Index (DMI)

To quantify the Indian Ocean Dipole (IOD), the Dipole Mode Index (DMI) dataset from the NOAA website is used (NOAA, 2017). The data consists of monthly values from January 1870 to December 2017. A positive DMI refers to a positive IOD and thus lack of precipitation over Indonesia and vice versa. This dataset has no missing values.

#### 4.2.5 Standardized Precipitation Evaporation Index (SPEI)

The data of the Standardised Precipitation-Evapotranspiration Index (SPEI) is obtained from a website from the Spanish Agency for Superior Scientific Investigations (Consejo Superior de Investigaciones Científicas – CSIC) (Vicente-Serrano *et al.*, 2018). The data dates back to January 1901. It offers long-time SPEI time series of a spatial resolution of 0.5 degrees. The time resolution is monthly. However, the website offers aggregated datasets of time-scales ranging between 1 and 48 months. For this study, the monthly dataset is used.

On the Website two types of datasets are available:

1. The SPEIbase is a revised dataset that is based on monthly precipitation and potential evapotranspiration (PET) from the Climatic Research Unit of the University of East Anglia and dates until December 2015. The PET is obtained by the FAO-56 Penman-Monteith model. This is the more robust of the two available SPEI datasets. This dataset is available as netCDFs for larger regions or as CSV files for single coordinates.
2. The SPEI Global Drought Monitor is an unrevised near real-time dataset. It is updated at the beginning of each month based on the mean temperature of the NOAA NCEP CPC GHCN\_CAMS gridded dataset and monthly precipitation sums from the Global Precipitation Climatology Centre (GPCC). This precipitation data is interpolated from an original resolution of 1° to the desired resolution of 0.5°. Due to the lack of real-time

data sources for more robust PET estimations, the PET is based on the Thornthwaite equation. As an example of the lower reliability of this near real-time product, the current drought of the summer 2018 in the Netherlands appears to be less strong than in the previous year, although this is not the case. This dataset is available as CSV files for single coordinates.

#### 4.2.6 Hansen deforestation maps

For analysing the trends in the VOD time series, the Hansen deforestation maps are used (Hansen *et al.*, 2013). It is based on Landsat imagery with a spatial resolution of approximately 30 by 30 m. It shows the yearly deforestation per pixel from 2000 to 2018. It also gives the overall increase in vegetation or forest in the same period. However, the increase is not split into the individual years.

#### 4.2.7 Yield data

The Directorate General of Estate Crops *et al.* (2016) of the Ministry of Agriculture of Indonesia published a report about the pepper production in Indonesia. It contains statistics on the yearly pepper field areas, the pepper production, export and import and yields. The data of this report is collected from the Estate Crops Province Level and from other institutions such as Board of Central Statistics, the Ministry of Industry, Ministry of Trade, the Central Bank of Indonesia and the publication of Estate Commodity Associations. The exact procedure of the collection of the yield data is not given. Additionally, the values of the year 2016 are preliminary values and the values of 2017 are estimations only. Therefore, the reliability of this data is uncertain as there is no information available on what the statistics are based.

### 4.3 Spatial patterns in VOD

#### 4.3.1 Comparison of VOD and NDVI to general land use patterns

In a first step, VOD and NDVI images are compared to a Google Maps image. For this purpose, the mean of the year 2016 (01.01.2016 to 31.12.2016) is calculated for VOD as well as for NDVI for two selected squares of 10 x 10 km, one on Bangka (*BSquare02*) and one on Lampung (*LSquare07*) (in Figure 31 and Figure 32). As an additional comparison *LSquare04* is used as well. Each of these squares includes several pepper fields. The Google Maps image is composed by different years. Although land uses changes relatively fast in this region it gives a broad idea of the present land uses.

The NDVI image is obtained by combining the *Nir* and the *Red Band* of the *Sentinel 2* data from the Google Earth Engine. Due to the high cloud occurrence, the clouds are masked out. To avoid the effect of cloud shadow that remains after the masking out the clouds, images with a cloudy pixel percentage of over 80% are excluded. This percentage was chosen in a process of trial error to obtain enough images in the period of one year. In Bangka, this leads to 19 images (35 before cloud filter) and in Lampung to 7 images (19 before cloud filtering). The NDVI images are then overlaid with contour lines of the VOD gradient in steps of 0.001 to show the similarity or the difference between the two spatial images.

#### 4.3.2 Derivation of spatial characteristics of VOD of pepper fields

The spatial distinguishability of pepper fields is assessed on the VOD images produced in the previous step (4.3.1). The distinguishability is cross-compared with the same NDVI images. *BSquare02* includes the pepper fields *BPepperField01*, *BPepperField02*, *BPepperField03* and *BPepperField04*. The pepper fields 02 and 03 exist since 2014, whereas *BPepperField04* exists since 2015 and *BPepperField01* since 2017. *LSquare07* includes *LPepperField05*, *LPepperField06* and *LPepperField07*. All these fields existed before 2012.

#### 4.3.3 Identification of spatio-temporal characteristics of large-scale VOD

Furthermore, a spatio-temporal analysis is conducted for *BSquare02* and *LSquare07* to see if spatial patterns become visible during a drought. For both locations, three situations (before, during and after a drought) are compared during the drought year 2015. For each situation, a 4-month VOD average is created per location

and compared during the drought year 2015 and the non-drought year 2016. The three periods vary in the two locations. The exact period per location of the resulting 6 images are shown in Table 8.

Table 8: Timeframe for the 4-month VOD mean in the drought and the non-drought year

Location	Label	Timeframe for the 4-month VOD mean			
		Drought year		Non-drought year	
		From	To	From	To
Bangka	Before the drought	01.03.2015	01.07.2015	01.03.2016	01.07.2016
	During the drought	01.07.2015	01.11.2015	01.07.2016	01.11.2016
	After the drought	01.11.2015	01.03.2016	01.11.2016	01.03.2017
Lampung	Before the drought	01.04.2015	01.08.2015	01.04.2016	01.08.2016
	During the drought	01.08.2015	01.12.2015	01.08.2016	01.12.2016
	After the drought	01.12.2015	01.04.2016	01.12.2016	01.04.2017

Next, the images from each situation are compared to their corresponding situation from the other year as follows.

$$(VOD_{\text{drought year}} - VOD_{\text{non-drought year}}) / VOD_{\text{non-drought year}}$$

The resulting image gives the increase or decrease in VOD with reference to the non-drought year in a specific period. Positive values indicate that the VOD in the drought year is higher and negative values indicate that the VOD in the drought year is lower.

## 4.4 Temporal patterns in VOD

### 4.4.1 Calculation of VOD anomalies

For the analysis, it is crucial to understand whether a VOD value is low due to season-related little vegetation in that period or due to atypical low moisture availability. For this purpose, time series anomalies are going to be analysed. The VOD anomaly is calculated as follows. The VOD data is given as time series of raw data with the actual daily values and as a time series of the moving 20-day average given in daily time steps as well. This average overcomes the issue of missing values and also fluctuations. The given average time series is used to calculate the climatology. Leap years are considered within this calculation. And only the VOD data from 15.08.2012 until the 01.05.2018 are used for the climatology. Next, the anomaly is calculated by subtracting the climatology from the VOD moving average time series.

$$VOD_{\text{Anomaly}} = VOD_{20} - VOD_{\text{Climatology}}$$

### 4.4.2 De-trending of VOD anomalies

According to the Hansen deforestation maps, the analysed area in Indonesia has experienced extensive deforestation (Hansen *et al.*, 2013). In these areas, agricultural vegetation is cultivated. As the purpose of the VOD in this study is to detect (drought conditions) differences in vegetation water content as a response to "short-term" water shortages, the long-term trends which can be either decreasing or increasing should be extracted from the time series. For this reason, the VOD anomaly time series is de-trended. A linear model is fit to the time series. This linear trend is then subtracted from the actual anomaly time series.

### 4.4.3 Derivation of temporal characteristics of VOD of pepper fields

The used downscaled VOD product gives dimensionless VOD values per 100 m x 100 m pixel, which is representative of the total water content in that pixel. However, it is important to consider the analysed field size taking into account that the resolution is only 1 ha. Furthermore, the downscaling method leads to a

radius of influence of several kilometres. This means that the adjacent land use should be taken into consideration for the interpretation, especially if a small area of the size of one pixel is analysed.

In order to assess whether the fields are distinguishable, the VOD anomaly time series of 17 fields are compared to the time series of the mean value of a square of 10 x 10 km. Then, the difference between the two time series is calculated and plotted together with the two original time series. Additionally, the mean of the absolute difference as well as the mean of the absolute anomaly of the field is calculated in order to calculate the mean difference as percentage of the field anomaly (see title of each plot).

Furthermore, the spatial analysis explained in further detail in 4.3 gives insight to the distinguishability of the individual pepper field. This analysis consists in the comparison of three aggregated images before, during and after a drought.

#### 4.4.4 Comparison of VOD to other drought indicators

In order to evaluate the added value through VOD as an alternative drought indicator, the VOD anomalies are cross-compared to the anomalies of other indices. Based on the comparison of the different drought indicators in section 2.2 and previous studies in Indonesia (see 3.1.1.1), four different proxies or indicators are chosen to compare with VOD: The Multivariate ENSO Index (ENSO), the Dipole Mode Index (DMI) that describes the Indian Ocean Dipole, the Standardized Precipitation Index (SPEI) and the Normalized Difference Vegetation Index (NDVI).

The correlation with other drought indices is based on the fields. The VOD anomaly time series of the 17 fields is compared with the anomaly time series of the other selected drought indices. For all drought datasets, the correlation with the VOD anomaly is tested with the Pearson correlation test and the Spearman Rank Test. The Pearson test gives a correlation coefficient  $r$  that ranges between -1 and 1, and expresses the degree to which two variables change correspondingly. The  $p$ -value indicates the probability to obtain the present result with a correlation coefficient of zero. The correlation coefficient is defined as statistically significant if the  $p$ -value is lower than 5%. (MedCalc, no date)

The Spearman Rank test gives the correlation coefficient  $r_s$ , ranging between -1 and 1, which indicates the strength of the link between the two datasets also for non-linear correlations. Again, the correlation is statistically significant when the  $p$ -value is under 5%. If both tests give similar correlations the two datasets are linearly correlated. If Spearman gives higher results than Pearson then the correlation is non-linear.

The tests are conducted in python by using `pearsonr` and `spearmanr` function from the `scipy.stats` package as follows.

```
p = pearsonr (VOD_anomaly, OtherIndicator_Anomaly)
```

```
s = spearmanr (VOD_anomaly, OtherIndicator_Anomaly)
```

Both functions return the correlation coefficient and the 2-tailed  $p$ -value.

##### 4.4.4.1 MEI

As the MEI is given in bimonthly values, the VOD anomaly data has to be aggregated to monthly data. Next, the correlation lag functions between the two time series is plotted as follows with the `xcorr` function in the `matplotlib.pyplot` package in Python.

```
ax.xcorr(a- mean(a), b- mean(b), usevlines=False, maxlags=8, normed=True)
```

Where  $a$  and  $b$  are the two sequences of scalars of the anomaly time series that are compared. This line returns a plot in which the x-axis represents the lag, from minus to positive, and y-axis values show correlation coefficient in each time lag. Here, the maximum possible lag is set to 8 months. These functions show at which positive or negative lag the correlation is the highest. The negative lag is the significant one here, as the vegetation and thus, the VOD reacts slower to global patterns such as the ENSO. A negative lag

means that the VOD time series shifts from 0 to 8 months earlier and, thus, the visible effects of the ENSO are artificially occurring at the same time as the ENSO. This negative lag takes place when the most negative correlation occurs. Then, the two time series are plotted with the respective calculated maximum correlation lag and the statistical tests are conducted on the lagged time series.

#### **4.4.4.2 DMI**

The Dipole Mode Index (DMI) is given in monthly values from January 1870 to December 2017. Thus, the overlapping time period with the analysed VOD time series is only from August 2012 to December 2017. Also here the VOD is aggregated to monthly values and the lag function is applied to find the maximum correlation between the two datasets. Then, both time series are plotted under consideration of the lag and the statistics are calculated.

#### **4.4.4.3 SPEI**

As mentioned in 4.2.4, there is more robust data available until 2015 and less robust data available until the present. The more robust dataset is used as a netCDF in order to obtain the mean of the polygon to have the same maximum resolution of the product as it will be used for the VOD product. One of the strongest droughts seems to be at the end of 2015, when the short time series ends. Therefore, also the unrevised dataset is included. This dataset is only given for a single coordinate.

The plot includes the VOD anomalies as well as the two different SPEI anomaly time series. The statistical analysis showing the correlation between the different time series is done as follows. First the correlation between the revised and the unrevised SPEI is calculated to understand how different or similar these two datasets are from each other. Next, the VOD is compared to the long and unrevised SPEI and then to the short and revised SPEI. The correlation of the SPEI with the VOD is calculated without time lag as they are supposed to occur simultaneously.

#### **4.4.4.4 NDVI**

Since the NDVI is also given as a spatial time series in a netCDF, the NDVI data is extracted, in analogy to the SPEI data extraction, as the mean NDVI value of each pepper field polygon. As described in 4.2.2, the time interval of the NDVI dataset is not homogeneously 16 days. For this reason, a rolling mean of 18 days is applied to the NDVI dataset filling all the empty days. The resulting artificially created daily NDVI anomalies are aggregated to monthly values to have a fair comparison with the other indices. These monthly NDVI and VOD anomalies are plotted without time lag and the corresponding statistics are calculated.

#### **4.4.5 Comparison of NDVI to other drought indicators**

In order to put the results from 4.4.4 into perspective, the same analysis is conducted comparing the NDVI to the MEI, the DMI, the short SPEI and the long SPEI. The methodology is in analogy to the VOD analysis. All calculations are based on monthly values as well. Time lags are only applied for the MEI and the DMI.

#### **4.4.6 Comparison of yields to VOD**

The national yearly pepper yields are calculated by dividing the yearly pepper production given in tons by the yearly pepper cultivation area given in hectares. The values of 2016 are preliminary values and the ones of 2017 are estimated values only. Nevertheless, national pepper production in tons and the area of pepper fields in hectare are plotted from 2012 to 2017. The provincial production is not used as it only contains data from 2015 and estimates of 2016 and 2017. This time period is too short to detect trends.

## 5 RESULTS & DISCUSSION

This chapter describes and discusses the results. First, the general spatial performance of VOD is discussed. Then, spatial and temporal characteristics of VOD of pepper fields are compared to their surroundings. Next, VOD anomalies are compared to other drought indicator anomalies. Further, VOD anomalies are compared qualitatively to yield data. Lastly, a roadmap to convert VOD into a drought index is proposed.

### 5.1 Spatial patterns

#### 5.1.1 VOD and NDVI

This section discusses the spatial similarity between VOD and NDVI in terms of their representation of the overall land use. Figure 33 shows the Google Earth images of the *LSquare07* and *BSquare02* including some clearly detectable land uses. Most of the other areas are small agricultural fields with different crops. As the land use changes relatively fast in this region, the Google Earth image only gives a general idea of the land use. Figure 34 and Figure 35 show the comparison between NDVI and VOD on the example of *BSquare02* and *LSquare07*. Each figure includes an NDVI image, an image where the NDVI is overlaid by VOD contour lines with a difference of 0.001 and a VOD image.

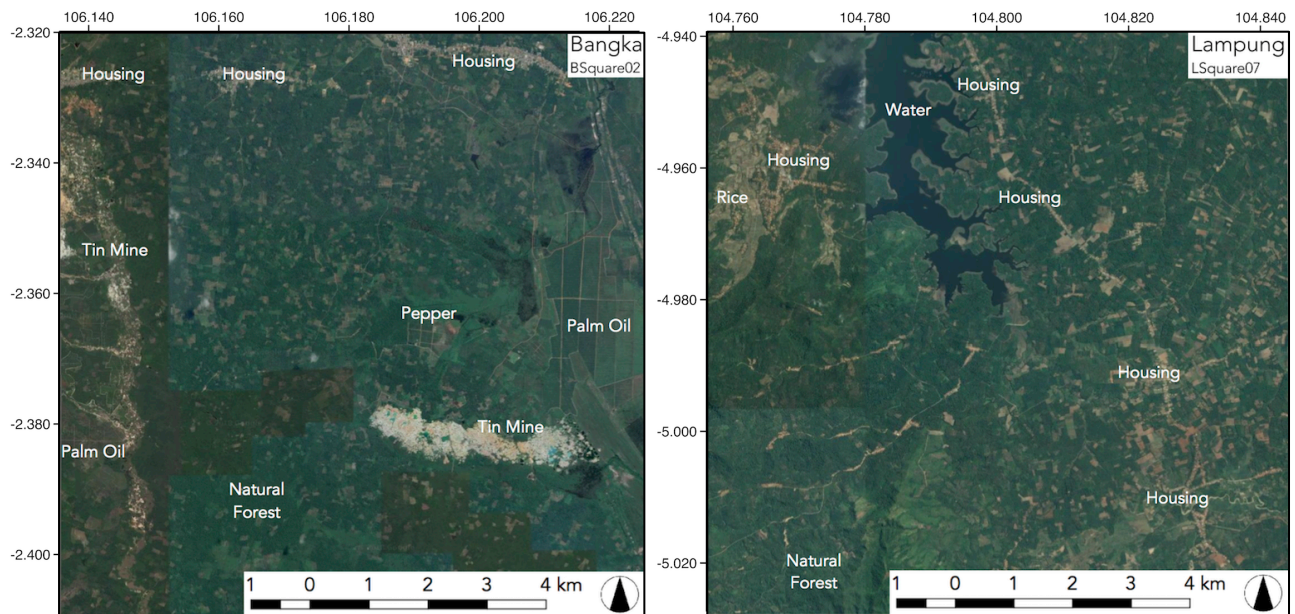


Figure 33: Google Earth image of *BSquare02* (left) and *LSquare07* (right)

As the NDVI is derived from the 10-m-resolution Sentinel 2 imagery, the spatial resolution is high enough to identify most of the land uses and even some fields. However, as mentioned in 4.3 the temporal resolution in this area is very low. Even the one-year-mean has gaps of the cloud mask in *LSquare07* (see white areas in the northeast in Figure 35). In *BSquare02*, the villages are characterized by bare soil and light vegetation. The tin mines contain bare soil, light vegetation and turbid water. The large palm oil plantation in the east is identifiable through the separation of rectangular streets with lower NDVI values. In *LSquare07*, the large water body in the north features clear and turbid water. The thin lines, appearing as lighter vegetation, represent streets with houses along them. The rice fields in the west, feature lighter vegetation.

The VOD has a much coarser scale with a pixel size of 100 x 100 m. It has to be considered that these images are aggregated over one year and do therefore differ from single day images. In section 4.3.2, VOD images

of single days are discussed. These images show that the values only have 2 decimals (see Figure 40). This leads to relatively large areas with the same value. However, each day, the footprints are located in different points. Therefore, other proportions of footprints are used every day to obtain the downscaled VOD of a certain pixel. Additionally, the sensor's inaccuracy of 1 to 2 K when measuring the brightness temperature contributes to inter-daily variations. In the moment, that a moving average is applied or an aggregated image over a certain period is generated as for this analysis step (see Figure 34 and Figure 35), the larger homogeneous areas of the single day images become more heterogeneous and gradients become smoother as mean values have more than 2 decimals. Therefore, in both locations, water surfaces, like the tin mines are clearly detectable by lower VOD values. In *BSquare02*, the VOD seems to capture gradients of denser vegetation, such as the natural forest, to lighter vegetation, like the tin mine. Remarkable is the gradient from west to east in *LSquare07*, which prevails regardless of actual differences in vegetation density.

The comparison of the different VOD images with their corresponding NDVI image shows the difference between the two locations. In *BSquare02*, the contour lines mainly match the variation in vegetation greenness of the NDVI. Especially, the shape of the high density NDVI in the mid-south-west is very similar to the gradient in VOD values. An exception is the north-eastern corner, which shows the lowest values in VOD but not in the NDVI. The slight mismatch between the two images could be partly originated by a different spatial distribution of leafy vegetation (sensitivity of NDVI) and of woody vegetation (sensitivity of VOD).

In *LSquare07*, the VOD contour lines barely match differences in NDVI. The gradient from west to east seems to be dominant over small variations. The presence of the water body could contribute to this effect. Moreover, to understand the performance of VOD in Lampung, a second square (*LSquare04*) is analysed. The results are shown in the Appendix 8.2. In this example, the horizontal gradient is not present but there is a wave-shaped gradient, which is caused by the border of a swath. To avoid these patterns, images including a swath edge should be excluded.

The results suggest that the NDVI represents the land use properly. However, to produce satisfactory results, images over extremely long periods have to be aggregated due to the high cloudy cover. The VOD in turn does not face these temporal issues, but has a lower spatial resolution. Temporal aggregation leads to a smoother gradient and also a slight heterogeneity. Important to mention is, that the spatial performance of VOD varies per location. In the selected area in Bangka, VOD is very similar to NDVI, representing the land use properly. On Lampung, the VOD in the analysed area does not seem to capture spatial differences. Surface water bodies and swath edges seem to have a negative impact on the spatial performance of VOD.

### 5.1.2 Derivation of spatial characteristics of VOD of pepper fields

The two selected squares contain several pepper fields (see Figure 34 and Figure 35). As mentioned in 5.1.1, the spatial resolution of NDVI is high enough to identify some field shapes in general. For this reason, it is used as reference to see if the vegetation density from the fields is actually different to the surroundings, which is required to distinguish a pepper field in the VOD image. In *BSquare02*, *BPepperField01* is not distinguishable, as it only exists since 2017. *BPepperField02* and *BPepperField03* have partly different NDVI values compared to the surrounding, but are not homogenous within the same field. *BPepperField04* is clearly distinguishable due to its size. In Lampung, all fields exist since 2012 or earlier. However, the pepper plants in these fields are supported by trees. For this reason, they only differ slightly from their surroundings. The VOD does not allow for a detection of smaller fields. This is to be expected since the small fields only have a weak contrast in the higher-resolution NDVI. Possible explanations are similar surrounding vegetation density, the coarse resolution and the previously mentioned slight heterogeneity caused by temporal aggregation. Only the 36-ha-large *BPepperField04* is clearly recognizable in the VOD image.

Summarizing, most of the fields do not have different spatial characteristics of VOD compared to their surroundings. This is caused by a combination of field size, coarse resolution, similar surrounding vegetation density, heterogeneous VOD and the radius of influence. Only the pepper field of 36 ha size is detectable.

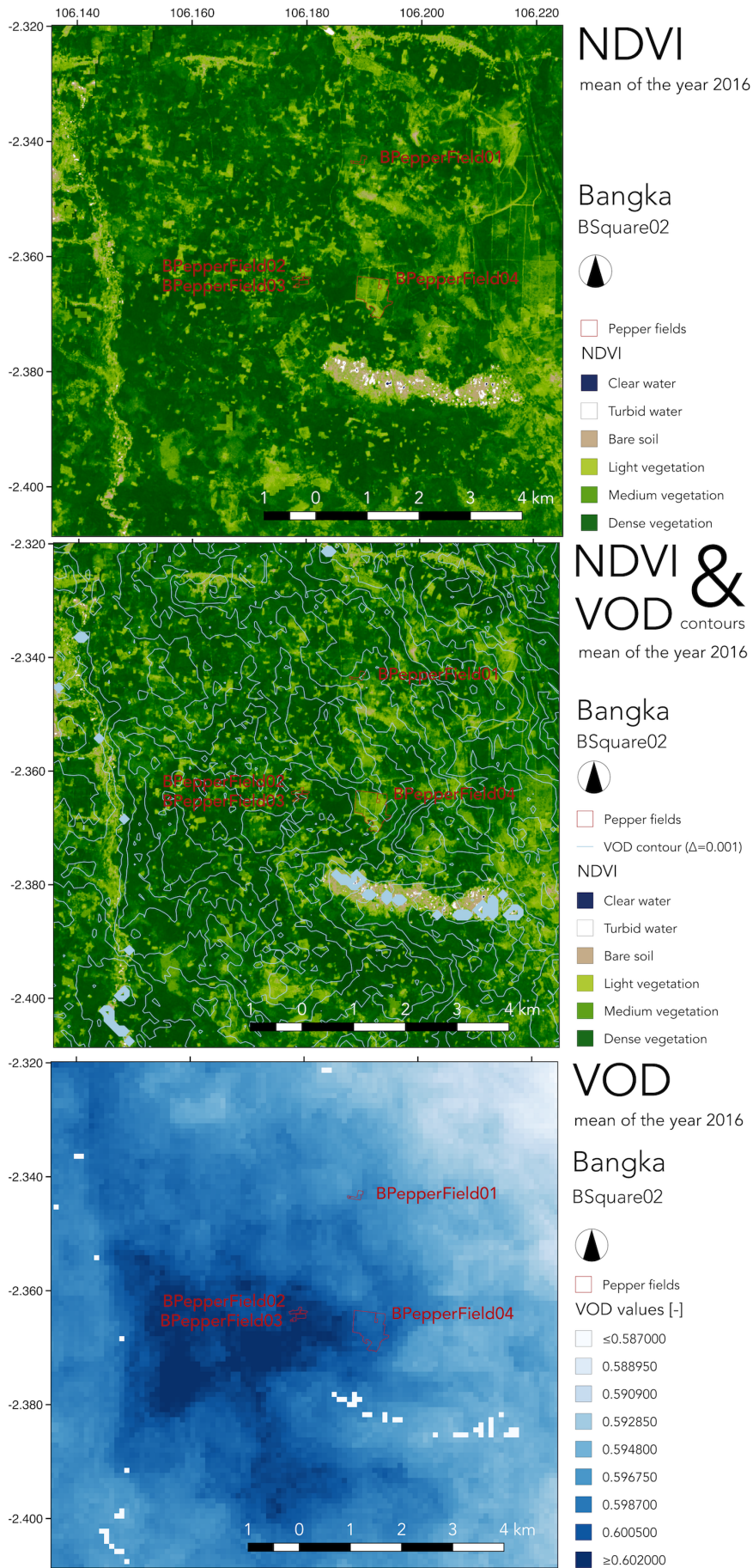


Figure 34: Mean NDVI (top), mean NDVI with VOD contours (middle) and mean VOD (bottom) of 2016 of BSquare02

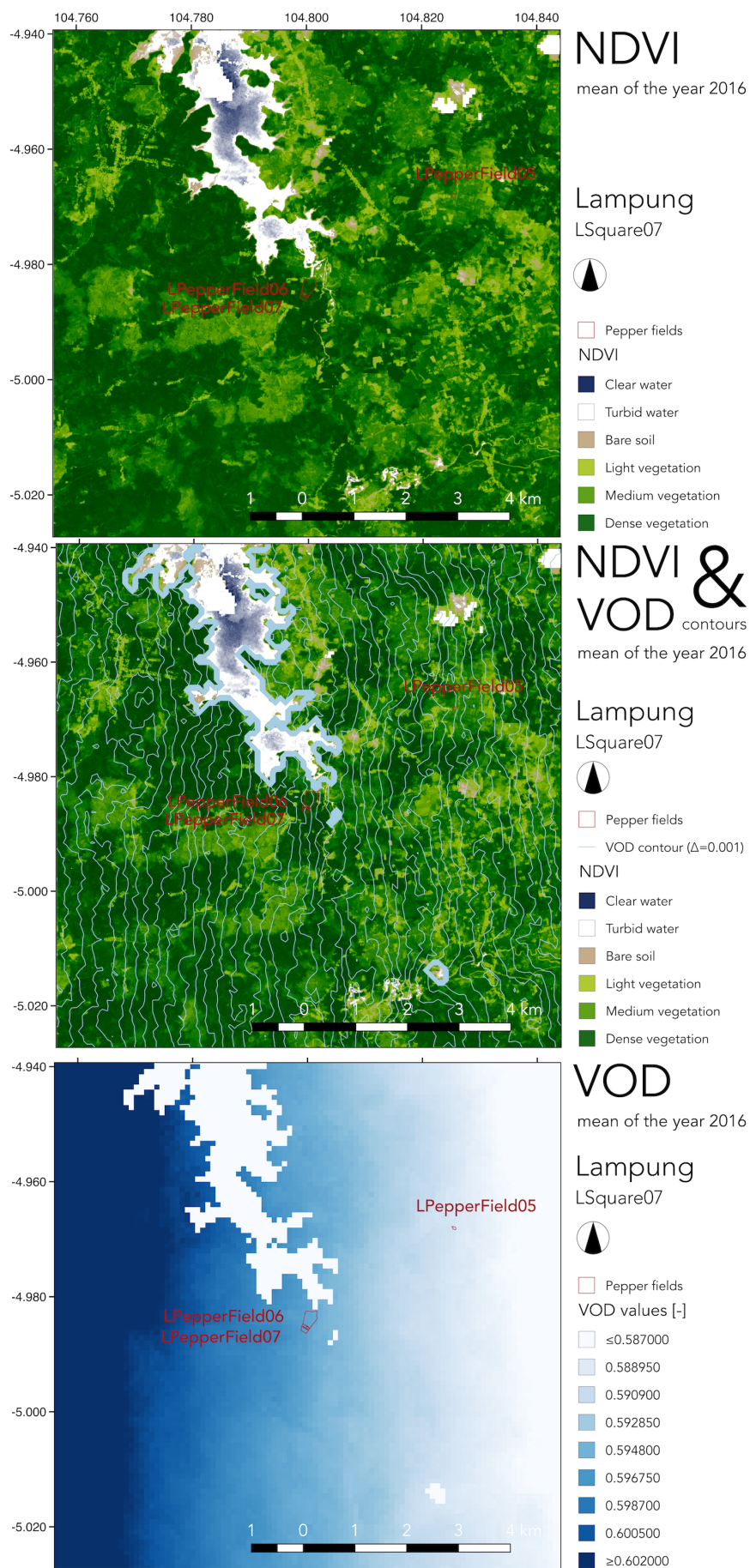


Figure 35: Mean NDVI (top), mean NDVI with VOD contours (middle) and mean VOD (bottom) of 2016 of LSquare07

### 5.1.3 Spatial changes in large-scale VOD over time

This section gives further information on the spatial patterns of large-scale VOD during a drought. This can help in assessing, whether large-scale VOD can be used to describe droughts in pepper fields. Figure 36 shows the 4-monthly VOD anomaly before, during and after the drought of 2015 in *BSquare02* and *LSquare07*. The anomalies are given as a percentage of the normal year 2016. Each plot has a different scale. The mean, minimum and maximum value per image are summarized in Table 9.

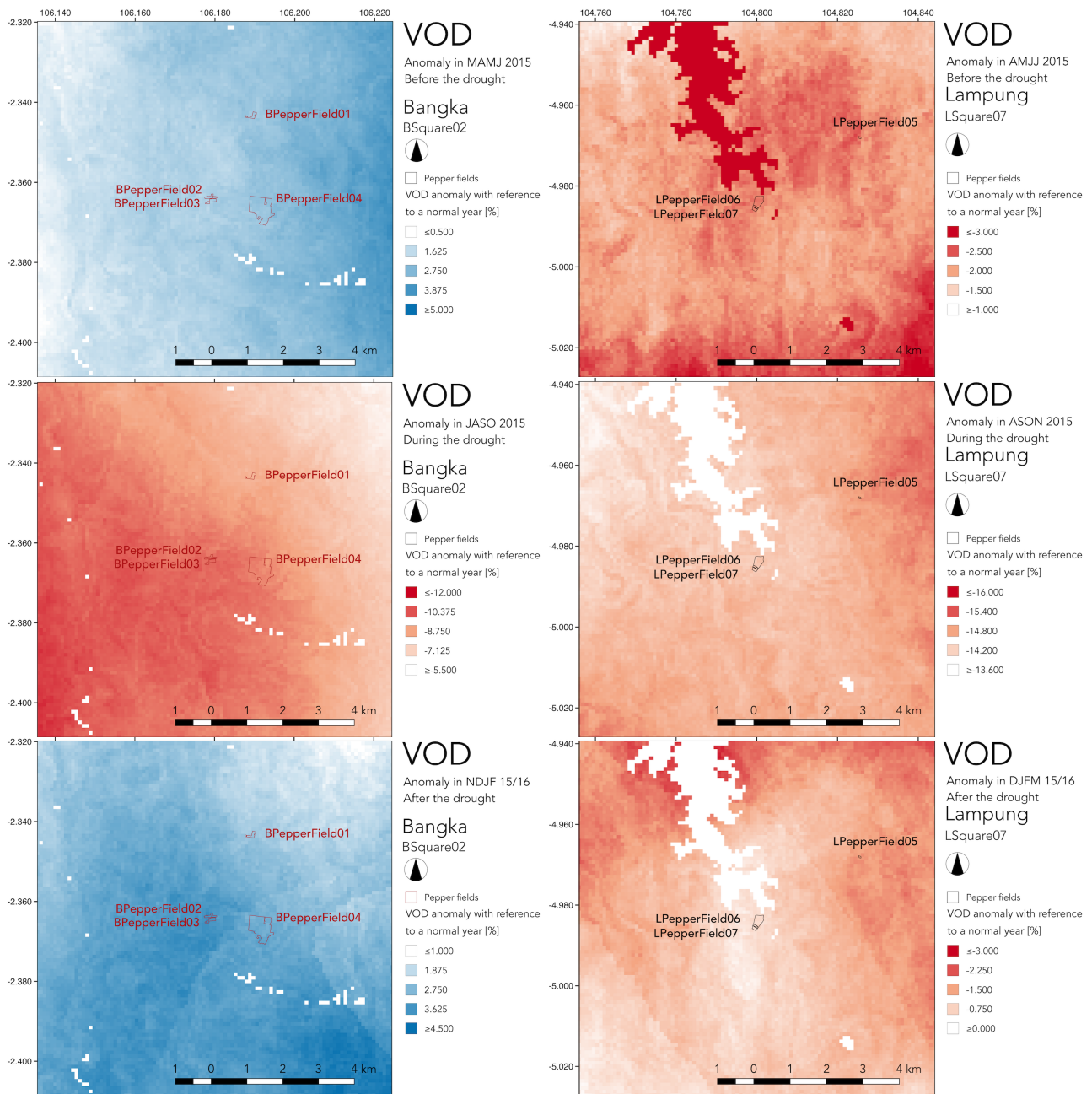


Figure 36: 4-monthly VOD anomaly before, during and after the drought in *BSquare02* (left) and *LSquare07* (right)

Table 9: Mean, min and max anomaly before, during and after the drought in 2015 with reference to the normal year 2016

Area	Before			During			After		
	Mean	Min	Max	Mean	Min	Max	Mean	Min	Max
BSquare02	+2.2%	+0.4%	+4.1%	-9.0%	-11.6%	-5.7%	+3.0%	+0.8%	+4.6%
LSquare07	-2.2%	-3.0%	-1.1%	-14.1%	-15.3%	-13.6%	-1.2%	-2.7%	-0.1%

In *BSquare02*, on average the anomalies develop from +2.2% before the drought, to -9.0% during the drought and then back to +3.0% after the drought. The percentages within the same image vary within a range of 3.7 points before, 5.9 points during and 3.8 points after the drought. These are relatively large variations within the same image considering the difference between a non-drought and a drought situation is only a 6-point difference. During the drought, the highest differences are in the southwest. In this same area, the VOD reaches the highest values after the drought. In the north-east, the VOD anomaly during the drought is lower. Nevertheless, after the drought the VOD anomaly does not reach as positive values as in the southwest. These anomalies are based on one normal year only. Ideally, the anomaly should be based on the mean of all non-drought years between 2012 and 2018. This means that the sign of the values closer to zero should not be over-rated as they could still be part of a negative anomaly if the non-drought mean would be slightly different. Together, the three images of *BSquare02* indicate that the drought in the southwest is stronger and concentrated over a short period whereas in the northeast it is less strong but spread over a longer period.

In *LSquare07*, the anomalies develop on average from -2.2% before the drought, to -14.1% during the drought and then back to -1.2% after the drought. And the percentages within the same image differ within a range of 1.9 points before, 1.6 points during and 2.6 points after the drought. The smaller differences within the same image lead to a more homogeneous pattern for the three periods. Interestingly, the pattern observed in the one-year aggregates disappears in the anomaly. However, a new pattern of diagonal edges with strong contrasts becomes visible in both locations for the period after a drought. This could be caused by the shape of the physical temperature distribution, which is used for the VOD retrieval in the LPRM (see 2.3.2.6). The temperature is based on a higher frequency with smaller footprints and, thus, less overlap. These edges could also be caused by swath edges.

This analysis shows that spatio-temporal characteristics can vary within a square of 10 x 10 km. For this reason, the following temporal analysis (in 5.2) is conducted on the fields rather than on the large squares.

## 5.2 Temporal patterns

### 5.2.1 Effect of applying a moving average or temporal aggregation

For the temporal analysis, it should be considered, that the used VOD data set is a moving average. For the comparison of VOD with other drought indicators, the time series is even aggregated to monthly data. As explained in 5.1.1, the varying position of the footprints and the sensor uncertainty lead to inter-daily VOD fluctuations, which are shown in the example time series of *BPepperField06* in Figure 37). By taking the moving average of 20 days, on which this entire analysis is based, this effect smoothens.

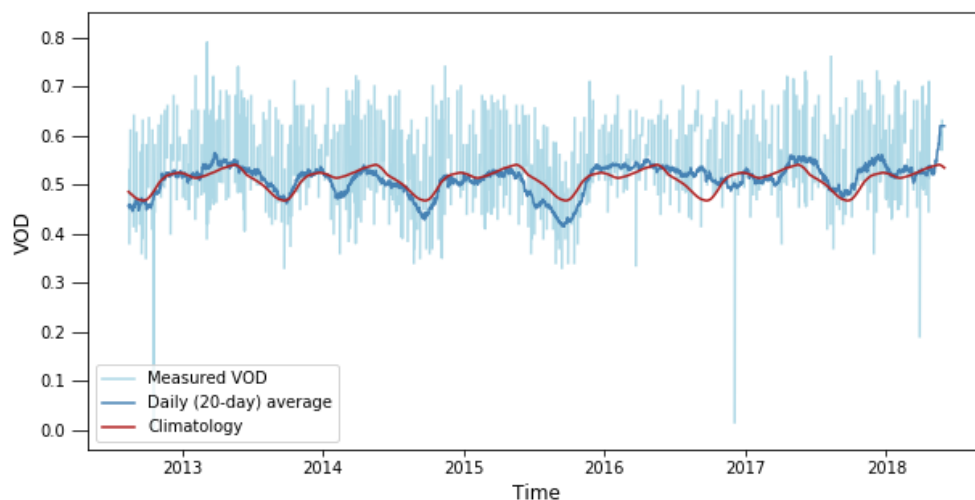


Figure 37: VOD (X-Band) time series of *BPepperField06* – raw data, moving average and climatology

### 5.2.2 VOD trends

The de-trending of the VOD time series for the different fields results in decreasing trends in some areas and in increasing trends in other areas. Especially in Bangka, all fields show an increasing trend and in Lampung they show between almost no trend and a decreasing trend (see Table 10).

Table 10: Increasing or decreasing trends of the VOD anomaly time series per pepper field

Location	Field/Square number	Anomaly trend of <i>PepperField</i>	Anomaly trend of <i>Square</i>
Bangka	01	0.00001146	0.00001142
	02	0.00001164	0.00001198
	03	0.00001197	0.00001198
	04	0.00001075	0.00001180
	05	0.00001282	0.00001478
	06	0.00001002	0.00000958
	07	0.00001129	0.00001089
	08	0.00001542	0.00001441
	09	0.00000838	0.00001015
	10	0.00000843	0.00001015
Lampung	01	-0.00000194	-0.00000325
	02	-0.00000030	-0.00000125
	03	-0.00000052	-0.00000114
	04	-0.00000027	-0.00000114
	05	-0.00000793	-0.00000519
	06	-0.00000865	-0.00000558
	07	-0.00000865	-0.00000558

The most probable reason for the decreasing trends in Lampung is the rapid rate of deforestation in the region stated by Hansen (2013) (see 4.4.2). Apart from the yearly decreasing rate given for each year from 2000-2017, the Hansen maps also show an increase in forests. However, the increase is given as one value from the period 2000 to 2012. Thus, the analysed period for this study is not included. For this reason, a net increase or decrease per location cannot be calculated. Nevertheless, according to the Hansen maps, in the period from 2000 to 2012, the forest cover gain in Bangka was much higher than in Lampung. Probably, this trend could have been similar to the period from 2012-2018 of the present study. Possible reasons for increasing trends on Bangka are re-growing plantations such as palm oil or rubber replacing previously burned areas for agriculture. In Lampung, there are several areas that are under protection where deforestation is prohibited. However, the exact location of these natural reserves is not known. Nevertheless, this could explain the lack of trend in certain time series.

### 5.2.3 Derivation of temporal characteristics of VOD of pepper fields

Overall, the absolute VOD values in Bangka and Lampung are quite similar. The mean of the means of the time series per pepper field in Bangka is 0.5660 ( $\sigma$ : 0.0327). In Lampung, the mean VOD value is 0.5661 ( $\sigma$ : 0.0375). The pepper fields in Lampung have a higher vegetation cover, as the supporting life trees had either a large canopy or the pepper plants were very dense. The VOD does not seem to saturate in this area.

For a better understanding of the VOD, the anomalies for pepper fields are compared to the anomalies of the surrounding 100 km<sup>2</sup>-sized squares. Results are shown in Appendix 8.3.1. Four example fields are selected: *BPepperField02* and the large industrial *BPepperField04* in Bangka as well as *LPepperField03* and *LPepperField07* in Lampung. *BPepperField02* exists since 2014, *BPepperField04* since 2015, *LPepperField03* since 2014 and *LPepperField07* since 2002 (see Figure 38). Visually, in most cases, like *BPepperField02* and *BPepperField04*, the differences are around  $\pm 0.005$ . This corresponds to 5 to 10% of the field anomalies. The exact percentages are shown in each plot. These are higher due to the offsets in the time series, which are discussed later. The difference is caused by a different magnitude of values and not by a time lag.

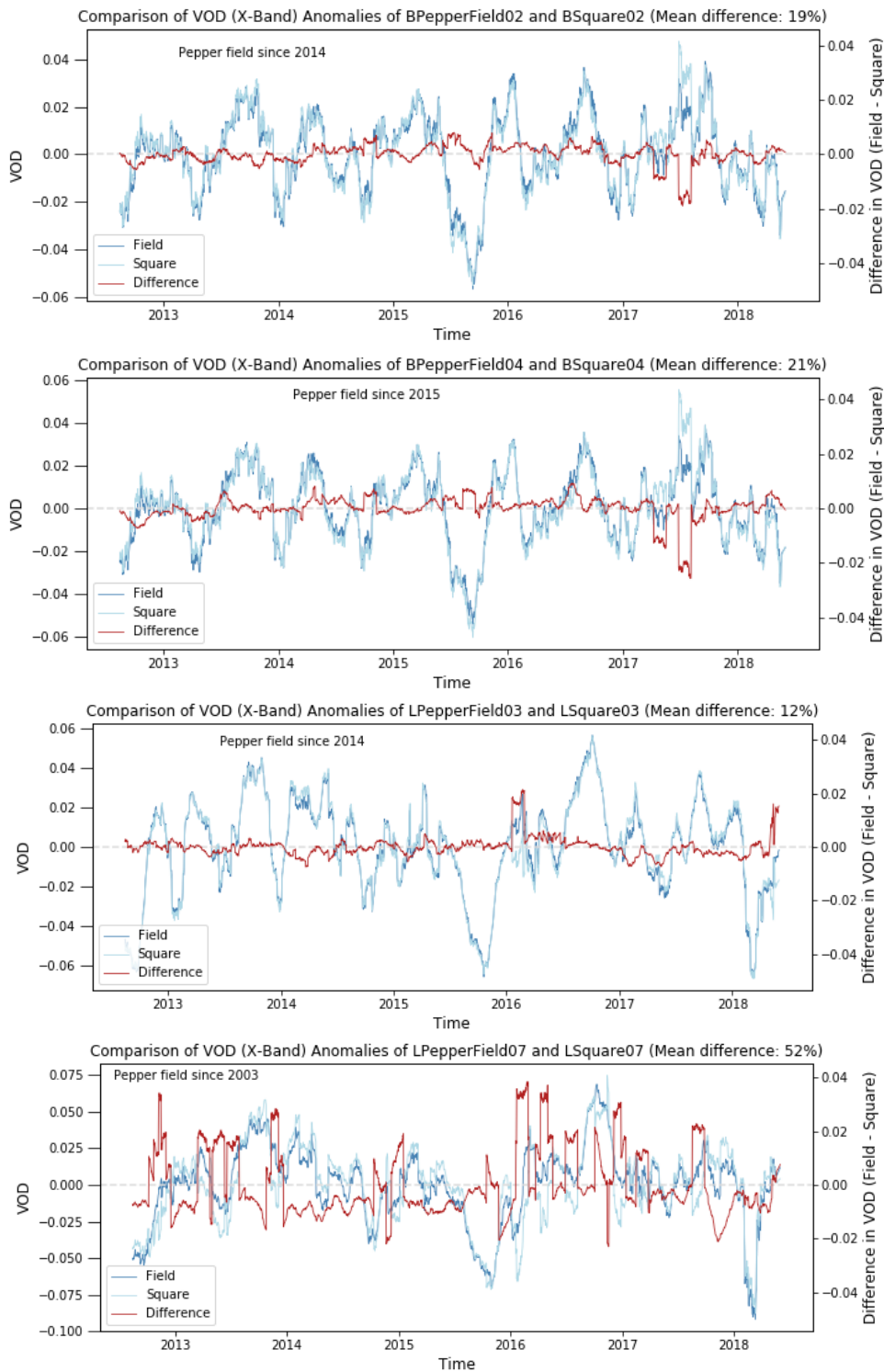


Figure 38: VOD anomalies of fields and squares in *BSquare02*, *BSquare04*, *LSquare03* and *LSquare07*

On Bangka, the fields exist since recent years. This helps to compare the difference between before and after their existence. However, the difference plots are equally irregular before and after the existence of the pepper fields. In most cases, the prior land use was natural forest, which would react differently than the less dense pepper fields. However, detailed land use maps of prior moments in time would be useful here. Not even the large *BPepperField04* is different before and after its existence.

The largest deviations are in *LSquare05*, *LSquare06* and *LSquare07*. All these fields exist since the beginning of the time series or even before. Therefore, it is difficult to make this comparison. These three fields are all located almost within the same square including a large water body (see Figure 32). If the exact boundary of

the surface water or its temperature is not known, errors are introduced in the downscaling method. Possibly, this is the reason for the larger variation over time of the square compared to the pepper field. Slightly smaller disparities are visible in *LPepperField02*, *LPepperField03* and *LPepperField04*. These three fields are all in the same area, which contains a large amount of pepper fields. For this reason, the surrounding is slightly more homogeneous and similar to the field itself.

There are several factors influencing the temporal changes of the value of a single pixel. In the first place, the value is influenced by the variations of aboveground biomass amount. Furthermore, the downscaled pixel value is obtained by combining the data of several footprints. This leads to a radius of influence of several kilometres for a single pixel. The accuracy of this downscaling method is unknown. Thus, also changes in the surrounding impact on the anomaly of the single pixel. Next, as explained in section 5.2.2, the varying composition of the downscaled pixel value and the sensor uncertainty lead to unnatural inter-daily variations in the VOD. By taking a 20-day moving average, the impact on the time series is reduced but not eliminated. In this part of the analysis, the anomaly of a field, which is composed by a few pixels, is compared to the anomaly of a large surrounding, which contains a much larger number of pixels, that are all influenced by these different factors. This means that there is evidently a difference between the anomalies of the pepper field and the anomalies of the square. However, this cannot be attributed only to the actual differences in land use because there are too many factors influencing the downscaled and averaged value of a pixel.

To see whether there is a relation between the  $VOD_{\text{Difference}}$  and the  $VOD_{\text{Square Anomaly}}$ , scatterplots are produced separating the data in before and after the pepper field existence (see Appendix 8.3.2). However, these plots do not reveal a meaningful relationship.

In several of the plots there are offsets present, like in mid 2017 of *BPepperField02* and *BPepperField04*. These offsets are caused by the anomaly time series of the squares. In Bangka, the offsets are negative, meaning that suddenly the square has a more positive VOD anomaly than the field. In Lampung, the offsets are positive caused by a sudden negative anomaly of the square of a less positive anomaly than in the field.

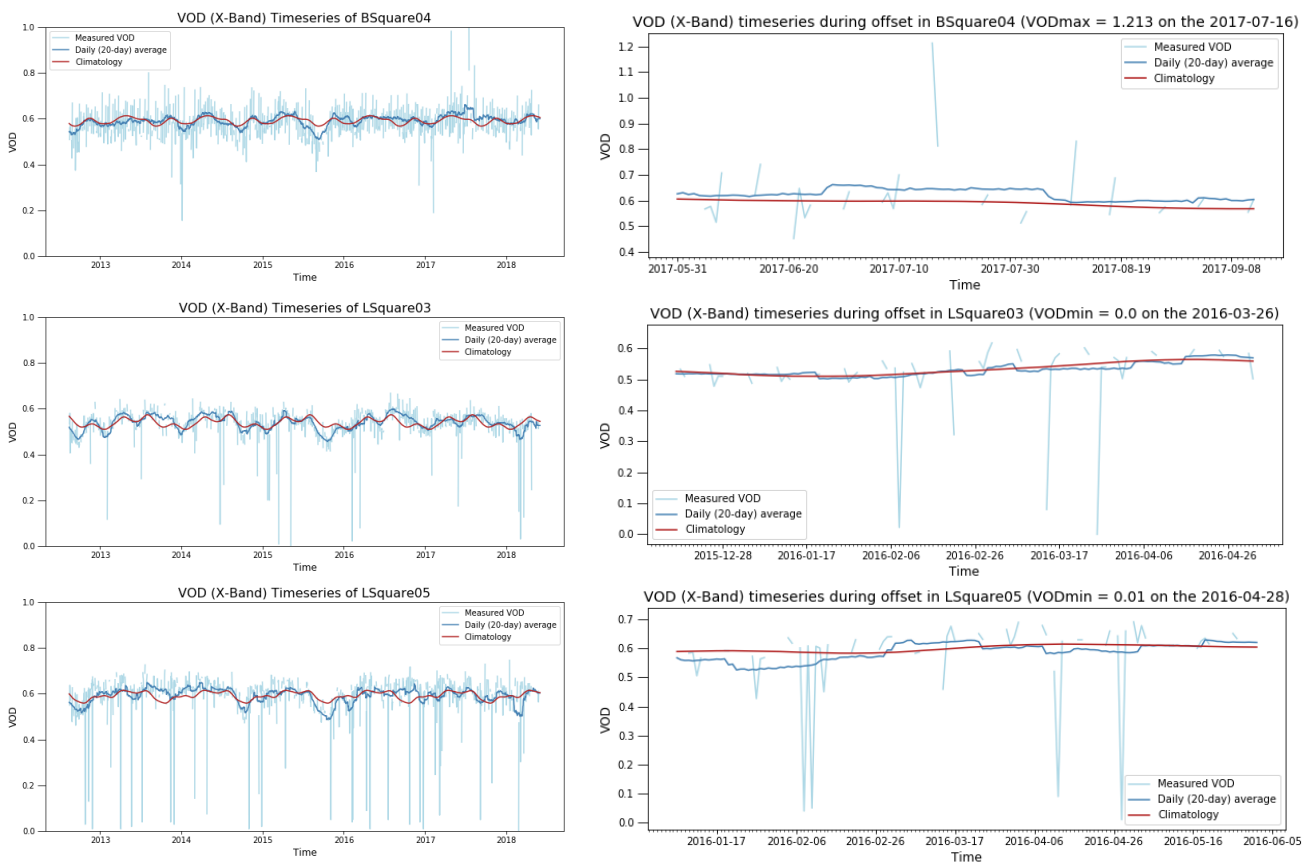


Figure 39: VOD time series of selected fields in the entire period (left) and a selected period during the offset (right)

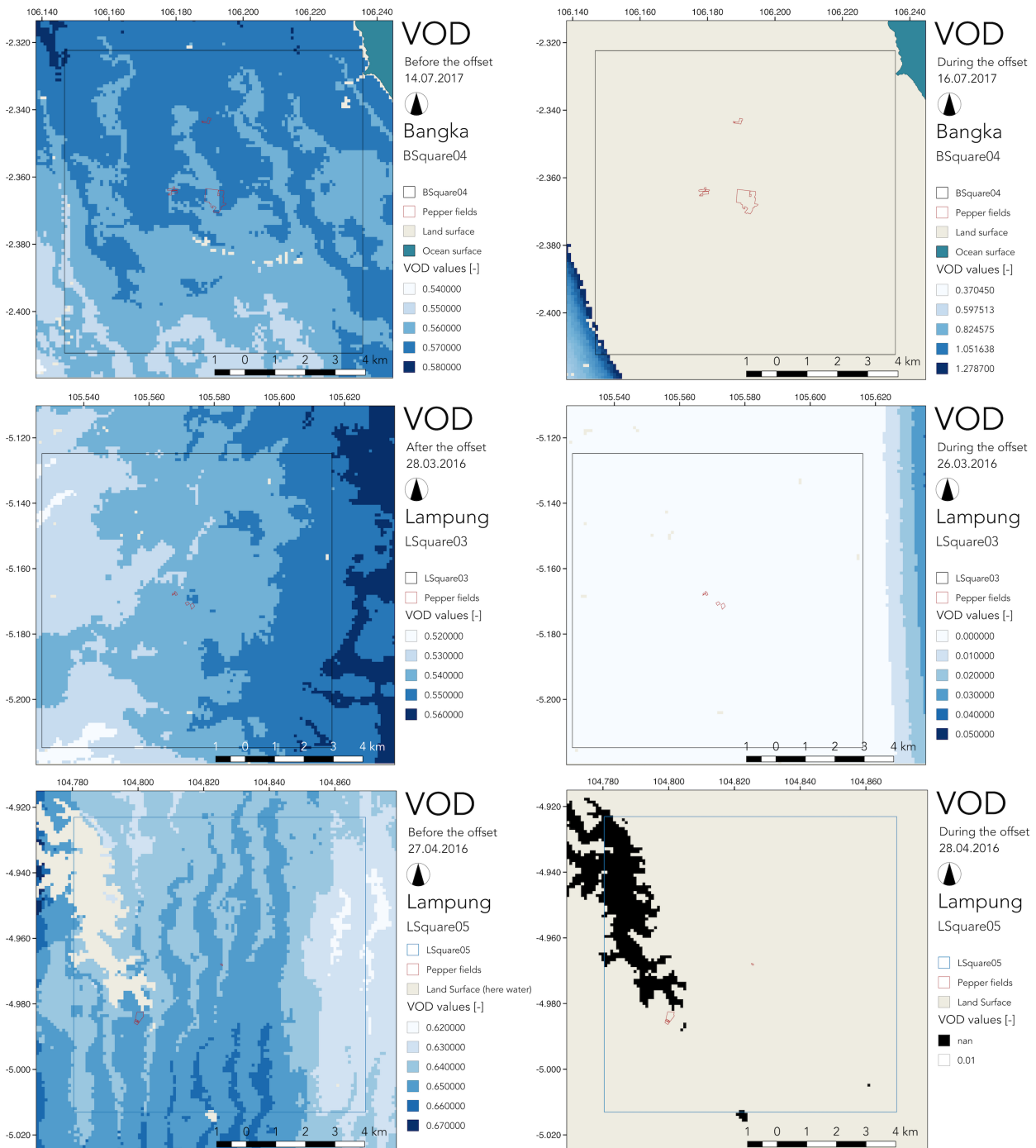


Figure 40: Spatial VOD images before or after and during offset of selected fields

To obtain an insight to these offsets, the periods when these offsets occur are extracted in the time series of the VOD (see Figure 39). Here, the effect of an extreme peak on the 20-day moving average becomes visible. In order to see the difference between these peak days and a normal day, the individual VOD images are shown in Figure 40. These images show that there are several kinds of errors generating the observed offsets. In the case of *BSquare04*, it appears that the coastline is shifted on the day of the offset with some very high VOD values at the boundary. As a consequence, only very few and high value pixels are counted as part of the mean as the rest has no value as it is counted as water surface. This results in a very high mean value. The fields on this day do not have a value at all and are, therefore, filled by the normal values through the moving average in the time series. In the case of *LSquare03*, on the day of the offset, most of the square contains zero values. In the east, there is a deep gradient towards higher VOD values. In this area, there are

no large surface water bodies in the surrounding. In *LSquare05*, during the offset, the land surface seems to have no values and the water body a nan-value. For a certain reason, the mean value of that day is 0.01 although no pixel is visible with this value. In the three cases, the reasons of the error occurrence are unknown. Further investigation is needed.

Summarizing, the anomalies of the pepper fields are different to the anomalies of their surroundings. However, this cannot be attributed only to the actual differences in land use as there are too many factors influencing the downscaled and averaged value of a pixel. The differences seem to be generated by the fact that, when comparing pepper fields to the squares, two different groups of pixels are compared that are influenced by the following factors. First, the values vary with the actual changes of the aboveground biomass in the square but also of the surrounding because the downscaling method leads to a radius of influence of several kilometres. Second, the values fluctuate on a daily basis due to the varying location of the footprints leading to a different composition of footprints for the same pixel on different days. This is confirmed by the fact that the irregular differences are also present for the period before the area was a pepper field. Fields with rather homogeneous land use in the surroundings have a smaller difference as the surrounding on average might react more similar to the small pixel. This analysis reveals the existence of different errors that lead to offsets in the normal VOD time series and propagates to the anomalies. However, the reason for the occurrence of these errors is unclear

#### **5.2.4 VOD, NDVI and other drought indicators**

The aim of this analysis is to compare the indicators of the El Niño Southern Oscillation (ENSO) and the Indian Ocean Dipole (IOD) as well as the meteorological drought indicator Standardized Precipitation Evaporation Index (SPEI) to the VOD data. To put this comparison into context, the same indicators are compared to the Normalized Difference Vegetation Index (NDVI), which is often used as a comparable tool to VOD. For these correlations, it should be kept in mind that VOD and NDVI are independent datasets. The VOD is a measure of aboveground biomass and its water content. For this reason, it measures the response of the vegetation to the hydrological conditions such as precipitation, temperature or groundwater storage. The VOD anomalies are hence expected to be correlated to the anomalies of the tested indicators but not to 100%. Vegetation does not fluctuate as fast as precipitation does for example. The vegetation is capable of buffering extreme conditions to a certain extent. This buffer represents the added value that VOD gives over the ENSO, the IOD or the SPEI. This part of the study aims at verifying the existence of this added value.

##### **5.2.4.1 Overview of correlations with other indices**

Table 11 summarizes the Pearson and Spearman correlations  $r$  of other indicators with VOD. More specifically, it shows the mean and the standard deviation of all analysed fields per location (Bangka or Lampung). Furthermore, the amount of statistically significant results is given per location and indicator. Analogically, Table 12 compares the results between the NDVI and other indicators.

Field-specific Pearson and Spearman correlations with VOD are shown in Figure 41. In these plots, statistically insignificant results ( $p > 5\%$ ) are set to zero. These spider plots show if the degree in correlation is similar for all indicators within the same field. Based on these two figures, fields are selected to further discuss the individual indicators in the following sub-chapters. All anomaly plots are shown in Appendix 8.4.1.1, 8.4.2.1 and 8.4.3. The correlations of VOD and NDVI with the ENSO and the IOD are calculated with the time lag that results in the highest correlation. The relation between lag time and correlation coefficient for the ENSO are shown in Appendix 8.4.1.2 and 8.4.1.3 and for the IOD in Appendix 8.4.2.2 and 8.4.2.3.

For all indicators, the Pearson correlation is similar to the Spearman correlation (see Table 11). This means that the variables are linearly related. If Spearman would be much higher than Pearson, the relationship would rather be non-linear.

When comparing the correlations of other indicators with VOD (Table 11) with the correlations of other indicators with NDVI (Table 12), it stands out that overall correlations with NDVI are lower and fewer correlations are statistically significant. This is most probably linked with the cloud cover in this area as seen in the spatial analysis. The NDVI used for the temporal analysis is taken from MODIS, which has an integrated way of compensating the cloud cover (see 4.2.2). However, if the cloud cover is too high there might not be enough data available to compensate for the high cloud cover. Furthermore, extremely high aerosol concentrations that often occur during peat fires in extreme droughts can impede a proper representation of the actual state through NDVI (see 3.1.1.2). The saturation of NDVI at high vegetation intensity could possibly also contribute to difficulties in representing the high NDVI peaks and leading to lower correlations.

Figure 41 shows that, in Bangka, Fields 01 to 04 have lower Pearson correlations than Fields 05 to 10. These four fields are all on the same spot in Bangka. Here, the fields might have a higher resistance to droughts, either through higher groundwater levels, higher soil moisture or more drought-resistant vegetation. The difference in correlation between Fields 05 to 10 to Field 01 to 04 for the ENSO and the IOD is much higher than for the SPEI. This could indicate that in the area of Field 01 to 04 the precipitation is influenced more by other phenomena than the ENSO and the IOD. In Lampung, the correlations are relatively homogeneously distributed over the different fields.

Table 11: Summary of correlations between VOD anomalies and other drought indices

Index		Pearson			Spearman		
		Mean correlation $r$	$\sigma$ of correlation	Amount of fields with $p < 5\%$	Mean correlation $r_s [-]$	$\sigma$ of correlation [-]	Amount of fields with $p < 5\%$
ENSO (MEI)	Bangka	-0.50	0.22	10/10	-0.58	0.04	6/10
	Lampung	-0.40	0.05	7/7	-0.35	0.06	7/7
IOD (DMI)	Bangka	-0.37	0.09	9/10	-0.36	0.07	6/10
	Lampung	-0.57	0.04	7/7	-0.53	0.06	7/7
SPEI (long)	Bangka	0.58	0.12	10/10	0.53	0.11	10/10
	Lampung	0.34	0.04	7/7	0.32	0.08	7/7
SPEI (short)	Bangka	0.45	0.10	10/10	0.49	0.05	6/10
	Lampung	-	-	0/7	-	-	0/7
NDVI	Bangka	0.31	-	1/10	0.30	-	1/10
	Lampung	0.30	0.02	4/7	0.26	0.02	4/7

Table 12: Summary of correlations between NDVI and other drought indices

Index		Pearson			Spearman		
		Mean correlation $r$	$\sigma$ of correlation	Amount of fields with $p < 5\%$	Mean correlation $r_s [-]$	$\sigma$ of correlation [-]	Amount of fields with $p < 5\%$
ENSO (MEI)	Bangka	-0.28	-	1/10	-	-	0/10
	Lampung	-0.43	0.06	4/7	-0.34	0.07	5/7
IOD (DMI)	Bangka	-0.30	0.00	2/10	-	-	0/10
	Lampung	-0.33	0.06	4/7	-0.37	0.03	3/7
SPEI (long)	Bangka	-0.28	0.00	2/10	-0.11	0.32	3/10
	Lampung	-	-	0/7	-	-	0/7
SPEI (short)	Bangka	-	-	0/10	-	-	0/10
	Lampung	-0.38	0.05	2/7	-0.42	0.03	2/7

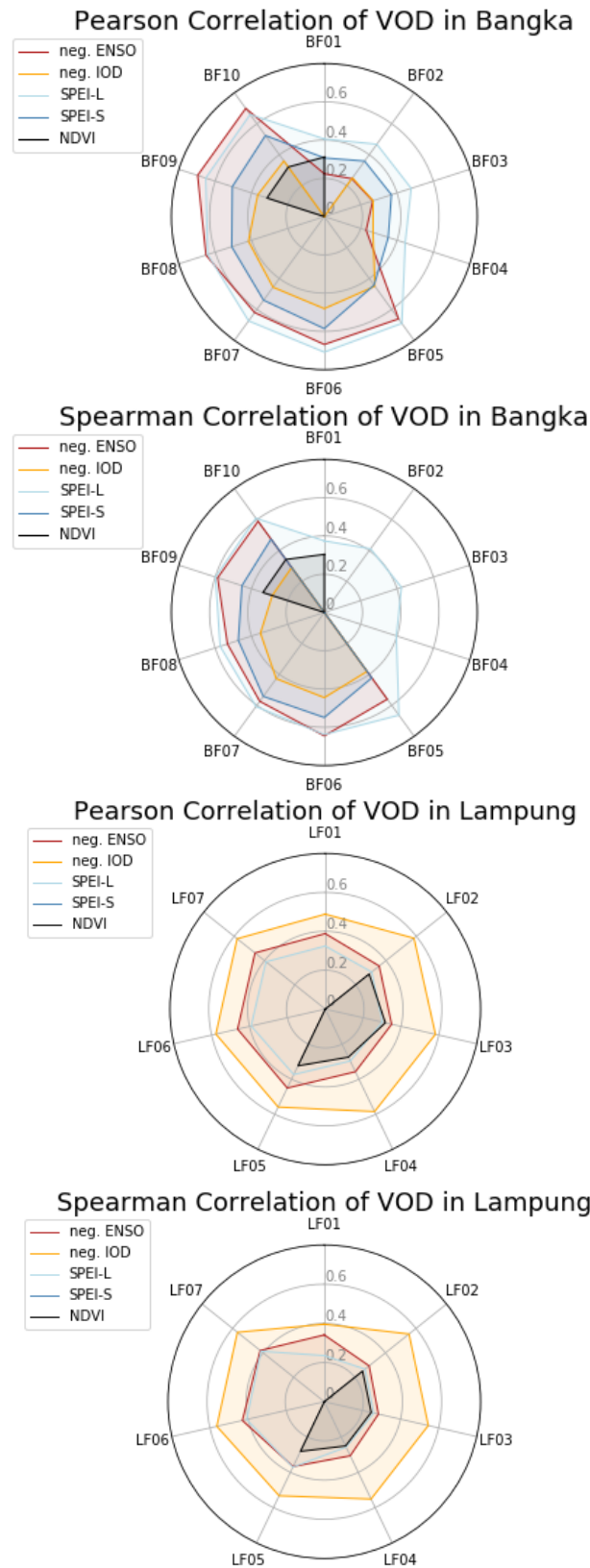


Figure 41: Field-specific Pearson and Spearman correlations of VOD and other drought indicators

The spider plots of the NDVI present mainly statistically insignificant results and are therefore not shown. In Bangka, Field 04 has a Pearson correlation of 0.3 and Field 09 and 10 have a correlation with the IOD of -0.3. On Lampung in Fields 02, 05, 06 and 07, Pearson and Spearman correlations with both the ENSO and the IOD are around -0.4.

#### 5.2.4.2 ENSO (MEI)

The Multivariate ENSO Index (MEI), which is a measure of the ENSO, is negatively correlated with the VOD and NDVI (see Table 11 and Table 12). This is to be expected as a high positive MEI value indicates an El Niño year in which droughts occur, meaning that the VOD (and NDVI) is probable to reach a minimum. It should be taken into account that ENSO (and IOD) are indicators of weather phenomena that influence the climate in the study area. Correlations only occur during extreme events such as ENSO maxima leading to precipitation deficit in the study area and generating an agricultural drought, which could then probably be seen in the VOD. In previous studies, the correlation for low ENSO and precipitation in the wet season has shown to be low (Hendon, 2003; Chang *et al.*, 2004). For this reason, correlations for ENSO should be interpreted with caution. The correlations between the VOD and the ENSO are between -0.22 and -0.70.

Figure 42 shows the anomaly time series of VOD, NDVI and MEI in selected fields in Bangka and Lampung. The ENSO anomaly time series presents one distinguishing large positive anomaly, which coincides with the drought of 2015/2016 found in literature and reported by the farmers during the field visit.

#### VOD and MEI

The time lag leading to the maximum correlation between the MEI and the VOD is between zero and six months (see Appendix 8.4.1.2 and 8.4.1.3). In some fields, the maximum correlation is very clear and in other fields there are two lag times that lead to similar results. The different lag times can be explained by the evolution of climate, or by different conditions such as soil moisture making some vegetation reacting slower to droughts or drought resistance of certain plants. In previous studies the ENSO has found to be related to droughts in Indonesia (Hendon, 2003; D'Arrigo *et al.*, 2008). The different time lags leading to maximum correlations indicate that the fields respond differently to the climate conditions related to the ENSO. This bears an added value of VOD over the ENSO.

*BPepperField04* is an example of a weaker correlation between VOD and MEI (Pearson: -0.23) and *BPepperField06* an example of one of the stronger correlations (Pearson: -0.67). The correlation in *BPepperField04* is calculated without a time lag, whereas *BPepperField06* gave a maximum correlation at a lag of 5 months. Even though the correlation with *BPepperField04* is very low, the extreme drought event of 2015 is captured by the VOD. *LPepperField03* is an example of a lower correlation between VOD and MEI on Lampung (Pearson: -0.28) and *LPepperField06* an example of one of the stronger correlations in Lampung (Pearson: -0.43). Also here, the representation of the drought in 2015 is rather similar.

In 2015, the positive ENSO peak matches the negative VOD peak. The VOD anomaly plots of Lampung, feature a negative peak, reaching almost the magnitude of the peak in 2015. However, the ENSO anomaly plot does not have a peak in this period. The VOD anomaly in 2012 could either be related to factors other than the ENSO or to faulty VOD data as the spatial analysis showed partly incoherent results in Lampung.

#### NDVI and MEI

The MEI of *BPepperField04* is statistically significantly correlated with the NDVI (Spearman: 0.28), whereas *BPepperField06* is not statistically significantly correlated. In general, the NDVI anomalies fluctuate much more. On one hand, this can be explained by the fact that NDVI is more sensitive to leafy part of the vegetation whereas VOD is also sensitive to the woody part of the vegetation and probably changes in leaves occur faster than in the woody parts. On the other hand, NDVI does not feature a clear pattern representing the drought. Of the 17 fields, only four (*BPepperField08*, *LPepperField05*, *LPepperField06* and *LPepperField07*) have a clear peak in 2015, which is much stronger than other peaks in the anomaly. This rather indicates that issues with cloud cover and aerosols lead to low NDVI data quality.

In short, VOD and ENSO anomalies have a correlation coefficient between -0.22 and -0.70. In all plots, the VOD anomalies represent the drought event of 2015, which is characterized by a strong positive ENSO anomaly. The negative VOD anomaly of 2012 in Lampung is not related to the ENSO. In contrary, there are only very few NDVI anomaly plots that have remarkably different patterns during the drought period.

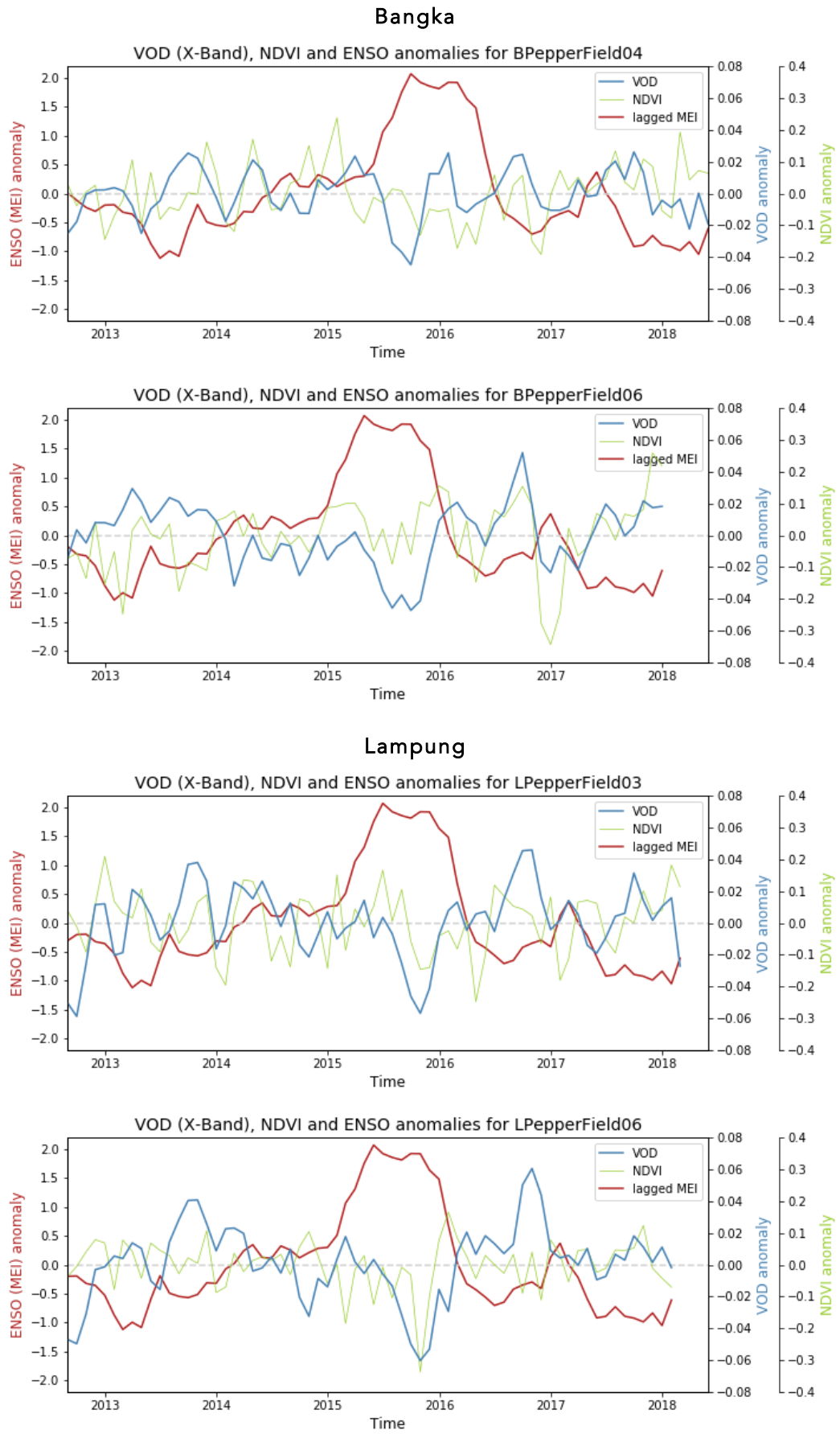


Figure 42: VOD, NDVI and MEI anomalies for selected Pepper Fields in Bangka (top) and Lampung (bottom)

### 5.2.4.3 IOD (DMI)

The DMI is a measure of the Indian Ocean Dipole (IOD). In analogy to the MEI, the DMI is negatively correlated with the VOD and NDVI (see Table 11 and Table 12). Also here, high positive DMI values lead to a lack of precipitation in Indonesia increasing the probability of agricultural droughts, generating low VOD and NDVI values. As explained in 5.2.4.2, the correlation between DMI and VOD or NDVI has to be interpreted with caution.

Figure 43 shows the VOD, NDVI and DMI anomalies of the same fields as in 5.2.4.2. The maximum correlation between the DMI and the VOD occurred with time lags between 0 and 3 months (see Appendix 8.4.2.2 and 8.4.2.3). The time lag is shorter compared to the one for the MEI-VOD correlations. A possible reason is the fact, that the Indian Ocean Dipole is concentrated on a smaller geographic area compared to the ENSO. Interesting to observe is that the DMI has several positive anomalies: one in the beginning of the time series, one in the period of the 2015/2016 drought and another one in 2017. The positive anomaly of 2017 follows on a period with a strong negative anomaly.

#### VOD and DMI

The correlation between VOD and DMI is between -0.25 and -0.58. *BPepperField04* has a correlation of -0.27 (Pearson), *BPepperField06* of -0.48 (Pearson) and *LPepperField03* as well as *LPepperField06* have a correlation of -0.58 (Pearson). Visually, the correlations in the different fields are quite similar (see Figure 43). The VOD has its strongest negative anomaly in 2015/2016, when a large positive DMI anomaly occurs. However, the larger positive DMI anomaly of 2017 is represented as a much less pronounced negative anomaly in the VOD. The anomaly plots in Figure 43 show that, in certain fields like *BPepperField04* there is almost no negative anomaly peak. In other fields like *BPepperField06*, *LPepperField03* or *LPepperField06*, there is a negative but smaller peak compared to 2015. The fact that the VOD does not show a strong decrease in 2017 is probably related to the prior negative IOD peak, which leads to above average precipitation. This can lead to a groundwater recharge in this period, which creates a buffer for the vegetation to resist below-average precipitation until a certain extent. This storage capacity can vary per location depending on soil characteristics and existing soil moisture or groundwater levels. For the positive IOD anomaly peak in the beginning of the time series, the period prior to the anomaly is not included in the analysis and no argument can be made in this context. Nevertheless, the fields in Lampung show a negative anomaly peak in the beginning of the time series that almost reach the magnitude of the anomaly in 2015. In Lampung, correlations between VOD and the DMI are stronger than between VOD and MEI, whereas in Bangka it is the opposite (see Figure 41). This could mean that the climate in Lampung is more influenced by the ENSO than by the IOD and in Bangka, the DMI has a stronger influence, which makes sense as Lampung is closer to the Indian Ocean, where the IOD takes place and Bangka is closer to the Pacific where the ENSO mainly takes place. This would be interesting to prove by cross comparing with the NDVI. However, the correlations are not sufficient to draw conclusions here.

#### NDVI and DMI

As explained in the comparison with the MEI, the NDVI anomalies in all fields, behalf of *BPepperField08*, *LPepperField05*, *LPepperField06* and *LPepperField07* do not show a significant decrease in 2015/2016. As a result, correlations are weak or statistically insignificant.

To sum up, VOD and DMI have correlations between -0.25 and -0.58. The strongest VOD anomaly occurs in 2015 simultaneous to a large positive DMI anomaly. The largest positive DMI anomaly occurs in 2017 just after a strong negative peak. However, the VOD anomaly in most fields does not have a strong negative peak in 2017. Probably, the prior above-average rainfall increased the groundwater levels and soil moisture, buffering the subsequent below-average rainfall. This storage capacity varies per location depending on soil characteristics. The VOD in Lampung appears to be more influenced by IOD whereas the VOD in Bangka seems to be more influenced by the ENSO, which is reasonable due to their location.

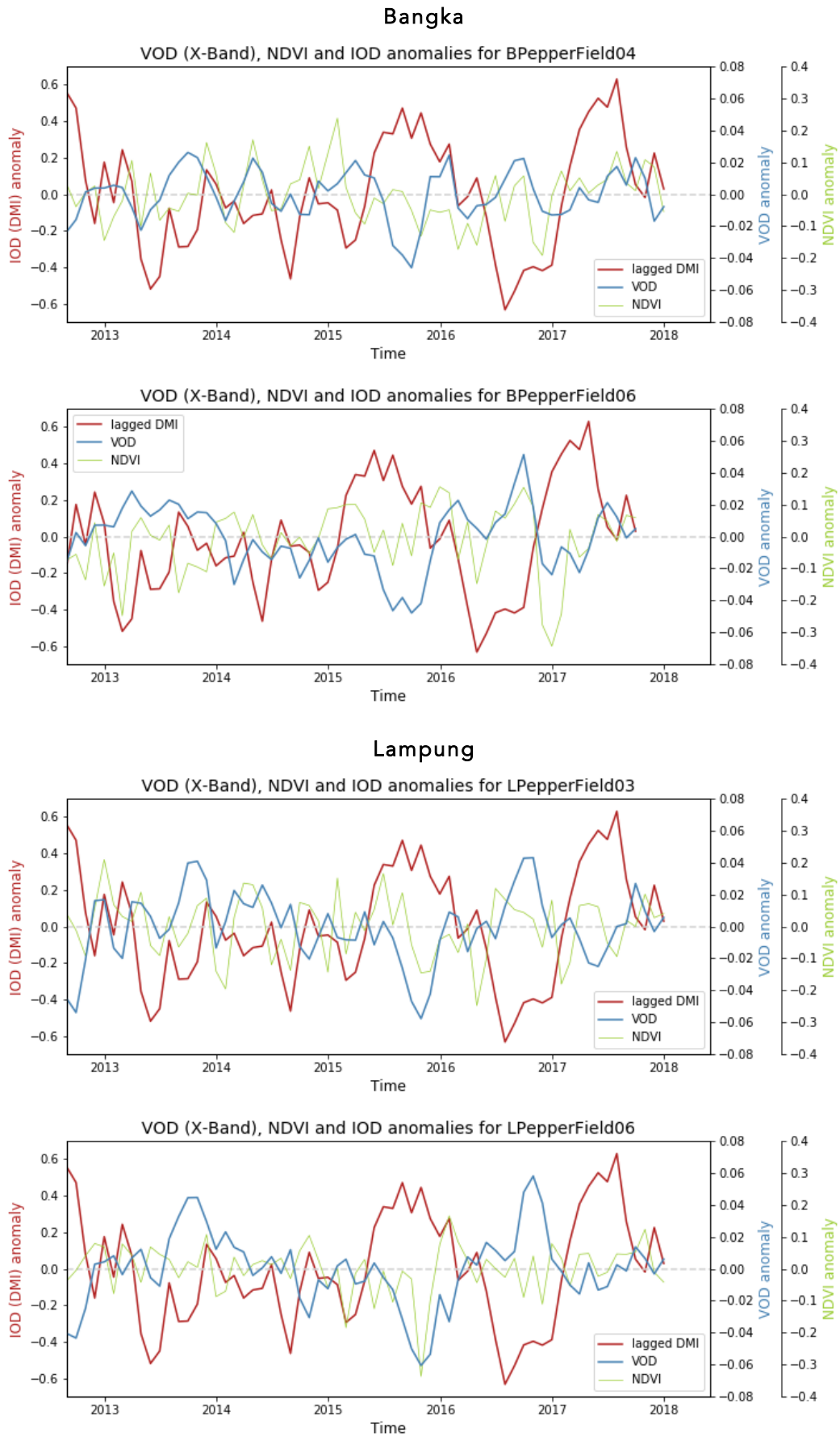


Figure 43: VOD, NDVI and IOD anomalies for selected Pepper Fields in Bangka (top) and Lampung (bottom)

#### 5.2.4.4 SPEI

The SPEI is an indication of water availability through the consideration of precipitation and evaporation (see 2.2.1.2). On the monthly time scale it monitors water storage, such as soil moisture, which responds quickly to precipitation anomalies. A higher SPEI means more rain and less evaporation, enhancing vegetation growth and leading to higher VOD and vice versa. Here, correlations are more relevant, because local precipitation is a more direct contributor to agricultural drought in a certain location than the global ENSO or IOD values. For this reason, the correlations are calculated without a time lag.

Figure 44 shows the anomalies of VOD, NDVI and SPEI in selected fields. It includes the revised and short SPEI time series as well as the long and unrevised SPEI time series. In Bangka, the two SPEI time series match relatively well with each other (Pearson: 0.83). However, in Lampung, the time series differ much more leading to lower correlations between the two SPEI datasets (Pearson: 0.12), especially in the period from mid 2012 to mid 2014. A possible explanation could be the different method to calculate the evaporation.

#### VOD and SPEI

Table 11 shows that overall correlations are significant but not high. This means, that also factors other than precipitation and evaporation influence the VOD. The correlations are positive, which is to be expected as explained earlier. The VOD anomalies and the long SPEI anomalies have a mean Pearson correlation of 0.48 for both provinces together and of 0.58 for Bangka only. The Pearson correlation coefficient between the VOD and the short SPEI is on average 0.45, which is composed by the values in Bangka only since all fields in Lampung give statistically insignificant results. This means that the correlations with the long SPEI are stronger although they are supposed to be less robust. Remarkably is the lack of statistically significant results of the correlation between VOD and the short SPEI index in Lampung. Despite the supposed higher data quality of the short time series, the shorter time series includes less extreme events. The time series ends in 2015 during the drought event. This explains lower or insignificant correlations for the short SPEI dataset. It would be interesting to compare the VOD to a longer revised SPEI time series to analyse the impact on the correlation. For the long unrevised SPEI time series, the correlations are stronger in Bangka than in Lampung. The mismatch between the two SPEI datasets could explain these results.

Figure 44 reveals two interesting points. First, in 2014, the negative anomaly of the short SPEI is much stronger than the one in 2015. However, similar to observations in 5.2.4.3, prior to 2014 there was a long period with positive SPEI anomalies. The negative VOD anomaly is not as pronounced as the one of 2015. Second, the negative VOD anomaly in 2015 appears a few months after it appears in both, the long and the short, SPEI. These two observations are probably caused by the buffer that the vegetation offers to climatic conditions and show the potential of the added value the VOD bares.

#### NDVI and SPEI

In comparison to the MEI and the DMI, the two SPEI datasets correlate much less with NDVI. This is due to the larger changes between minima and maxima of the SPEI over shorter time periods. The MEI and DMI anomalies have less variation within the same year making correlations possible.

Summarizing, the VOD anomalies are correlated on average 0.48 with the long revised SPEI and 0.45 with the short unrevised SPEI anomalies. In many fields, the correlations with the short time series are lower or statistically insignificant because the time series includes fewer extremes. In Lampung, the long SPEI differs strongly from the short SPEI, indicating low data quality in Lampung for the long SPEI time series. This results in weaker correlations in Lampung for the long dataset. The VOD anomaly coincides with the strong SPEI anomaly in 2015. In 2014, the SPEI features a much stronger negative anomaly. However, the VOD does not feature a strong anomaly here, which is probably related to the previous period positive SPEI anomalies recharging the hydrological system and providing a buffer for the vegetation. Additionally, the VOD starts to decline after the SPEI anomaly, which indicates that meteorological and agricultural droughts do not occur

simultaneously. These two observations probably show the added value of VOD. Correlations between the NDVI and the other indicators are even lower than compared to the other indicators.

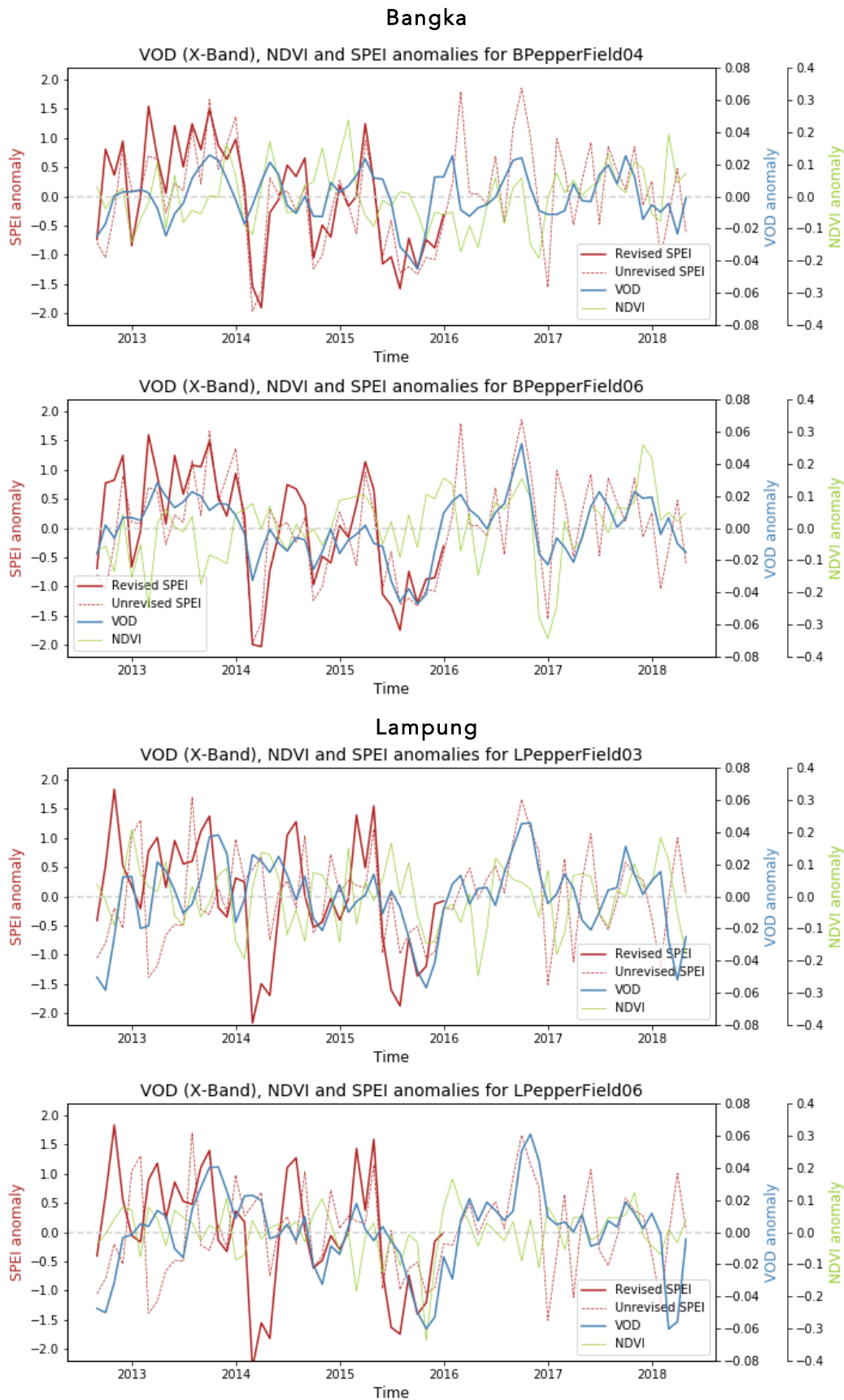


Figure 44: VOD, NDVI and SPEI anomalies for selected Pepper Fields in Bangka (top) and Lampung (bottom)

### 5.2.5 Yields and VOD

The selected drought indicators or proxies that are compared with the VOD all show a drought in 2015. However, these are rather primarily based on precipitation. Therefore, it is important to prove that this drought is also an agricultural drought.

Figure 45 shows yield per year in Indonesia. This plot is based on a report of the Directorate General of Estate Crops of the Ministry of Agriculture of Indonesia. The exact procedure of the collection of the yield data is not given. Additionally, the values of 2016 are preliminary values and the ones of 2017 are estimated values only. For this reason, this analysis is qualitative only.

The pepper yield in Indonesia relies on the climate as fields are not irrigated (see 3.1.2). In 2015, the yield drops compared to the previous year, which coincides with the droughts visible in the VOD anomaly time series as well as the reported droughts and lower yields in 2015 from farmers during the field visit. Furthermore, the lower production in 2012 could be related to the negative VOD anomalies in Lampung, that are of the same magnitude as of 2015. Nevertheless, the time prior to 2012 should be analysed to be able to make a consistent conclusion on this point.

Although only qualitatively, this graphic provides evidence for the drought of 2015/2016 described in the literature and by the farmers.

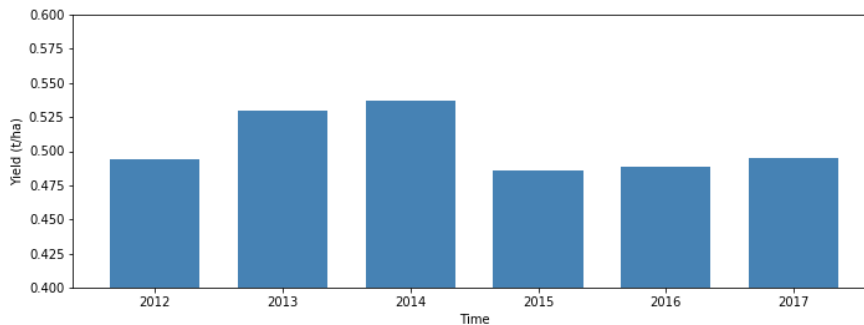


Figure 45: Yearly pepper yield from 2012 to 2017 of Indonesia (Directorate General of Estate Crops *et al.*, 2016)

## 5.3 Guideline to convert VOD to a drought index

This previous analysis shows that there is potential to use VOD as a drought proxy but also room for improvement, especially on the data quality. The presented guideline proposes steps to take in order to convert VOD into a drought index (see Figure 46). This guideline is based on the recent drought work of Liu *et al.* (2018). In that study, VOD and other indicator time series are aggregated or interpolated bi-linearly from their original resolution of  $0.05^\circ$  (C-Band) to monthly data with a spatial resolution of  $0.10^\circ$  (corresponding to ca. 10 km). The pixel-specific VOD climatology is based on the monthly values of non-drought years. The anomalies are then calculated with reference to this non-drought climatology. The anomalies are standardised by dividing the pixel-specific anomaly by the corresponding pixel-specific standard deviation within the reference period. In the present study, the reference period was 7 years. Through this standardisation, the anomaly of each grid cell represents the deviation from the non-drought average for the same months within the reference period.

The base for a suitable index is a high-quality input. For the VOD, this means to solve certain issues that become evident through this study. With the help of detailed land use maps, the accuracy of the downscaling could be assessed. Furthermore, the masking out of surface water bodies should be improved and then the influence of the inevitable errors caused by surface water on the downscaled results should be evaluated. By combining these steps, the actual spatial resolution can be estimated. In order to approximate the temporal resolution, the effect of temporal averaging has to be assessed. The fluctuations in the VOD time series are inevitable as the sensor has an uncertainty of 1 to 2 Kelvin, when measuring the brightness temperature. Additionally, the previously explained varying footprint location contributes to the fluctuation.

Possibly, there is an optimum length of the moving average window. For different purposes, the required time scale can vary. Therefore, a drought variable should be capable to quantify droughts at various time scales. Drought analyses are more commonly conducted on a yearly time scale followed by a monthly time scale. For agricultural droughts, a monthly time scale seems to be more appropriate (Mishra et al., 2010). However, within the *SpiceUp* project, farmers might be interested in shorter time scales in order to decide whether it would be beneficial to irrigate, whereas the company *Verstegen*, that buys the pepper might be interested in monthly values. For this reason, it is beneficial to maintain the highest temporal resolution possible. Moreover, an essential point to develop a drought index of different resolutions is a sufficient long-time series in which several drought events have occurred. Here, a data length of at least 15 years is suggested. Due to the offset between AMSR-E and AMSR-2, only the latter dataset is used in this work. However, in order to obtain time series of more than 15 years, it would be convenient to understand why there is this offset. As a last step of the improvement on data quality, a technique should be developed to exclude faulty images. This could be executed by excluding values if they vary more than a certain threshold compared to their previous value. Next, the pixel-specific climatology based on normal years without droughts could be calculated, just as in the work of Liu et al. (2018). Then, the pixel-specific anomaly can be estimated which is then normalized in a next step by dividing the anomaly by the pixel-specific standard deviation.

The present study reveals that the meteorological drought index SPEI and VOD are correlated to a certain extent. It also shows that the VOD reacts after a time lag on anomalies in the SPEI and also that if a positive SPEI anomaly is followed by a strong negative SPEI anomaly the impact on the VOD can be reduced. For this reason, the relationship between VOD and a meteorological drought indicator, as for instance SPEI, can be modelled for the region of interest in order to be able to predict the future behaviour of VOD. For this purpose, in analogy to the VOD, pixel-specific SPEI climatology of non-drought years should be calculated. Then, the pixel-specific anomaly can be obtained, which is then also standardised like the VOD. This makes a comparison between the two anomalies possible. Finally, it should be determined at which frequency the VOD gives the best results (C-Band, X-Band or L-Band).

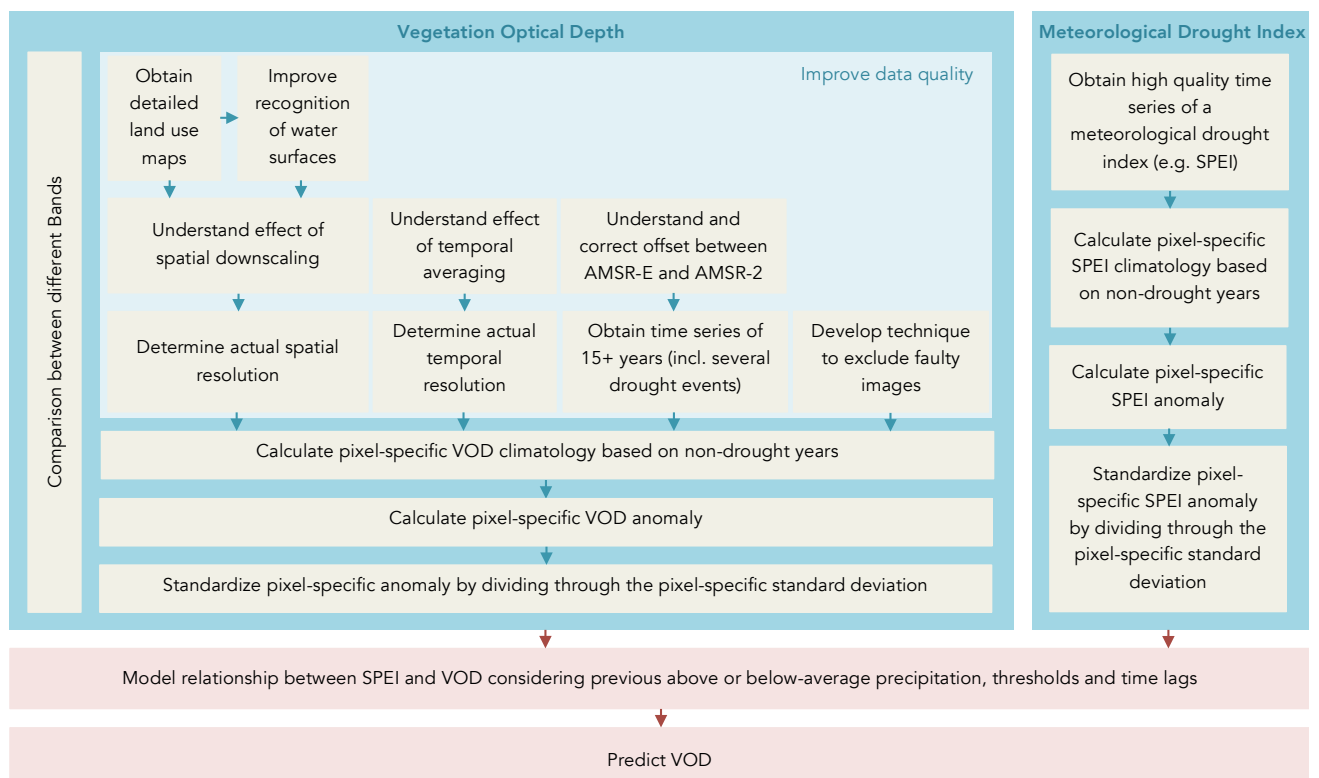


Figure 46: Road map to convert VOD into an agricultural drought predictor

# 6 CONCLUSIONS & RECOMMENDATIONS

## 6.1 Conclusions

The main purpose of this thesis is to analyse the potential of the VOD dataset of VanderSat for agricultural drought monitoring on the case study of pepper fields in the regions of Bangka and Lampung in Indonesia by answering the following four research questions. Hereafter, a conclusion of each question is given, followed by a final conclusion.

### **How does the VOD of pepper fields compare to large-scale VOD?**

The spatial analysis reveals that the fields are too small to detect differences in spatial characteristics in VOD compared to the surroundings. Apart from the field size, the slightly heterogeneous VOD pattern and similar surrounding vegetation density contribute to this difficulty. However, the 36-ha-large pepper field is distinguishable due to its size and its contrast in vegetation density with the surrounding. The spatio-temporal analysis shows that within a square of 10 x 10 km differences in drought intensity and drought duration exist. This result suggests that smaller areas should be used to represent the VOD.

The temporal analysis shows that the VOD anomaly of the pepper fields differs slightly in magnitude compared to the larger-scale surroundings. However, this difference is the same as in the period prior to the existence of the pepper field. Therefore, the fluctuations seem to be rather related to the downscaling method and the temporal averaging.

### **How does the VOD compare with other drought indicators? Does it have an added value over NDVI?**

In the spatial analysis, NDVI proves to have a much higher spatial resolution and to represent land use properly. However, the temporal resolution of NDVI is very low. An aggregation period of a year is required to produce a nearly cloud-free composite. In contrast, VOD does not face the temporal issue but has a coarser spatial resolution. The downscaling method in combination with temporal averaging seems to cause a smoother gradient but also a slightly heterogeneous pattern. The spatial performance of VOD varies per location. In the analysed area in Bangka, VOD is very similar to NDVI, representing the land use properly. In the selected area in Lampung, VOD does not capture spatial differences. Surface water bodies could cause this negative impact on the spatial performance of VOD.

The temporal correlations between VOD and other drought indicators are significant but not high, suggesting that factors other than precipitation influence the VOD, as for example, different groundwater levels or drought resistance of certain plants. This is supported by the fact that some fields present higher or lower correlations for all analysed indicators. All three indicators as well as the VOD show strong anomalies during the drought of 2015. The NDVI only features a peak in 2015 in a few fields. The ENSO and the VOD are correlated on average by -0.46. The IOD and the VOD are on average correlated by -0.46 as well. Interestingly, the VOD does not peak in 2017 during the strongest positive IOD anomaly. Probably, this can be attributed to the prior negative IOD anomaly leading to above-average rainfall recharging groundwater levels and soil moisture, which buffers the subsequent below-average rainfall. The VOD anomalies are correlated on average by 0.48 with the long revised SPEI and by 0.45 with the short unrevised SPEI anomalies. In many fields, the correlations with the short time series are lower or statistically insignificant because the time series includes less extreme events. The most negative anomaly of the SPEI occurs in 2014 after a long period of positive anomalies. However, the VOD anomaly is less pronounced compared to 2015. Again, this is an indication that VOD is able to capture the buffering characteristic that the vegetation and soil have to climatic variations. Additionally, the VOD starts to decline some time after the SPEI anomaly, which indicates that meteorological and agricultural do not occur simultaneously and reveals the added value that VOD bares. Due to the high cloud cover, and probably also the aerosol concentration, the NDVI delivers mainly statistically insignificant results with all indicators.

**How does the VOD capture agricultural drought events?**

Although only qualitatively proven, the pepper yields, which indicate the agricultural drought, fall within the same period where VOD shows an extreme drought event. This provides qualitative evidence for an agricultural drought occurring in the same period mentioned in the literature and where the farmers have reported an extreme drought.

**How can the VOD be transformed to an agricultural drought indicator?**

This study proposes a guideline on the conversion of VOD to a drought indicator. The steps that are necessary to obtain a more robust VOD dataset are listed. The guideline suggests modelling the VOD anomalies based on the anomalies of a meteorological drought indicator like SPEI. This is an attempt to make use of the predictive value of the VOD that the results of this study reveal: the observed time lag between the SPEI and the VOD and also the influence of prior above-average rainfall on the course of the VOD during below-average rainfall.

In conclusion, this case study shows that VOD is able to capture agricultural droughts and, therefore, it bears promising potential as an agricultural drought indicator. The added value of VOD over NDVI is especially relevant for other tropical regions with a high cloud cover as in this case study. Possibly, saturation issues will arise when VOD is applied to denser vegetation areas. This study also reveals several data quality issues and questions the actual resolution of VOD. It remains uncertain if certain peaks of other indicators observed in the present study are not as pronounced in VOD due to the vegetation buffer or due to erroneous VOD data. Therefore, further analysis is recommended in the following section.

**6.2 Recommendations**

For future studies in this field, it is recommended to better understand the accuracy of VOD as well as the here used downscaling method. As this is an independent dataset, its accuracy is difficult to assess. It would be useful to quantify the amount of biomass that corresponds to certain VOD values. Detailed yield data would be a helpful asset to test the accuracy of VOD. Moreover, further case studies in other climates and vegetation densities should be conducted. Most of the recommendations are mentioned in the proposed guideline to convert VOD to an agricultural drought indicator in section 5.3. Apart from determining the actual spatial resolution with the help of detailed land use maps, an improved recognition and exclusion of surface water bodies in the downscaling method is proposed within the guideline. Furthermore, it is recommended to determine the optimum moving average length for the VOD time series that fluctuate strongly over short periods due to sensor inaccuracies and the downscaling method. Additionally, the development of a method to exclude faulty images is recommended. Moreover, it is important to look at longer time series including several droughts. Moreover, due to data availability, this study is based on X-Band VOD. However, it is suggested to look at C-Band VOD, which has a lower frequency and longer wavelengths and can, therefore, penetrate deeper into the vegetation.

**Acknowledgements**

I would like to thank Susan and Richard for the supervision in the first place and also my thesis committee (Edo and Philip) for great suggestions. Further, I thank my colleagues at VanderSat who were of great help, especially Nina for accompanying me during the field visit. Without the help of PT CAN it would have been impossible to select fields and to obtain an insight view on the situation. A special thanks to Hatami, Ikhsan and Saepul for receiving me and organizing this extraordinarily well-planned fieldwork. I am also grateful for the farmers who took their time to answer all my questions. Thanks to Evert-Jan for putting me in contact with PT CAN. And finally, I would like to thank my family and friends, in particular, Clara Sofie, Luis, Britta and Alvaro for giving me moral support, reviewing my report and helping me in decision making processes.

## 7 BIBLIOGRAPHY

- Affairs, D. M. of F. (2018) *About G4AW*. Available at: <https://g4aw.spaceoffice.nl/en/about-g4aw/> (Accessed: 10 June 2018).
- Agboma, C. O., Yirdaw, S. Z. and Snelgrove, K. R. (2009) 'Intercomparison of the total storage deficit index (TSDI) over two Canadian Prairie catchments', *Journal of Hydrology*. Elsevier B.V., 374(3–4), pp. 351–359. doi: 10.1016/j.jhydrol.2009.06.034.
- Andela, N. et al. (2013) 'Global changes in dryland vegetation dynamics (1988-2008) assessed by satellite remote sensing: Comparing a new passive microwave vegetation density record with reflective greenness data', *Biogeosciences*, 10(10), pp. 6657–6676. doi: 10.5194/bg-10-6657-2013.
- Ashok, K., Guan, Z. and Yamagata, T. (2003) 'Influence of the Indian Ocean Dipole on the Australian winter rainfall', *Geophysical Research Letters*, 30(15), pp. 3–6. doi: 10.1029/2003GL017926.
- Aulia, M. R. et al. (2016) 'Drought Detection of West Java's Paddy Field Using MODIS EVI Satellite Images (Case Study: Rancaekek and Rancaekek Wetan)', *Procedia Environmental Sciences*. Elsevier B.V., 33, pp. 646–653. doi: 10.1016/j.proenv.2016.03.119.
- Australian Government - Bureau of Meteorology (no date) *El Niño - Detailed Australian Analysis*. Available at: <http://www.bom.gov.au/climate/enso/enlist/index.shtml> (Accessed: 3 September 2018).
- Bannari, A. et al. (1995) 'A review of vegetation indices', *Remote Sensing Reviews*, 13(1–2), pp. 95–120. doi: 10.1080/02757259509532298.
- Boyer, J. S. (1982) 'Plant Productivity and Environment', *Science*, 218(4571), pp. 443–448. doi: 10.1126/science.218.4571.443.
- Bulsink, F., Hoekstra, A. Y. and Booij, M. J. (2010) 'The water footprint of Indonesian provinces related to the consumption of crop products', *Hydrology and Earth System Sciences*, 14(1), pp. 119–128. doi: 10.5194/hess-14-119-2010.
- Carrão, H. et al. (2015) 'An empirical standardized soil moisture index for agricultural drought assessment from remotely sensed data', *International Journal of Applied Earth Observation and Geoinformation*. Elsevier B.V., 48, pp. 74–84. doi: 10.1016/j.jag.2015.06.011.
- Carrão, H., Naumann, G. and Barbosa, P. (2016) 'Mapping global patterns of drought risk: An empirical framework based on sub-national estimates of hazard, exposure and vulnerability', *Global Environmental Change*, 39, pp. 108–124. doi: 10.1016/j.gloenvcha.2016.04.012.
- Ceccato, P., Flasse, S. and Gregoire, J.-M. (2002) 'Designing a spectral index to estimate vegetation water content from remote sensing data Part 2. Validation and applications', *Remote Sensing of Environment*, 82, pp. 198–207.
- Chang, C. P. et al. (2004) *On the Relationship between Western Maritime Continent Monsoon Rainfall and ENSO during Northern Winter*.
- Chiew, F. H. S. et al. (1998) 'El Nino/Southern Oscillation and Australian rainfall, streamflow and drought: Links and potential for forecasting', *Journal of Hydrology*, 204(1–4), pp. 138–149. doi: 10.1016/S0022-1694(97)00121-2.
- Choi, M. et al. (2013) 'Evaluation of drought indices via remotely sensed data with hydrological variables', *Journal of Hydrology*. Elsevier B.V., 476, pp. 265–273. doi: 10.1016/j.jhydrol.2012.10.042.
- Choudhury, B. J. et al. (1979) 'Effect of Surface Roughness on the Microwave Emission from Soils', *Journal of Geophysical Research*, 84, pp. 5699–5706.
- Climate-Data.org (2012) *Cliamte: Indonesia*. Available at: <https://en.climate-data.org/country/101/> (Accessed: 12 June 2018).
- D'Arrigo, R. et al. (2006) 'Monsoon drought over Java , Indonesia , during the past two centuries', *Geophysical Research Letters*, 33(February), pp. 4–7. doi: 10.1029/2005GL025465.
- D'Arrigo, R. and Wilson, R. (2008) 'Short Communication El Niño and Indian Ocean influences on Indonesian drought', *International Journal of Climatology*, 28(January), pp. 611–616. doi: 10.1002/joc.
- Dai, A. (2011) 'Drought under global warming: A review', *Wiley Interdisciplinary Reviews: Climate Change*, 2(1), pp. 45–65. doi: 10.1002/wcc.81.
- Devendra, C. (2016) 'Rainfed agriculture: its importance and potential in global food security', *UTAR Agriculture Science Journal*, 2(2). Available at: <http://uasj.utar.edu.my/uasj/file/Agriculture April 2016.pdf>.
- Van Dijk, A. I. J. M. et al. (2013) 'The Millennium Drought in southeast Australia (2001-2009): Natural and human causes and implications for water resources, ecosystems, economy, and society', *Water Resources Research*, 49(2), pp. 1040–1057. doi: 10.1002/wrcr.20123.
- Ding, Y., Hayes, M. J. and Widhalm, M. (2013) 'Measuring economic impacts of drought: a review and discussion', *Disaster Prevention and Management: An International Journal*. doi: 10.1108/09653561111161752.
- Directorate General of Estate Crops et al. (2016) *Statistik Perkebunan Indonesia - Lada (Tree Crop Estate Statistics of Indonesia - Pepper)*. Available at: <http://ditjenbun.pertanian.go.id>.
- Fanin, T. and van der Werf, G. R. (2017) 'Precipitation – fire linkages in Indonesia ( 1997 – 2015 )', *Biogeosciences*, 14, pp. 3995-4008-14-3995–2017. doi: 10.5194/bg-14-3995-2017.

- Fernandes, K. et al. (2017) 'Heightened fire probability in Indonesia in non-drought conditions: the effect of increasing temperatures', *Environmental Research Letters*, 12(54002).
- Field, R. D. et al. (2016) 'Indonesian fire activity and smoke pollution in 2015 show persistent nonlinear sensitivity to El Niño-induced drought', *PNAS*, 113(33), pp. 9204–9209. doi: 10.1073/pnas.1524888113.
- Field, R. D., van der Werf, G. R. and Shen, S. S. P. (2009) 'Human amplification of drought-induced biomass burning in Indonesia since 1960', *Nature Geoscience*. Nature Publishing Group, 2(March), pp. 185–188. doi: 10.1038/NGEO443.
- Field, R. and Shen, S. (2008) 'Predictability of carbon emissions from biomass burning in Indonesia from 1997 to 2006', *Journal of Geophysical Research*, 113(June), pp. 1–17. doi: 10.1029/2008JG000694.
- Gao, B. (1996) 'NDWI A Normalized Difference Water Index for Remote Sensing of Vegetation Liquid Water From Space', 266(April 1995), pp. 257–266.
- Gaveau, D. et al. (2014) 'Major atmospheric emissions from peat fires in Southeast Asia during non-drought years: evidence from the 2013 Sumatran fires', *Scientific Reports*, 4, pp. 1–7. doi: 10.1038/srep06112.
- Hackert, E. C. and Hastenrath, S. (1986) 'Mechanisms of Java Rainfall Anomalies', *American Meteorological Society*, pp. 745–757.
- Hamada, J. et al. (2012) 'Interannual Rainfall Variability over Northwestern Java and its Relation to the Indian Ocean Dipole and El Niño-Southern Oscillation Events', *SOLA*, 8(1997), pp. 69–72. doi: 10.2151/sola.2012-018.
- Hansen, M. C. et al. (2013) 'High-Resolution Global Maps of 21st-Century Forest Cover Change', *Science*, 342(6160), pp. 850–853. Available at: <http://earthenginepartners.appspot.com/science-2013-global-forest>.
- Hayes, M. J. et al. (1999) 'Monitoring the 1996 Drought Using the Standardized Precipitation Index', *Bulletin of the American Meteorological Society*, 80(3), pp. 429–438.
- Hendon, H. H. (2003) 'Indonesian rainfall variability: Impacts of ENSO and local air-sea interaction', *Journal of Climate*, 16(11), pp. 1775–1790. doi: 10.1175/1520-0442(2003)016<1775:IRVIOE>2.0.CO;2.
- Herawati, H. and Santoso, H. (2011) 'Forest Policy and Economics Tropical forest susceptibility to and risk of fire under changing climate: A review of fire nature, policy and institutions in Indonesia', *Forest Policy and Economics*. Elsevier B.V., 13(4), pp. 227–233. doi: 10.1016/j.forpol.2011.02.006.
- Holmes, T. R. H. et al. (2009) 'Land surface temperature from Ka band ( 37 GHz ) passive microwave observations', *Journal of Geophysical Research*, 114(November 2008), pp. 1–15. doi: 10.1029/2008JD010257.
- Imgur Stack Exchange (no date) *Spectrum*. Available at: <https://i.stack.imgur.com/XEJPa.png> (Accessed: 4 September 2018).
- International Pepper Community (no date) *Country Profile: Indonesia*. Available at: <http://www.ipcnet.org/n/map/?path=map&page=id> (Accessed: 30 September 2018).
- Jackson, T. J. and O'Neill, P. E. (1990) 'Attenuation of Soil Microwave Emission by Corn and Soybeans at 1.4 and 5 GHz', *IEEE Transactions on Geoscience and Remote Sensing*, 28(5), pp. 978–980. doi: 10.1109/36.58989.
- Jackson, T. J. and Schmugge, T. J. (1991) 'Vegetation effects on the microwave emission of soils', *Remote Sensing of Environment*, 36(3), pp. 203–212. doi: 10.1016/0034-4257(91)90057-D.
- Jackson, T. J., Schmugge, T. J. and Wang, J. R. (1982) 'Passive microwave sensing of soil moisture under vegetation canopies', *Water Resources Research*, 18(4), pp. 1137–1142. doi: 10.1029/WR018i004p01137.
- de Jeu, R. A. M. et al. (2004) 'Remote sensing techniques to measure dew: The detection of canopy water with an L-band passive microwave radiometer and a spectral reflectance sensor', *Proceedings of SPIE Conference on Remote Sensing for Agriculture, Ecosystems, and Hydrology*, 5568, pp. 225–235. doi: 10.1117/12.573929.
- de Jeu, R. (2003) *Retrieval of Land Surface Parameters Using Passive Microwave Remote Sensing*. Vrije Universiteit Amsterdam.
- Jiao, W. et al. (2016) 'Evaluating an enhanced vegetation condition index (VCI) based on VIUPD for drought monitoring in the continental United States', *Remote Sensing*, 8(3). doi: 10.3390/rs8030224.
- Jones, M. et al. (2011) 'Remote Sensing of Environment Satellite passive microwave remote sensing for monitoring global land surface phenology', *Remote Sensing of Environment*. Elsevier Inc., 115(4), pp. 1102–1114. doi: 10.1016/j.rse.2010.12.015.
- Kachi, M. et al. (2014) 'Calibration and Validation Results of the Advanced Microwave Scanning Radiometer 2', *EUMETSAT Meteorological Satellite Conference*, 22-26 September, Geneva, Switzerland, 2(May).
- Kelley, C. P. et al. (2015) 'Climate change in the Fertile Crescent and implications of the recent Syrian drought', *Proceedings of the National Academy of Sciences*, 112(11), pp. 3241–3246. doi: 10.1073/pnas.1421533112.
- Keyantash, J. and Dracup, J. (2004) 'An aggregate drought index: Assessing drought severity based on fluctuations in the hydrologic cycle and surface water storage', *Water Resources Research*, 40(9), pp. 1–14. doi: 10.1029/2003WR002610.
- Keyantash, J. and National Center for Atmospheric Research Staff (Eds) (2018) *The Climate Data Guide: Standardized Precipitation Index (SPI)*. Available at: <https://climatedataguide.ucar.edu/climate-data/standardized-precipitation-index-spi> (Accessed: 16 March 2018).
- Kim, D., Byun, H. and Choi, K. (2009) 'Evaluation, modification, and application of the Effective Drought Index to 200-Year drought climatology of Seoul, Korea', *Journal of Hydrology*. Elsevier B.V., 378(1–2), pp. 1–12.

doi: 10.1016/j.jhydrol.2009.08.021.

Kogan, F. N. (1990) 'Remote sensing of weather impacts on vegetation in non-homogeneous areas', *International Journal of Remote Sensing*. Taylor & Francis, 11(8), pp. 1405–1419. doi: 10.1080/01431169008955102.

Köppen, W. and Geiger, R. (1936) *Handbuch der Klimatologie - Das geographische System der Klimate*. Berlin: Verlag von Gebrüder Borntraeger.

Krishnakumar, P. K. (2016) 'Pepper gets ready for bull run as output falls', *The Economic Times*, July. Available at:

<https://economictimes.indiatimes.com/markets/commodities/news/pepper-gets-ready-for-bull-run-as-indonesian-output-falls/articleshow/53296585.cms>.

Van Lanen, H. A. J. et al. (2013) 'Hydrological drought across the world: Impact of climate and physical catchment structure', *Hydrology and Earth System Sciences*, 17(5), pp. 1715–1732. doi: 10.5194/hess-17-1715-2013.

Langmann, B. et al. (2009) 'Vegetation fire emissions and their impact on air pollution and climate', *Atmospheric Environment*, 43, pp. 107–116. doi: 10.1016/j.atmosenv.2008.09.047.

Lestari et al. (2018) *Severe Drought Event in Indonesia Following 2015/16 El Niño/positive Indian Dipole Events, The International Conference on Theoretical and Applied Physics - IOP Conf.Series: Journal of Physics*. doi: 10.1088/1742-6596/1011/1/012040.

Lestari, R. K. et al. (2014) 'Increasing potential of biomass burning over Sumatra, Indonesia induced by anthropogenic tropical warming', *Environmental Research Letters*. IOP Publishing, 9(10). doi: 10.1088/1748-9326/9/10/104010.

Liu, Y. et al. (2007) 'TRMM-TMI satellite observed soil moisture and vegetation density (1998-2005) show strong connection with El Niño in eastern Australia', *Geophysical Research Letters*, 34(15), pp. 1–5. doi: 10.1029/2007GL030311.

Liu, Y. et al. (2012) 'Development and evaluation of a global long-term passive microwave vegetation product', *Geophysical Research Abstracts*, 14(1).

Liu, Y. et al. (2012) 'Global vegetation biomass change (1988-2008) and attribution to environmental and human drivers', *Global Ecology and Biogeography*, 22(6), pp. 692–705. doi: 10.1111/geb.12024.

Liu, Y. et al. (2013) 'Changing Climate and Overgrazing Are Decimating Mongolian Steppes', *PLoS ONE*, 8(2), pp. 4–9. doi: 10.1371/journal.pone.0057599.

Liu, Y. et al. (2018) 'Enhanced canopy growth precedes senescence in 2005 and 2010 Amazonian droughts', *Remote Sensing of Environment*. Elsevier, 211(March), pp. 26–37. doi: 10.1016/j.rse.2018.03.035.

Liu, Y. Y. et al. (2011) 'Global long-term passive microwave satellite-based retrievals of vegetation optical depth', *Geophysical Research Letters*, 38(18), pp. 1–6. doi: 10.1029/2011GL048684.

Liu, Y. Y. et al. (2015) 'Recent reversal in loss of global terrestrial biomass', *Nature Climate Change*, 5(5), pp. 470–

474. doi: 10.1038/nclimate2581.

Marlier, M. E. et al. (2013) 'El Niño and health risks from landscape fire emissions in Southeast Asia', *Nat Clim Chang*, 3, pp. 131–136. doi: 10.1038/nclimate1658.

Martínez-Fernández, J. et al. (2016) 'Satellite soil moisture for agricultural drought monitoring: Assessment of the SMOS derived Soil Water Deficit Index', *Remote Sensing of Environment*. Elsevier Inc., 177, pp. 277–286. doi: 10.1016/j.rse.2016.02.064.

MedCalc (no date) *Correlation Coefficient*. Available at: <https://www.medcalc.org/manual/correlation.php> (Accessed: 20 August 2018).

Medrilzam, M. et al. (2014) 'The socio-ecological drivers of forest degradation in part of the tropical peatlands of Central Kalimantan, Indonesia', *Forestry*, 87(August), pp. 335–345. doi: 10.1093/forestry/cpt033.

Meesters, A. G. C. A., Jeu, R. A. M. De and Owe, M. (2005) 'Analytical Derivation of the Vegetation Optical Depth From the Microwave Polarization Difference Index', *IEEE Transactions on Geoscience and Remote Sensing*, 2(2), pp. 121–123.

Mekis, E. and Vincent, L. (2004) 'Precipitation and temperature related climate indices for Canada', in *Proceedings of the 16th Symposium on Global Change and Climate Variations. Preprints of the 85th AMS Annual Meeting*. San Diego, California.

Mendicino, G., Senatore, A. and Versace, P. (2008) 'A Groundwater Resource Index (GRI) for drought monitoring and forecasting in a mediterranean climate', *Journal of Hydrology*, 357(3–4), pp. 282–302. doi: 10.1016/j.jhydrol.2008.05.005.

Miettinen, J., Shi, C. and Liew, S. C. (2016) 'Land cover distribution in the peatlands of Peninsular Malaysia, Sumatra and Borneo in 2015 with changes since 1990', *Global Ecology and Conservation*. Elsevier B.V., 6, pp. 67–78. doi: 10.1016/j.gecco.2016.02.004.

Mishra, A. K. and Singh, V. P. (2010) 'A review of drought concepts', *Journal of Hydrology*. Elsevier B.V., 391(1–2), pp. 202–216. doi: 10.1016/j.jhydrol.2010.07.012.

Mishra, A. K. and Singh, V. P. (2011) 'Drought modeling - A review', *Journal of Hydrology*. Elsevier B.V., 403(1–2), pp. 157–175. doi: 10.1016/j.jhydrol.2011.03.049.

Mo, T. et al. (1982) 'A model for microwave emission from vegetation-covered fields', *Journal of Hydrology*, 87(C13), pp. 11229–11237. doi: 10.1029/JC087iC13p11229.

Myneni, R. B. et al. (1995) 'The Interpretation of Spectral Vegetation Indexes', *IEEE Transactions on Geoscience and Remote Sensing*, 33(2), pp. 481–486.

NASA EOSDIS LP DAAC (2015) *MOD13A1 MODIS/Terra Vegetation Indices 16-Day L3 Global 500m SIN Grid V006 [Data set]*. doi: 10.5067/MODIS/MOD13A1.006.

National Drought Mitigation Centre - University of Nebraska (2018) *ENSO and Drought Forecasting*. Available at: <http://drought.unl.edu/Education/DroughtIn-depth/ENSO.aspx> (Accessed: 15 August 2018).

Van Nieuwstadt, M. G. L. and Sheil, D. (2005) 'Drought,

- fire and tree survival in a Borneo rain forest, East Kalimantan, Indonesia', *Journal of Ecology*, 93(1), pp. 191–201. doi: 10.1111/j.1365-2745.2005.00954.x.
- Njoku, E. and Kong, J. (1977) 'Theory for passive microwave remote sensing of near-surface soil moisture', *Journal of Geophysical Research*, 82(20). Available at: <http://onlinelibrary.wiley.com/doi/10.1029/JB082i020p03108/full>.
- NOAA (2017) *Dipole Mode Index (DMI) - Dataset*. Available at: [https://www.esrl.noaa.gov/psd/gcos\\_wgsp/Timeseries/DMI/](https://www.esrl.noaa.gov/psd/gcos_wgsp/Timeseries/DMI/) (Accessed: 5 April 2018).
- NOAA (2018) *Multivariate ENSO Index (MEI) - Dataset*. Available at: <https://www.esrl.noaa.gov/psd/enso/mei/> (Accessed: 15 August 2018).
- Owe, M., Jeu, R. De and Holmes, T. (2008) 'Multisensor historical climatology of satellite-derived global land surface moisture', *Journal of Geophysical Research*, 113(January), pp. 1–17. doi: 10.1029/2007JF000769.
- Owe, M., de Jeu, R. and Walker, J. (2001) 'A Methodology for Surface Soil Moisture and vegetation Optical Depth Retrieval Using the Microwave Polarization Difference Index', *IEEE Transactions on Geoscience and Remote Sensing*, 39, pp. 1643–1654. doi: 10.1109/36.942542.
- Owen, B. B. et al. (1961) 'The dielectric constant of water as a function of temperature and pressure', *The Journal of Physical Chemistry*. American Chemical Society, 65(11), pp. 2065–2070. doi: 10.1021/j100828a035.
- Owen, N. (2015) 'Beyond haze, El Nino drought poses poverty challenge for Indonesia', October. Available at: <https://www.reuters.com/article/us-indonesia-el-nino/beyond-haze-el-nino-drought-poses-poverty-challenge-for-indonesia-idUSKCN0SM2SK20151029> (Accessed: 6 September 2018).
- Page, S. et al. (2002) 'The amount of carbon released from peat and forest fires in Indonesia during 1997', *Letters to nature*, 420(November), pp. 61–65. doi: 10.1038/nature01131.
- Palmer, W. C. (1965) *Meteorological Drought*. 45. Washington D.C.
- Parinussa, R. M. et al. (2016) 'A Quasi-Global Approach to Improve Day-Time Satellite Surface Soil Moisture Anomalies through the Land Surface Temperature Input', *Climate*, 4(50). doi: 10.3390/cli4040050.
- Peel, M. C. et al. (2007) 'Updated world map of the Köppen-Geiger climate classification', *Hydrology and Earth System Sciences Discussions*, 4(2), pp. 439–473. Available at: <https://hal.archives-ouvertes.fr/hal-00298818>.
- Personal communication (2018) 'Interview with several farmers and employees of PT CAN during field visit in May and June 2018'.
- Pietrzak, J. and Katsman, C. (2017) 'Lecture of Physical Oceanography (Technical University of Delft)'.
- Princeton University (2013) *Terrestrial Hydrology Research Group*. Available at: [hydrology.princeton.edu](http://hydrology.princeton.edu) (Accessed: 16 October 2018).
- Ropelewski, C. F. and Halpert, M. S. (1987) 'Global and Regional Scale Precipitation Patterns Associated with the El Niño/Southern Oscillation', *Monthly Weather Review*, pp. 1606–1626. doi: 10.1175/1520-0493(1987)115<1606:GARSPP>2.0.CO;2.
- SADC Regional Remote Sensing Unit (2000) *The Standardized Precipitation Index*. Available at: <http://drought.unl.edu/portals/0/docs/spi-program-alternative-method.pdf>.
- van der Schalie, R. et al. (2017) 'The merging of radiative transfer based surface soil moisture data from SMOS and AMSR-E', *Remote Sensing of Environment*. Elsevier B.V., 189, pp. 180–193. doi: 10.1016/j.rse.2016.11.026.
- Van der Schalie, R. (2017) *Advancing soil moisture climate records through the integration of SMOS observations*. Vrije Universiteit Amsterdam.
- Schalie, R. Van Der et al. (2015) 'SMOS soil moisture retrievals using the land parameter retrieval model: Evaluation over the Murrumbidgee Catchment, southeast Australia', *Remote Sensing of Environment*, 163, pp. 70–79. doi: 10.1016/j.rse.2015.03.006.
- Schmugge, T. J. (1983) 'Remote Sensing of Soil Moisture: Recent Advances', *IEEE Transactions on Geoscience and Remote Sensing*, (3), pp. 336–344.
- Schoennagel, T. et al. (2005) 'ENSO and PDO variability affect drought induced fire occurrence in Rocky Mountain subalpine forests', *Ecological Applications - Ecological Society of America*, 15(6). doi: <https://doi.org/10.1890/04-1579>.
- Setiawan, A. M. et al. (2016) 'Utilization of near real-time NOAA-AVHRR Satellite output for El Niño induced drought analysis in Indonesia (Case study: El Niño 2015 induced drought in South Sulawesi)', *International Journal of Remote Sensing and Earth Sciences*, 13(2), pp. 87–94.
- Setiawan, A. M., Lee, W.-S. and Rhee, J. (2017) 'Spatio-temporal characteristics of Indonesian drought related to El Niño events and its predictability using the multi-model ensemble', *International Journal of Climatology*, 37(13), pp. 4700–4719. doi: 10.1002/joc.5117.
- Sheffield, J. et al. (2009) 'Global and continental drought in the second half of the twentieth century: Severity-area-duration analysis and temporal variability of large-scale events', *Journal of Climate*, 22(8), pp. 1962–1981. doi: 10.1175/2008JCLI2722.1.
- Shi, J. et al. (2008) 'Microwave vegetation indices for short vegetation covers from satellite passive microwave sensor AMSR-E', *Remote Sensing of Environment*. Elsevier Inc., 112(12), pp. 4285–4300. doi: 10.1016/j.rse.2008.07.015.
- Sholihah, R. I. et al. (2016) 'Identification of Agricultural Drought Extent Based on Vegetation Health Indices of Landsat Data: Case of Subang and Karawang, Indonesia', *Procedia Environmental Sciences*. Elsevier B.V., 33, pp. 14–20. doi: 10.1016/j.proenv.2016.03.051.
- Sloan, S. et al. (2017) 'Fire activity in Borneo driven by industrial land conversion and drought during El Niño periods, 1982–2010', *Global Environmental Change*.

- Elsevier Ltd, 47(October), pp. 95–109. doi: 10.1016/j.gloenvcha.2017.10.001.
- Sruthi, S. and Aslam, M. (2015) 'Agricultural Drought Analysis Using the NDVI and Land Surface Temperature Data; a Case Study of Raichur District', *Aquatic Procedia*. Elsevier B.V., 4(Icwrcoe), pp. 1258–1264. doi: 10.1016/j.aqpro.2015.02.164.
- Supari, Muharsyah, R. and Sopaheluwakan, A. (2016) 'Mapping Drought Risk in Indonesia Related to El-Niño Hazard', in *The 5th International Symposium on Earthhazard and Disaster Mitigation*. doi: 10.1063/1.4947413.
- Tacconi, L. (2016) 'Preventing fires and haze in Southeast Asia', *Nature Climate Change*. Nature Publishing Group, 6(7), pp. 640–643. doi: 10.1038/nclimate3008.
- The World Bank Group (2016) *Climate Change Knowledge Portal*. Available at: [http://sdwebx.worldbank.org/climateportal/index.cfm?page=country\\_historical\\_climate&ThisCCCode=IDN#](http://sdwebx.worldbank.org/climateportal/index.cfm?page=country_historical_climate&ThisCCCode=IDN#) (Accessed: 12 June 2018).
- The World Bank Group (2018) *Average Monthly Temperature and Rainfall for Indonesia from 1901-2015*. Available at: [http://sdwebx.worldbank.org/climateportal/index.cfm?page=country\\_historical\\_climate&ThisCCCode=IDN](http://sdwebx.worldbank.org/climateportal/index.cfm?page=country_historical_climate&ThisCCCode=IDN) (Accessed: 14 October 2018).
- The Worldbank (2017) *Agriculture, forestry, and fishing, value added (% of GDP)*. Available at: <https://data.worldbank.org/indicator/NV.AGR.TOTL.ZS?end=2016&locations=ID&start=2014> (Accessed: 13 August 2018).
- The Worldbank (2018) *The Worldbank in Indonesia - Overview*. Available at: <http://www.worldbank.org/en/country/indonesia/overview> (Accessed: 10 June 2018).
- TheGlobalEconomy.com (2016) *Indonesia: GDP share of agriculture*. Available at: [https://www.theglobaleconomy.com/Indonesia/Share\\_of\\_agriculture/](https://www.theglobaleconomy.com/Indonesia/Share_of_agriculture/) (Accessed: 6 September 2018).
- Torres, G. M., Lollato, R. P. and Ochsner, T. E. (2013) 'Comparison of drought probability assessments based on atmospheric water deficit and soil water deficit', *Agronomy Journal*, 105(2), pp. 428–436. doi: 10.2134/agronj2012.0295.
- Tremblay (2018) *Pepper History*. Available at: <http://www.peppermilltremblay.com/pepper.html> (Accessed: 22 August 2018).
- Tsakiris, G., Pangalou, D. and Vangelis, H. (2007) 'Regional drought assessment based on the Reconnaissance Drought Index (RDI)', *Water Resources Management*, 21(5), pp. 821–833. doi: 10.1007/s11269-006-9105-4.
- University Corporation for Atmospheric Research pursuant to NOAA (1994) *El Niño and Climate Prediction - Reports to the Nation on our Changing Planet*.
- VanderSat B.V. (2016) 'Method and system for improving the resolution of sensor data'. Gragner, Bruno. Available at: <https://patentimages.storage.googleapis.com/26/45/b9/558ca003879bee/EP3258413A1.pdf>.
- Vicente-Serrano, S. M. and Beguería, S. (2018) *SPEI - CSIC database*. Available at: <http://spei.csic.es/> (Accessed: 14 July 2018).
- Wadley, R. L. and Mertz, O. (2005) 'Pepper in a time of crisis: Smallholder buffering strategies in Sarawak, Malaysia and West Kalimantan, Indonesia', *Agricultural Systems*, 85(3 SPEC. ISS.), pp. 289–305. doi: 10.1016/j.agsy.2005.06.012.
- Wanders, N., van Lanen, H. A. J. and van Loon, A. F. (2010) *Technical Report No. 24 INDICATORS FOR DROUGHT CHARACTERIZATION*.
- Wang, J. R. and Choudhury, B. J. (1981) 'Remote sensing of soil moisture content, over bare field at 1.4 GHz frequency', *Journal of Geophysical Research*, 86(C6), pp. 5277–5282.
- Wang, J. R. and Schmugge, T. (1980) 'An Empirical Model for the Complex Dielectric Permittivity of Soils as a Function of Water Content', *IEEE Transactions on Geoscience and Remote Sensing*, 18(4), pp. 288–295. doi: 10.1109/TGRS.1980.350304.
- Weiss, E. A. (2002) *Spice Crops*. CABI. Available at: <https://books.google.de/books?id=RqqTdAwXev4C>.
- Wigneron, J. P. et al. (1993) 'Inversion of surface parameters from passive microwave measurements over a soybean field', *Remote Sensing of Environment*, 46(1), pp. 61–72. doi: 10.1016/0034-4257(93)90032-S.
- Wilheit, T. T. J. (1975) *Radiative transfer in a plane stratified dielectric*.
- Wilhite, D. A. (2000) 'Drought as a natural hazard: Concepts and definitions', *Drought: A Global Assessment*, pp. 3–18.
- World Food Programme (2016) *Indonesia - The Impact of Drought on Households in Four Provinces in Eastern Indonesia, February 2016*. Available at: <https://www.wfp.org/content/indonesia-impact-drought-households-four-provinces-eastern-indonesia-february-2016> (Accessed: 6 September 2018).
- Xue, J. and Su, B. (2017) 'Significant remote sensing vegetation indices: a review of developments and applications', *Journal of sensors*, Vol.2017, p. 17p. doi: 10.1155/2017/1353691.
- Ye, N. et al. (2015) 'Standing water effect on soil moisture retrieval from L-band passive microwave observations', *Remote Sensing of Environment*, 169, pp. 232–242. doi: 10.1016/j.rse.2015.08.013.
- Yirdaw, S. Z., Snelgrove, K. R. and Agboma, C. O. (2008) 'GRACE satellite observations of terrestrial moisture changes for drought characterization in the Canadian Prairie', *Journal of Hydrology*, 356(1–2), pp. 84–92. doi: 10.1016/j.jhydrol.2008.04.004.
- Yogesh, M. and Mokshapathy, S. (2013) 'Production and Export Performance of Black Pepper', *International Journal of Humanities and Social Science Invention*, 2(4), pp. 36–44.

## 8 APPENDIX

### 8.1 Details for the analysed fields

Name	Location	Area [ha]	Adjacent land use	Support type
BPepperField01	Bangka	2.27	NF	S
BPepperField02	Bangka	2.16	R + P + PO	Ts
BPepperField03	Bangka	2.20	R + P + PO	Ts
BPepperField04	Bangka	35.57	R + NF + PO	Ts
BPepperField05	Bangka	0.30	NF + PO + TM	S
BPepperField06	Bangka	1.07	PO + R	S + Ts
BPepperField07	Bangka	0.79	PO + R + CF	S
BPepperField08	Bangka	0.81	PO + P	S
BPepperField09	Bangka	0.15	NF	S
BPepperField10	Bangka	0.13	NF	TI + S
LPepperField01	Lampung	1.45	C + PO + Co + Ca + H	Ts
LPepperField02	Lampung	1.03	G + NF + H + P	Ts
LPepperField03	Lampung	0.98	P + NF + H	Ts
LPepperField04	Lampung	1.68	P + NF + H	Ts
LPepperField05	Lampung	0.30	NF + R + H + F	TI
LPepperField06	Lampung	1.60	P + PO + R + NF	Ts
LPepperField07	Lampung	6.44	P + PO + R + NF	TI

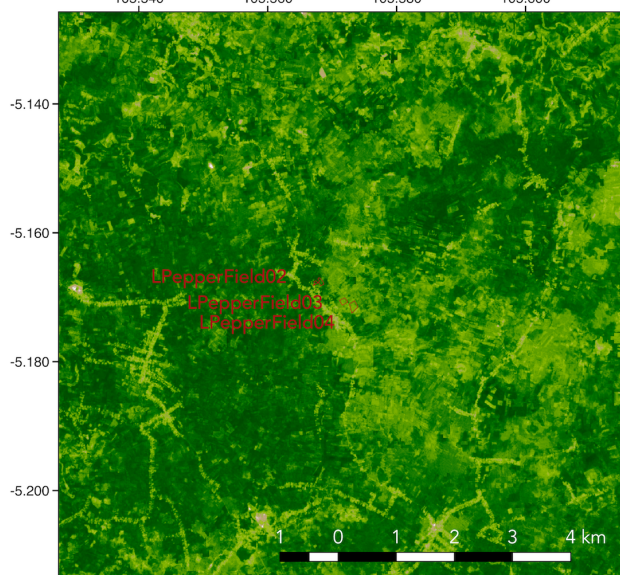
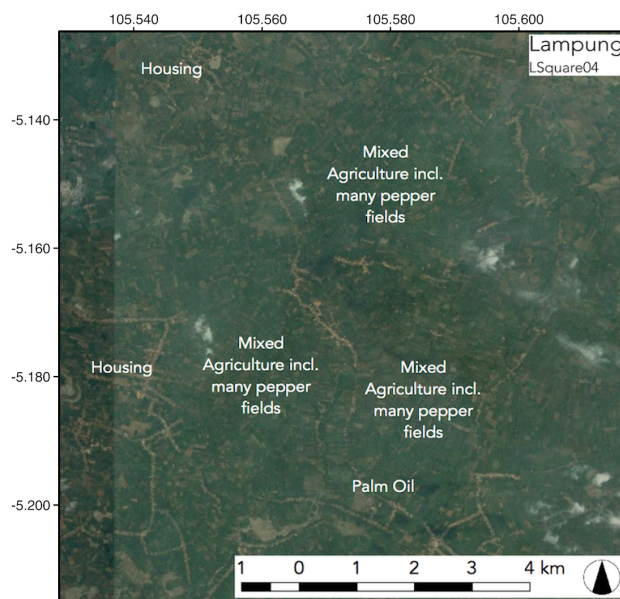
NF = Natural forest  
 R = Rubber  
 P = Pepper  
 PO = Palm oil

TM = Tin mines  
 CF = Cleared forest  
 C = Coffee  
 Co = Coconut

Ca = Cassava  
 H = Housing  
 G = Grass  
 F = Small Farms

S = Sticks  
 Ts = Trees with small canopy  
 TI = Trees with large canopy

## 8.2 Additional spatial analysis of *LSquare04*

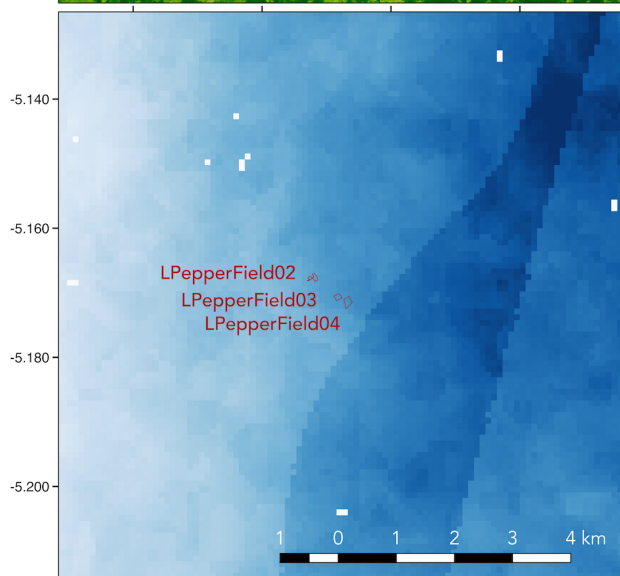


**NDVI**  
mean of the year 2016

Lampung  
LSquare04



- Pepper fields
- NDVI
- Clear water
- Turbid water
- Bare soil
- Light vegetation
- Medium vegetation
- Dense vegetation



**VOD**  
mean of the year 2016

Lampung  
LSquare04

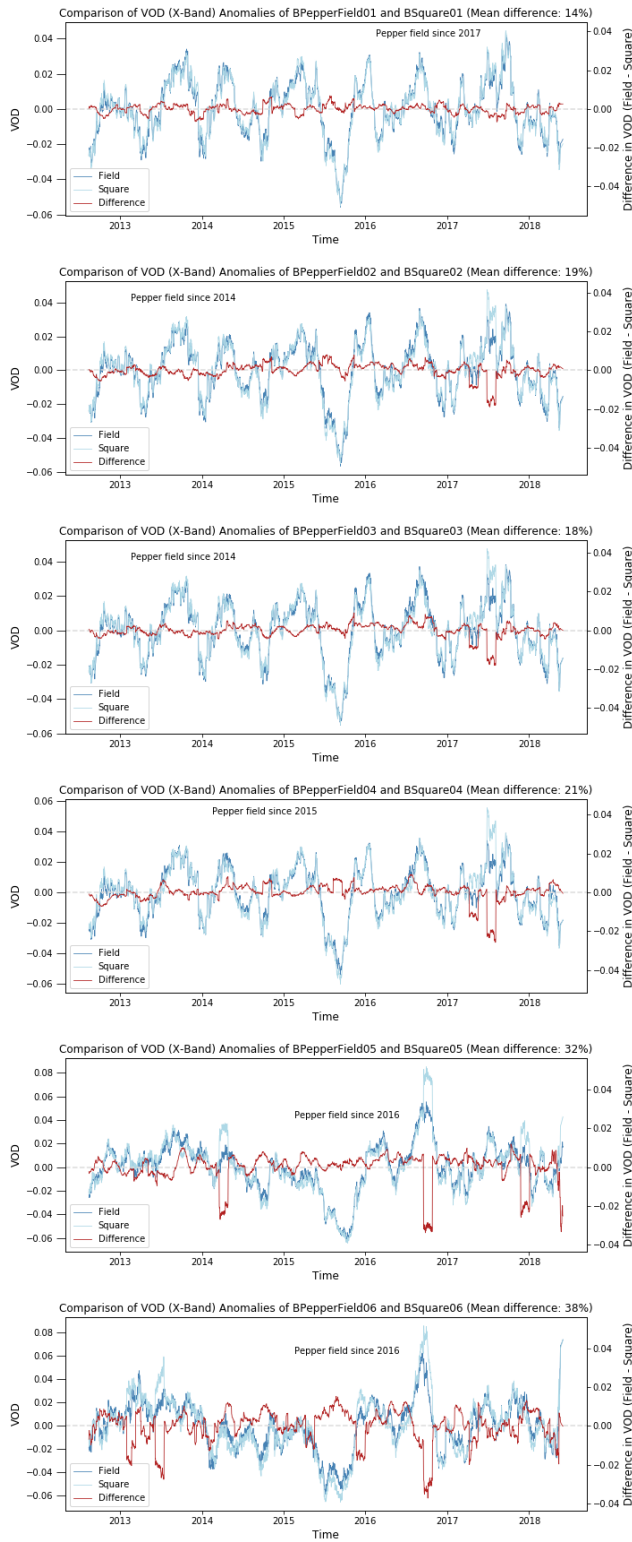


- Pepper fields
- VOD values [-]
- ≤0.541000
- 0.544250
- 0.547500
- 0.550750
- 0.554000
- 0.557250
- 0.560500
- 0.563500
- ≥0.566000

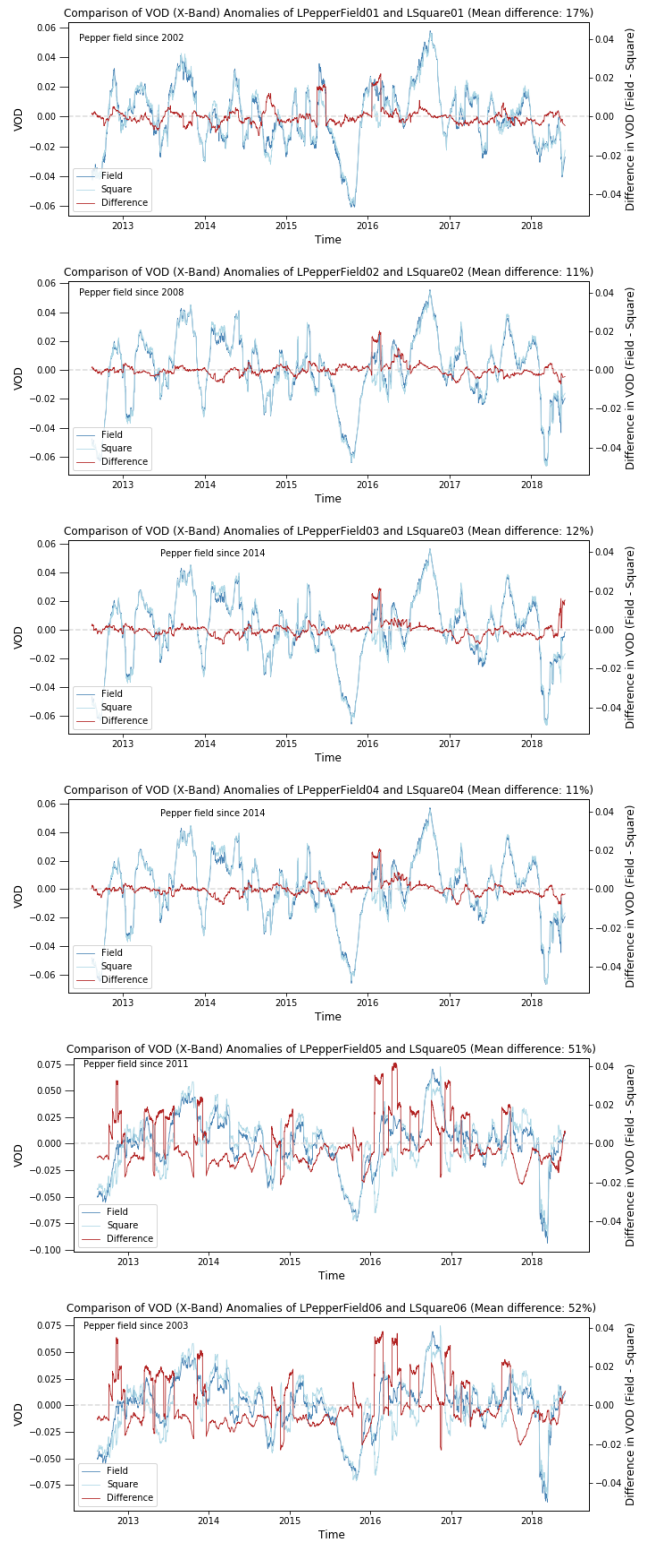
## 8.3 Pepper field versus large-scale surrounding

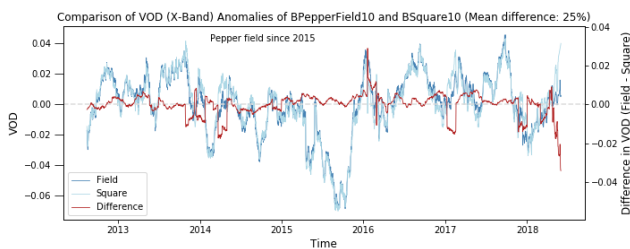
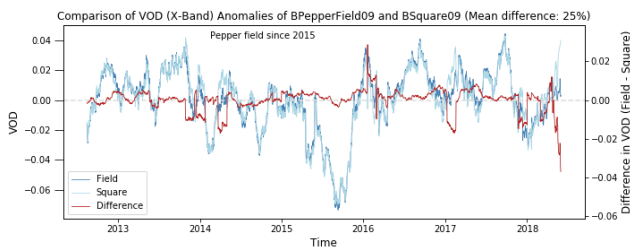
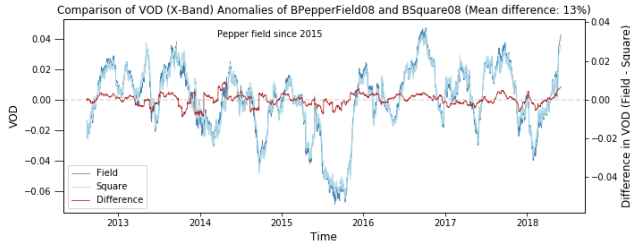
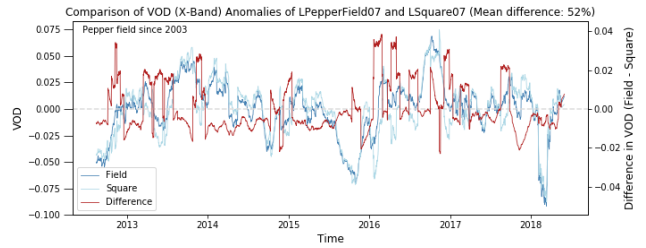
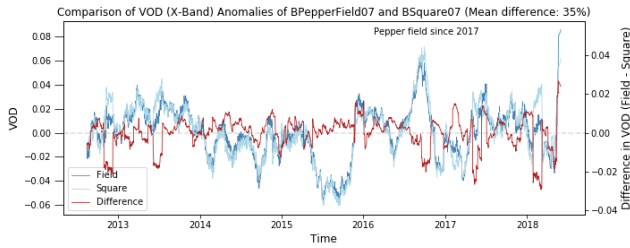
### 8.3.1 Anomaly time series

#### Bangka



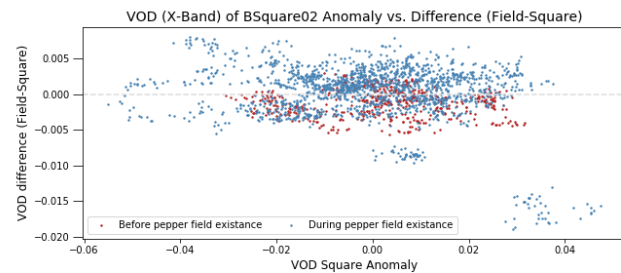
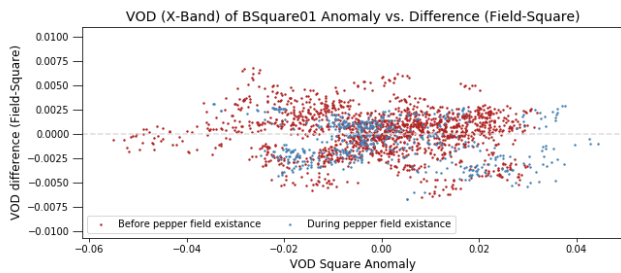
#### Lampung



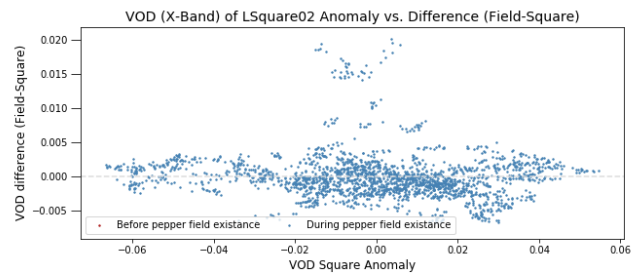
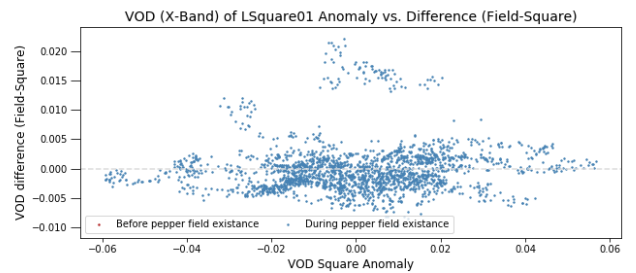


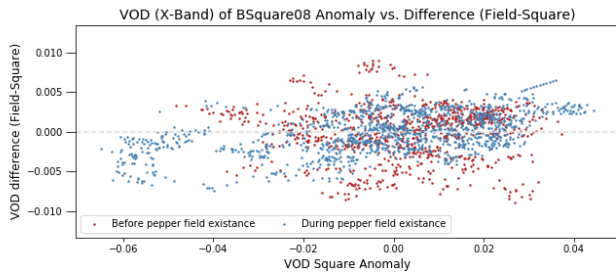
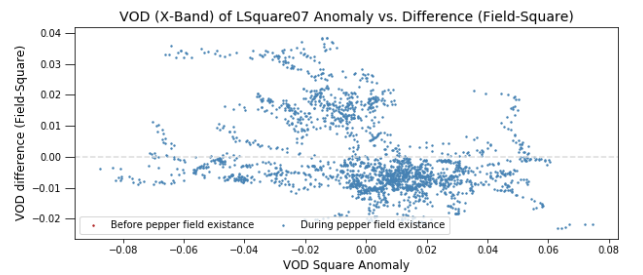
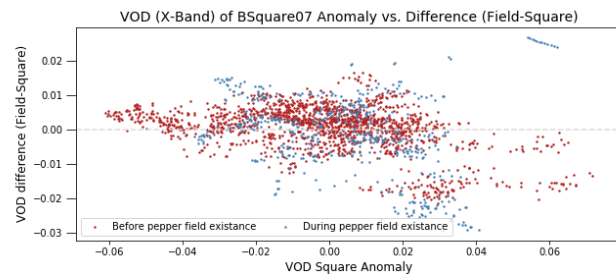
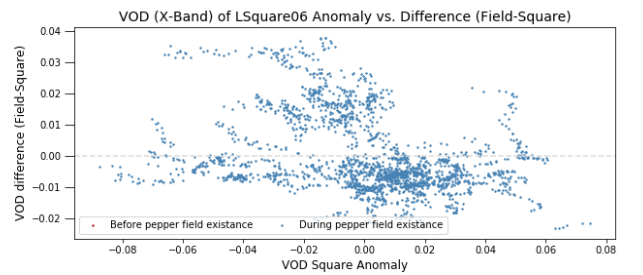
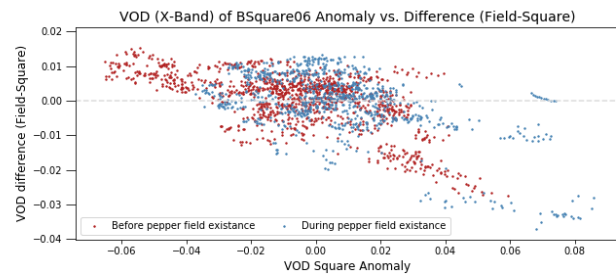
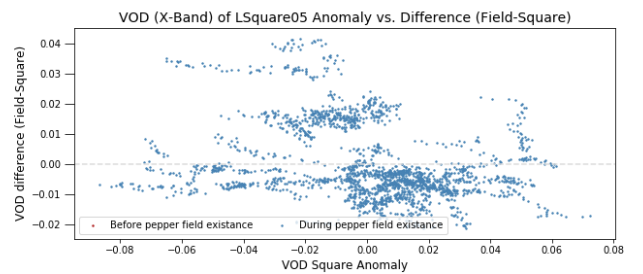
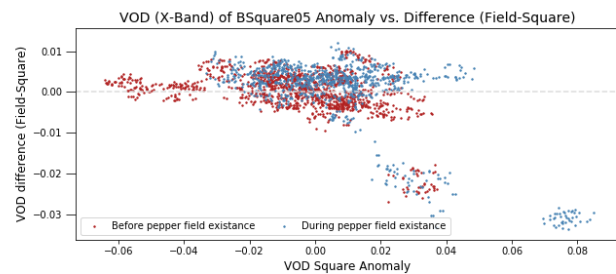
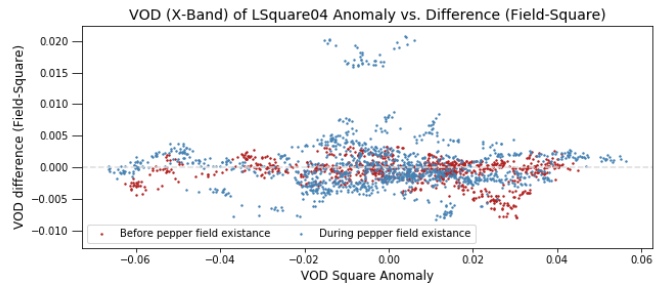
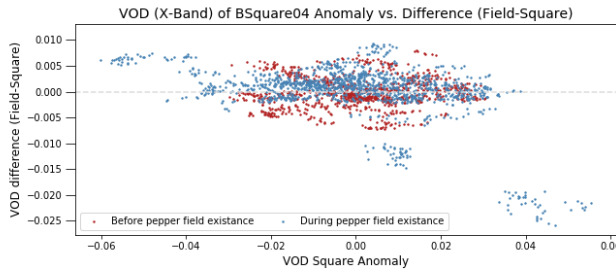
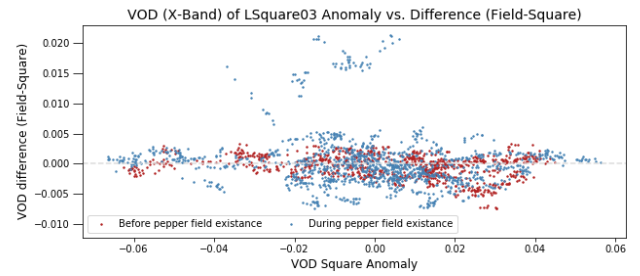
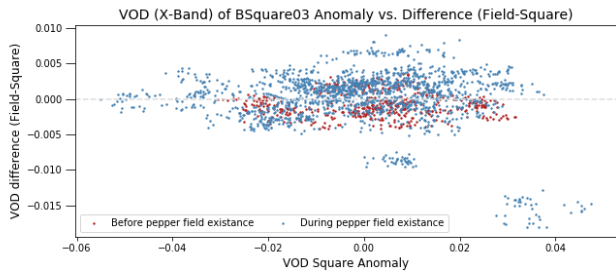
### 8.3.2 Scatter plots

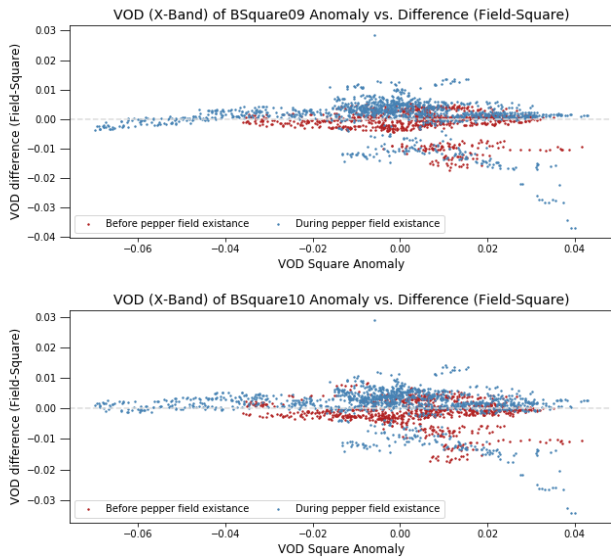
#### Bangka



#### Lampung





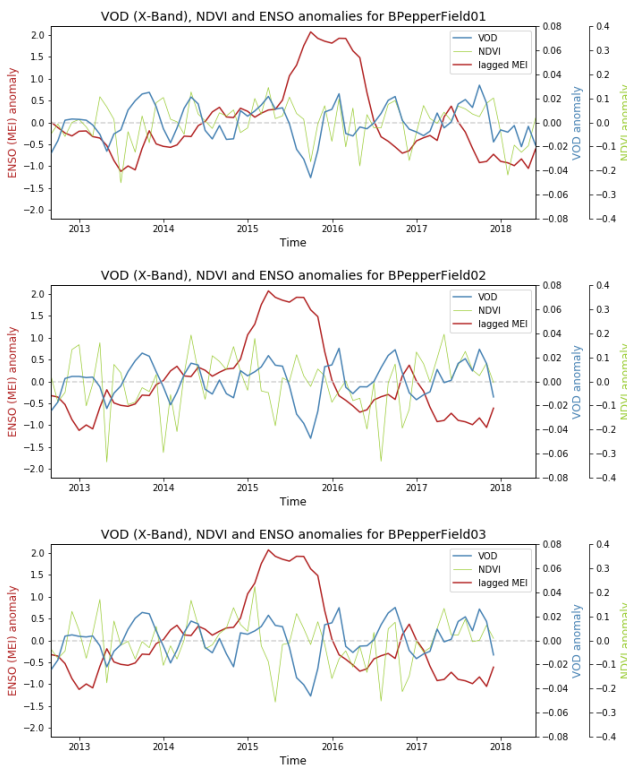


## 8.4 Correlations between different drought indices

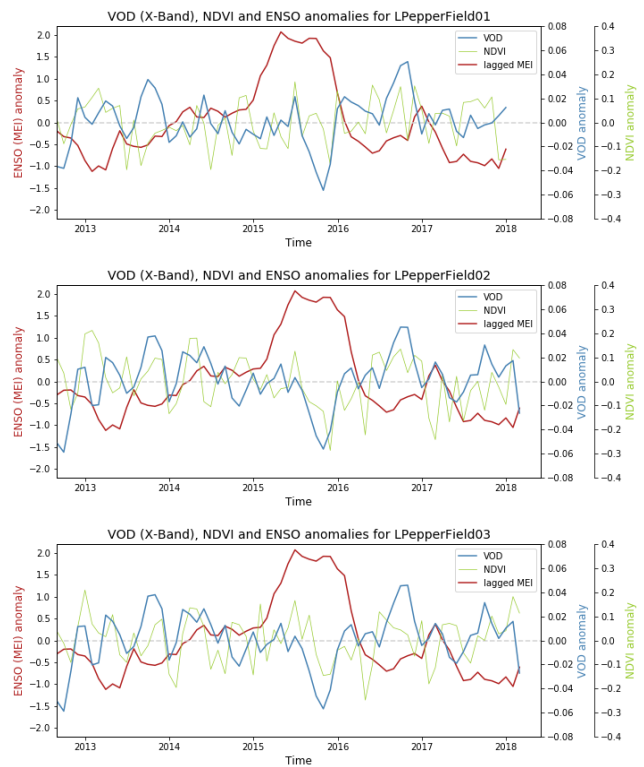
### 8.4.1 ENSO

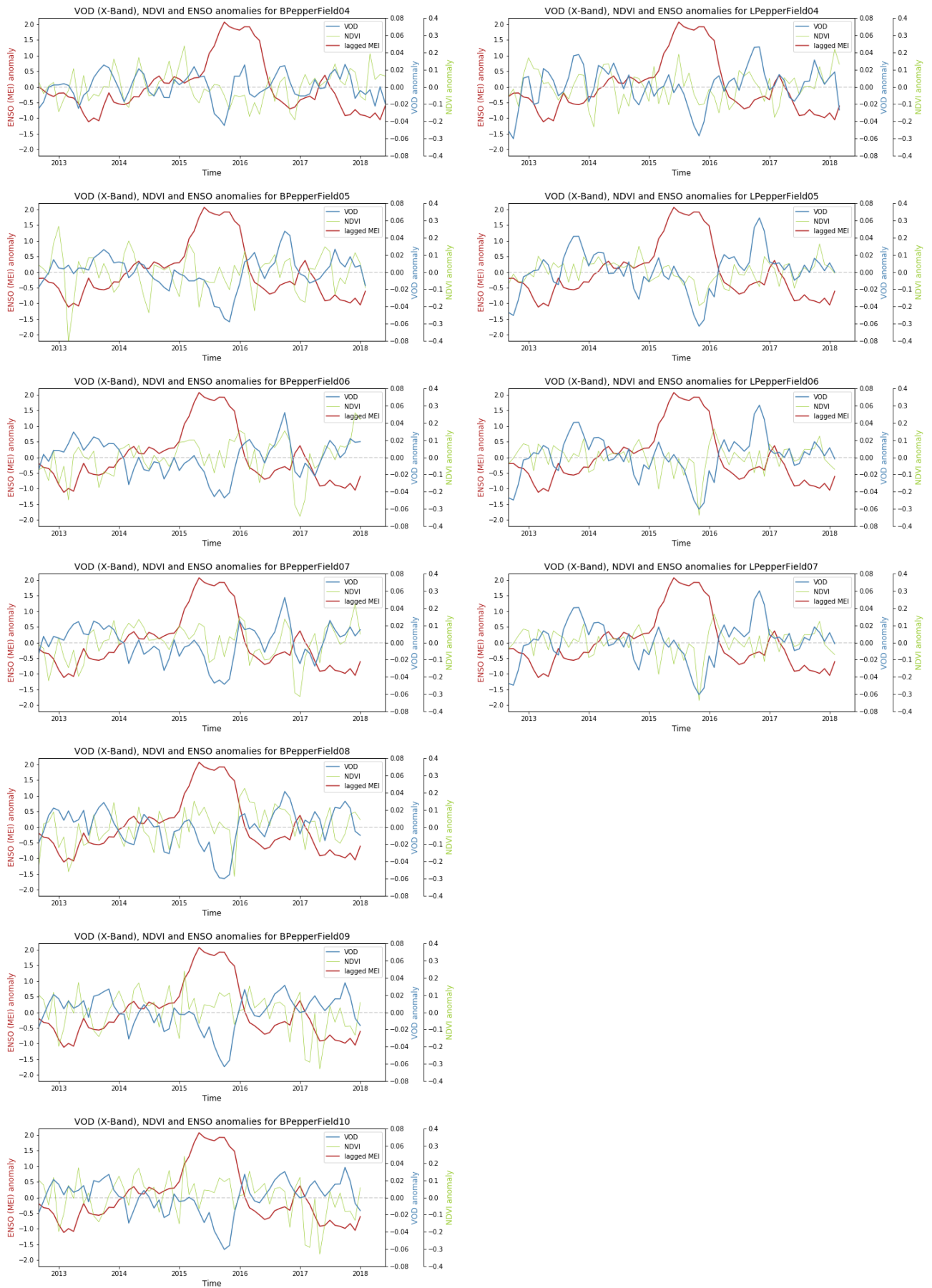
#### 8.4.1.1 ENSO anomaly time series

##### Bangka

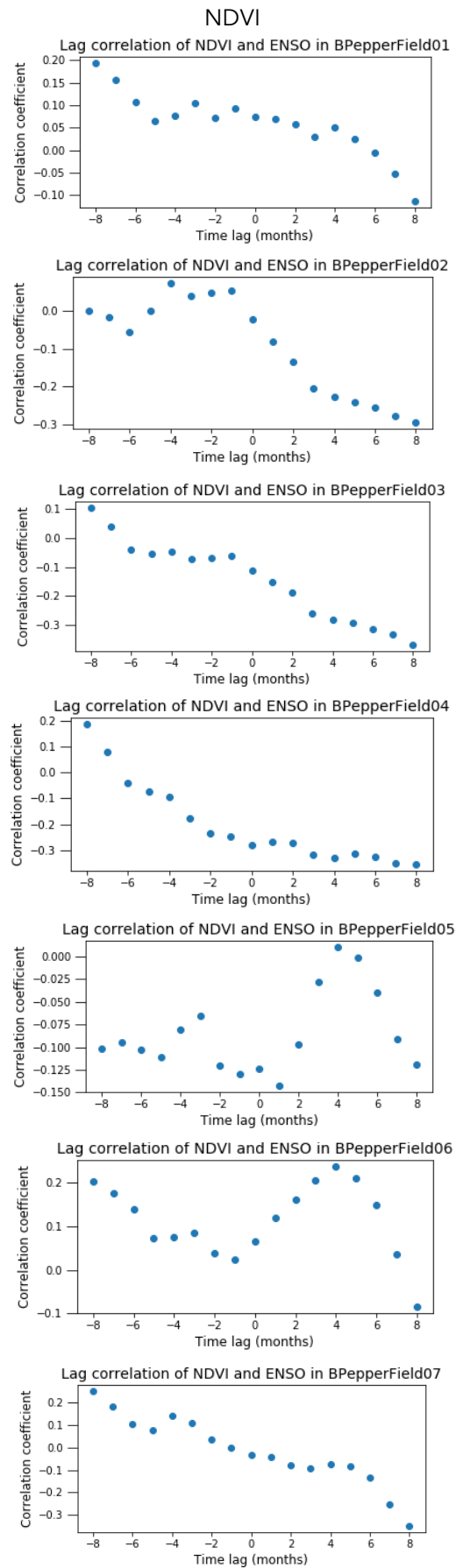
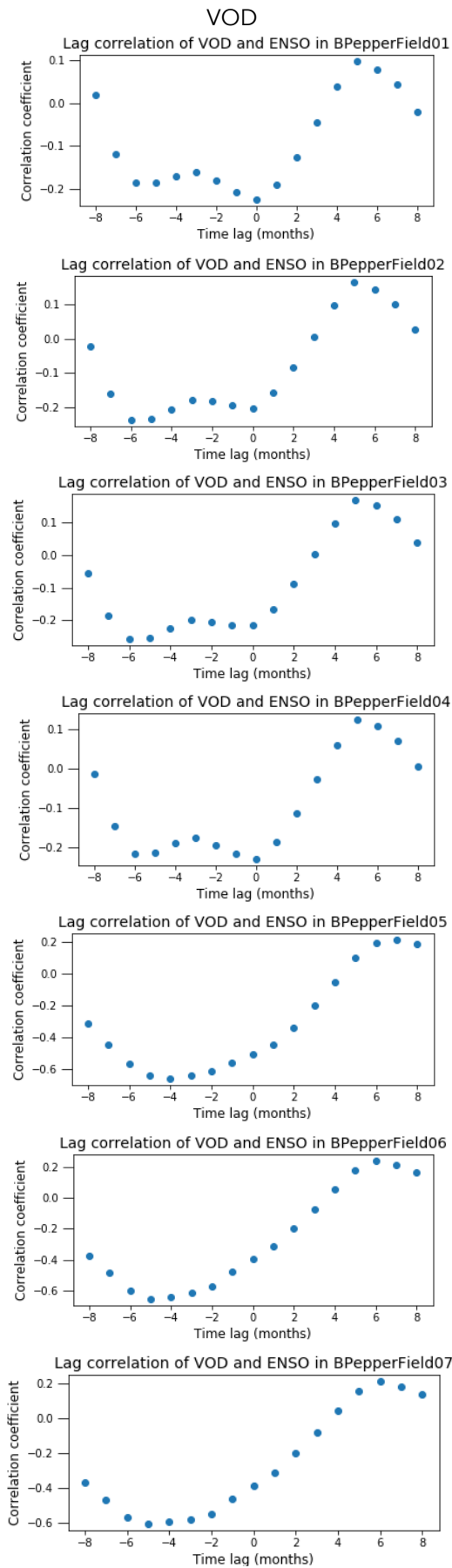


##### Lampung

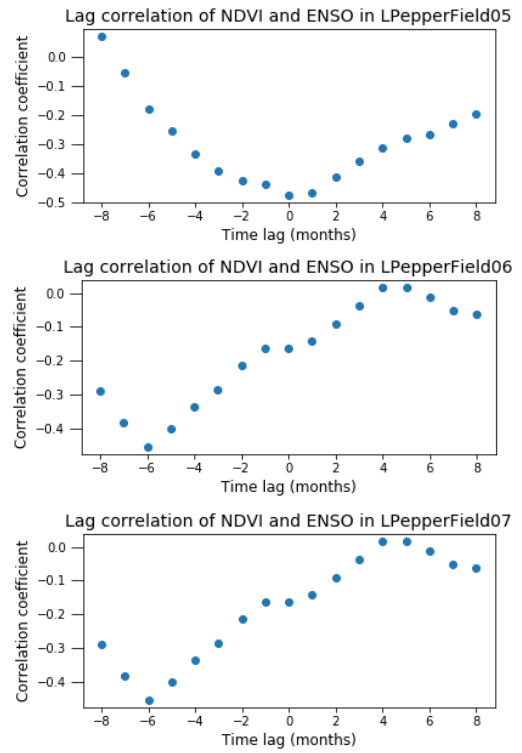
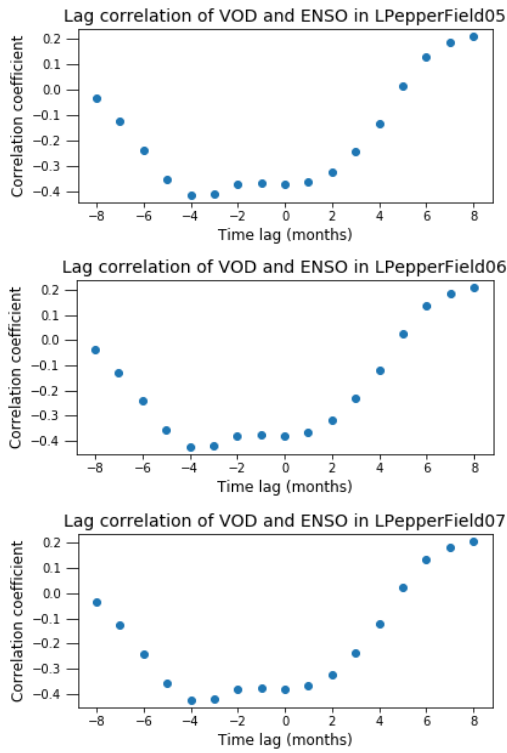




### 8.4.1.2 ENSO lag functions Bangka



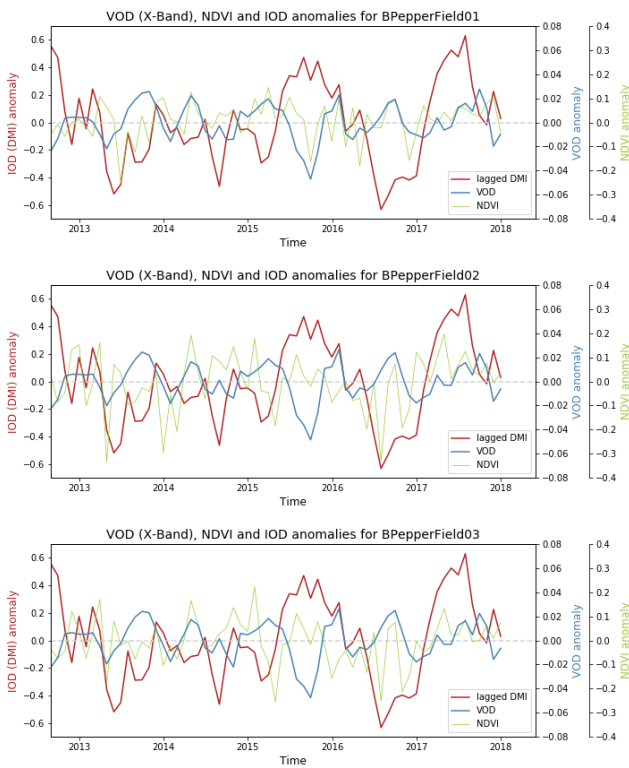




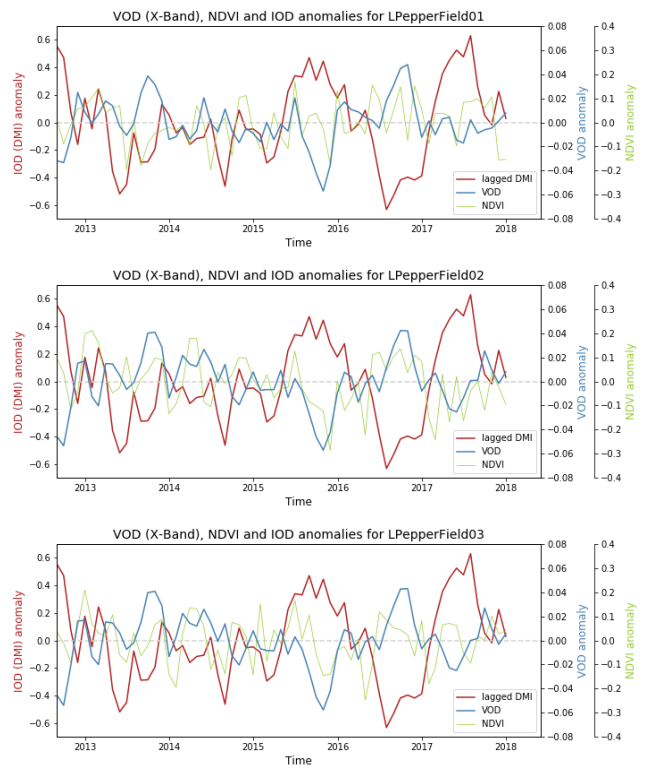
### 8.4.2 IOD

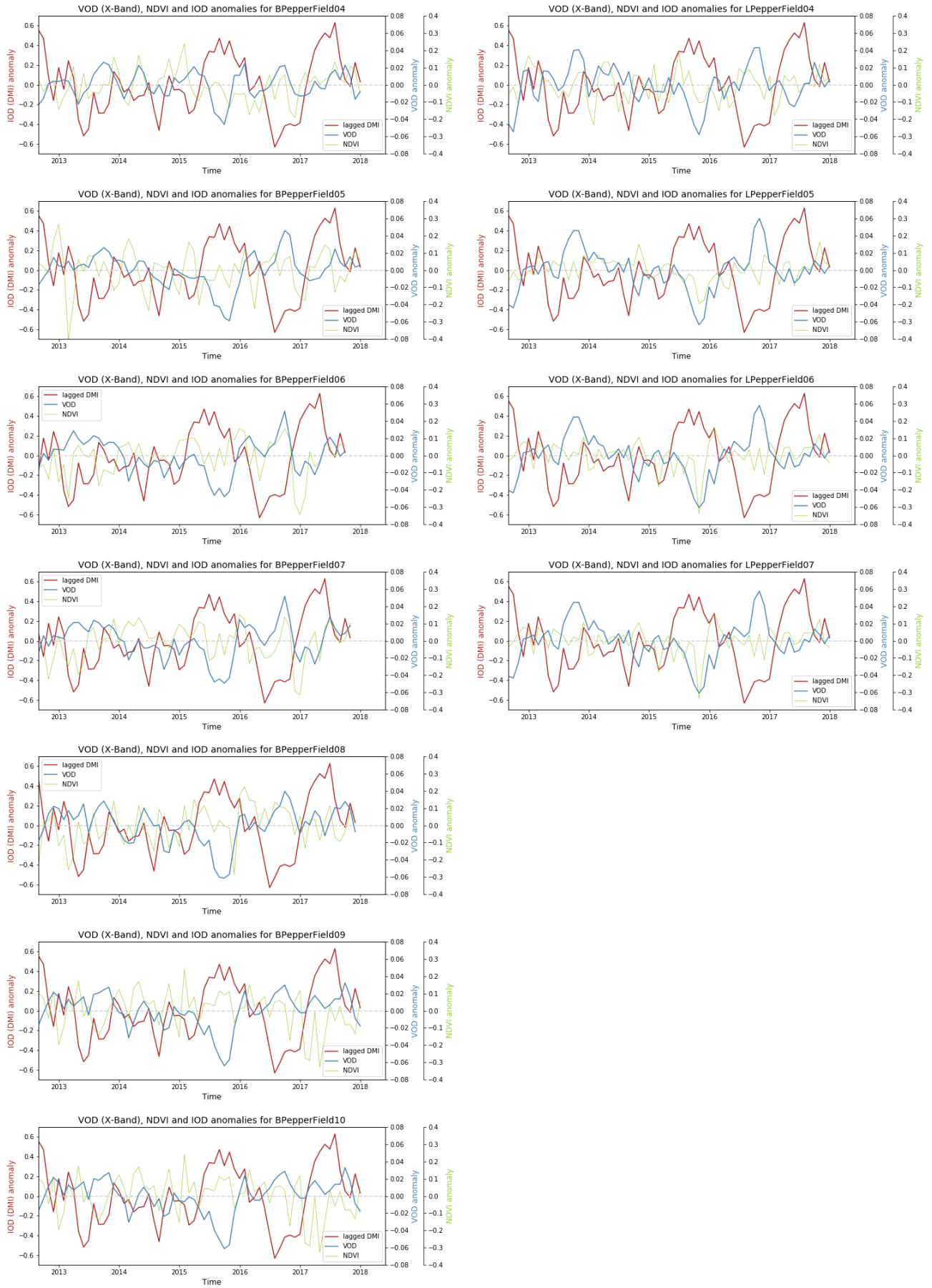
#### 8.4.2.1 IOD anomaly time series

##### Bangka

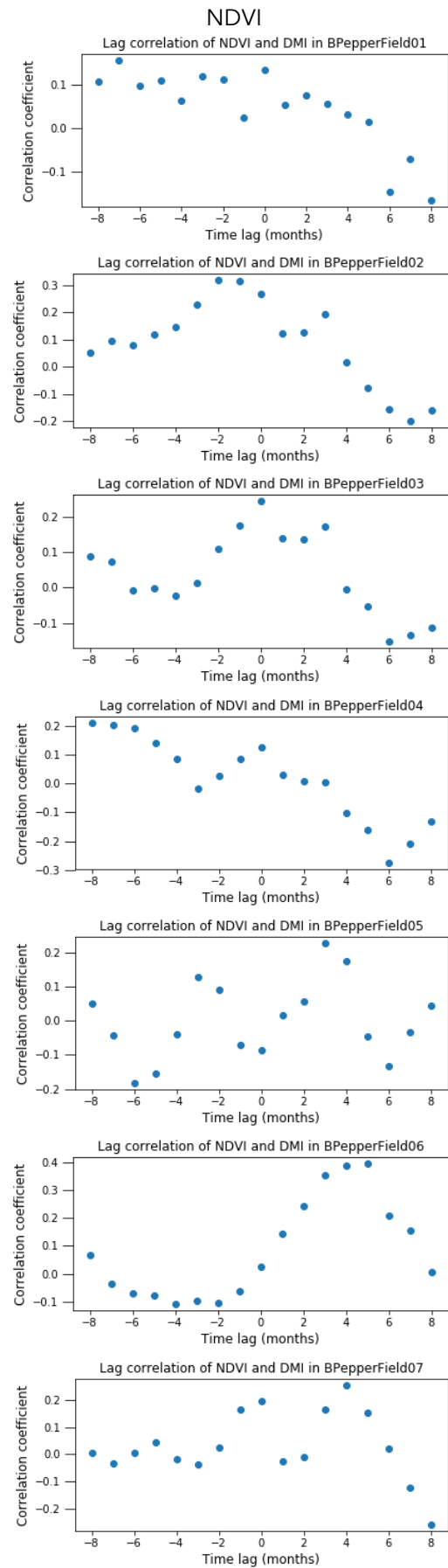
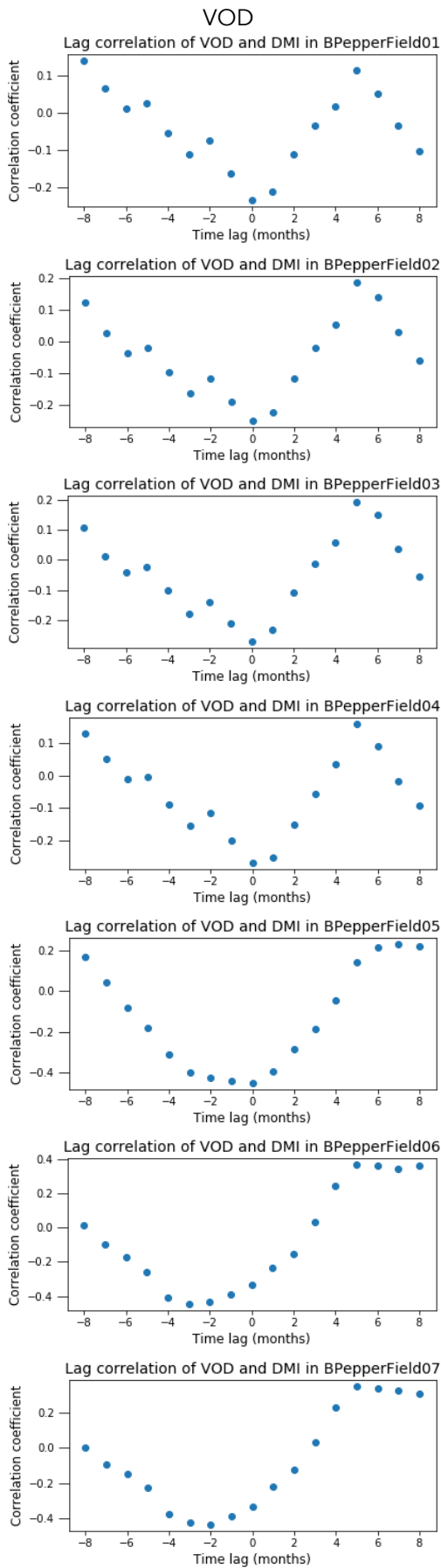


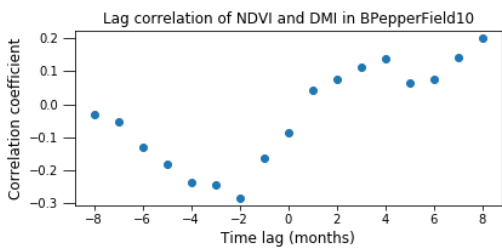
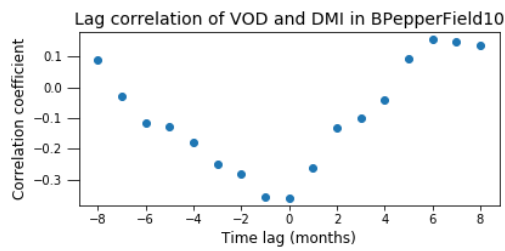
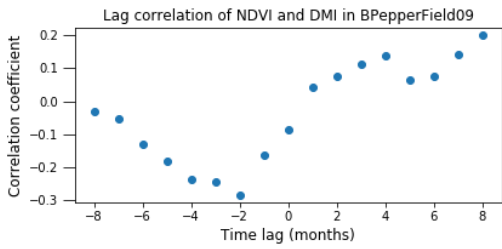
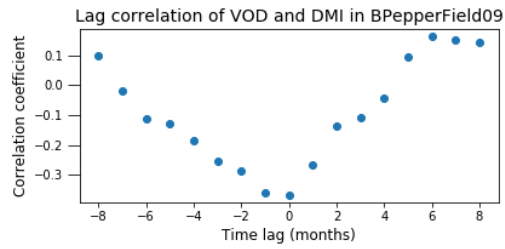
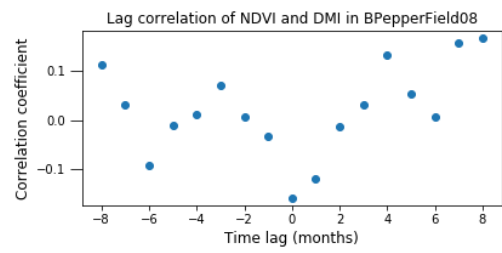
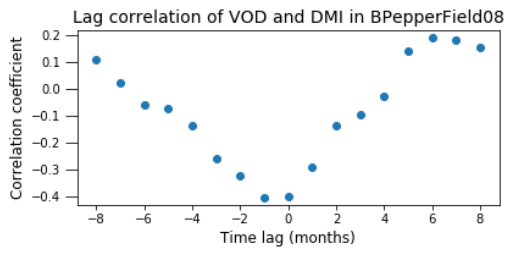
##### Lampung





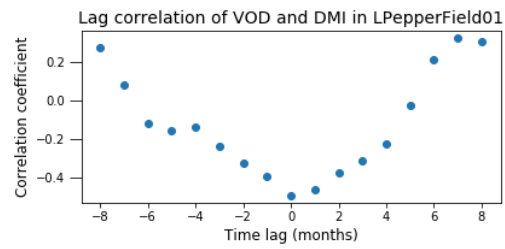
### 8.4.2.2 IOD lag functions Bangka



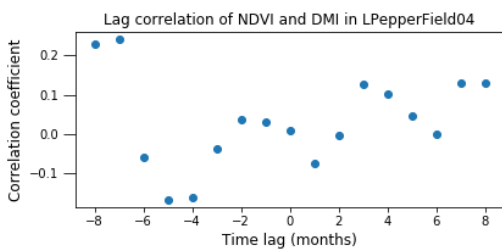
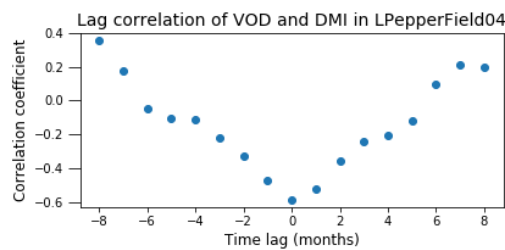
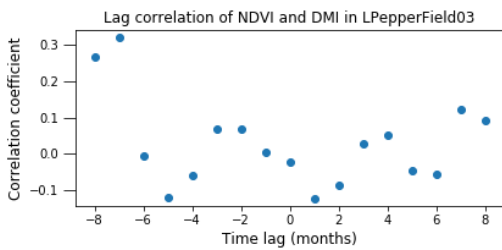
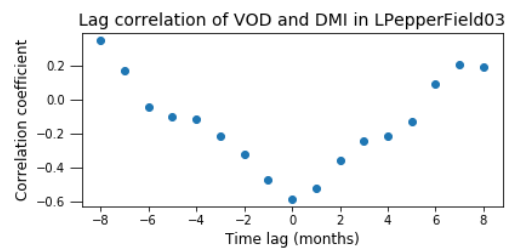
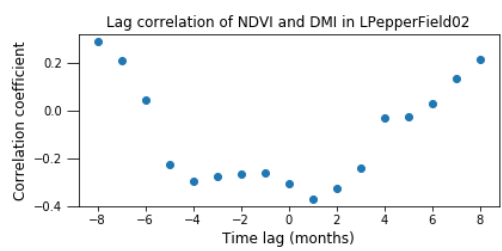
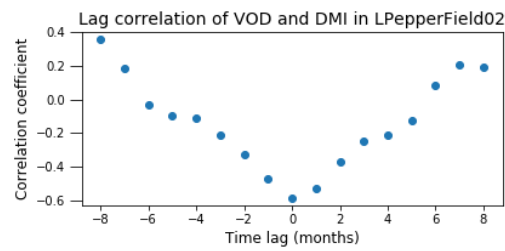
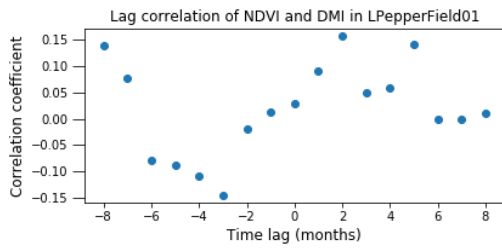


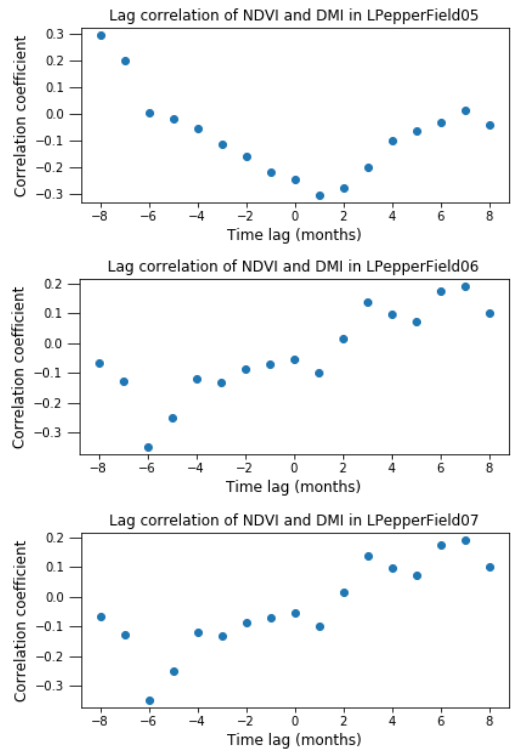
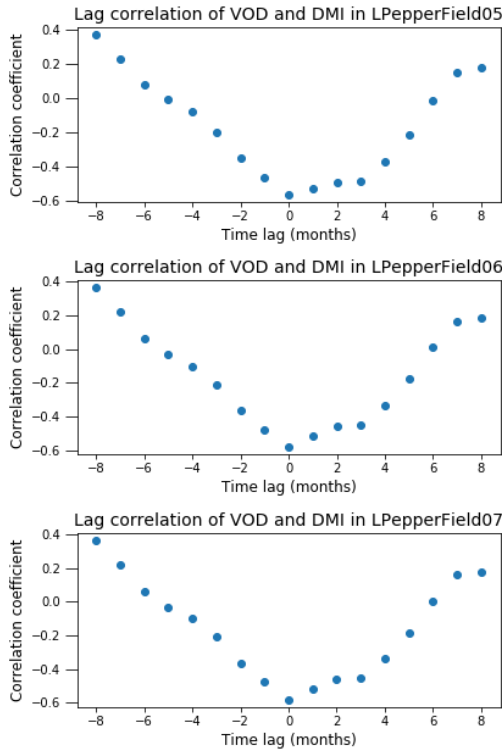
### 8.4.2.3 IOD lag functions Lampung

#### VOD



#### NDVI





**8.4.3 SPEI**

**Bangka**

**Lampung**

